JNC TJ8440 2001-001

亀裂ネットワークモデルによる解析

Fracture Network Modeling and Performance Assessment Support

（核燃料サイクル開発機構 契約業務報告書）

2001年2月

三菱商事株式会社

〒３１９－１１８４ 茨城県那珂郡東海村村松４番地４９
核燃料サイクル開発機構
技術展開部技術協力課
Inquiries about copyright and reproduction should be addressed to:
Technical Cooperation Section,
Technology Management Division,
Japan Nuclear Cycle Development Institute
4-49 Muramatsu,Tokai-mura,Naka-gun,Ibaraki 319-1184,
Japan

JNC TJ8440 2001-001
2001 年 2 月

亀裂ネットワークモデルによる解析

（核燃料サイクル開発機構 契約業務報告書）

吉添 誠* William Dershowitz**

要旨

本報告書は、平成 12 年度に Golder 社が実施した亀裂ネットワークモデルと性能評価を記述するものである。本報告書に記載された業務の主たる目的は、亀裂ネットワーク中の核種の移行経路をモデル化･評価することにおいて、JNC 殿を支援することであり、亀裂ネットワーク（DFN）モデル並びにチャンネルネットワーク（CN）モデルの両者のアプローチが取られている。加えて、Golder 社は、JNC 殿によるエスポの地下水移行モデル解析タスクフォース（AMTF）への参加を支援した。Golder 社は、AMTF の TASK4 における 5 メーター・スケールの亀裂ネットワーク移行経路の物質移行解析を実施するとともに、サイト特性調査と処分場の安全評価の統合化をめざした AMTF の TASK6 の進展にも寄与した。

Golder 社の平成 12 年度業務の詳細な情報は、本報告書の付属書に記されている。

本報告書は、三菱商事（株）が核燃料サイクル開発機構との契約により実施した業務に関するものである。
機構担当部課室：東海事業所　処分研究部　システム解析グループ
* 三菱商事株式会社
** Golder Associates Inc.

JNC TJ8440 2001-001
February, 2001

Fracture Network Modelling and Performance Assessment Support

Makoto Yoshizoe* and William Dershowitz**

Abstract

This report describes the Fracture Network Modelling and Performance Assessment Support performed by Golder Associates Inc. during the Heisei-12 (2000-2001) fiscal year. The primary objective of the work described in this report was to assist JNC in research related to characterization of solute transport pathways in fracture networks by the discrete fracture network (DFN) and channel network (CN) approaches. In addition, Golder supported JNC participation in the Äspö Modeling Task Force on of Groundwater Flow and Transport (AMTF). Golder carried out extensive analyses of flow and transport for a 5 meter scale fracture network pathway for AMTF Task 4, and assisted in development of AMTF Task 6 which will address the integration of site characterization and repository safety assessment.

Technical information about Golder Associates HY-12 support to JNC/Tokai is provided in the appendices to this report.

This work was performed by Mitsubishi Corporation under contract with Japan Nuclear Cycle Development Institute.
JNC Liaison: Waste Isolation Research Division
* Mitsubishi Corporation
** Golder Associates, Inc.

Report to:

Japan Nuclear Cycle Development Institute (JNC)
Tokai, Japan

Version 1.00

Fracture Network Modeling and Performance Assessment Support

Heisei-12
Progress Report

William Dershowitz
Thomas Doe
Dawn Shuttle
Thorsten Eiben
Aaron Fox
Kate Klise

February 14, 2001

ABSTRACT

This report describes the Fracture Network Modeling and Performance Assessment Support performed by Golder Associates Inc. during the Heisei-12 (2000-2001) fiscal year. The primary objective of the work described in this report was to assist JNC in research related to characterization of solute transport pathways in fracture networks by the discrete fracture network (DFN) and channel network (CN) approaches. In addition, Golder supported JNC participation in the sp Modeling Task Force on of Groundwater Flow and Transport (AMTF). Golder carried out extensive analyses of flow and transport for a 5 meter scale fracture network pathway for AMTF Task 4, and assisted in development of AMTF Task 6 which will address the integration of site characterization and repository safety assessment.

Technical information about Golder Associates HY-12 support to JNC/Tokai is provided in the appendices to this report.

TABLE OF CONTENTS

1. PROJECT OVERVIEW 2

2. TASK 2.4.2 DFN - CN PATHWAYS STUDY, LAPLACE TRANSFORM GALERKIN APPROACH 3

2.1 DFN Transport Equations 7
2.1.1 Time-domain Transport Equations 7
2.1.2 Laplace-transform Domain Transport Equations 10

2.2 Numerical Solution Procedure 12

2.3 Comparison of LTG Plates to LTG Pipes 13

3. TASK 3. INTERNATIONAL PROGRAMS 16

3.1 Task 3.1 Äspö Task Force Support 16
3.1.1 Task 3.1.1: Task 4 TRUE-1 Sorbing Tracer Transport Experiments 16
3.1.2 Task6: Performance Assessment Modeling Using Site Characterization Data (PASC) 21

4. CONCLUSIONS 25

5. REFERENCES 26

LIST OF TABLES

Table 1-1: HY-12 Task Summary 2
Table 2-1: Comparison of Breakthrough Curves from LTG Plates and LTG Pipes 14
Table 2-2: Performance Comparison between LTG Pipes and LTG Plates 15

LIST OF FIGURES

Figure 2-1: LTG Plate vs. LTG Pipe Network Verification Case 3
Figure 2-2: Tritium Transport for Verification Test LTG_T3 (log scale) 4
Figure 2-3: LTG and Ogata-Banks Comparison for Verification Test LTG_T2 5
Figure 2-4 LTG Pipe and LTG Plate Breakthrough for Case LTG_GT3 (Disersion=2.0m) 6
Figure 2-5: LTG Pipe and LTG Plate Breakthrough for Case LTG_GT2 7
Figure 3-1: Uranine Transport Model and Measurement 17
Figure 3-2: Cesium Transport Model and Measurement 18
Figure 3-3: Rubidium Transport Model and Measurement 19
Figure 3-4: Sodium Transport Model and Measurement 20

APPENDICES

Appendix A	Comparison of LTG Transport in Pipe (CN) and Plate (DFN) Fracture Networks
Appendix B	sp Task 4F2, Calibration of DFN Transport Modeling at the 10 m Scale
Appendix C	Learning from Recovery: Thoughts on Feature A Transport Experiments
Appendix D	Demonstration Simulations Tasks 6 Performance Assessment Modeling Using Site Characterization Data

1. PROJECT OVERVIEW

The primary objective of the Golder Associates work scope during HY-12 was to support JNC s evaluation of solute transport approaches for performance assessment. In addition, Golder Associates provided technical support to JNC for the sp project.

H-12 Tasks and the appendices in which they are reported are summarized in Table 1-1.

Task	Title	Appendix
2.4.2	DFN - CN Pathways Study, Laplace Transform-Galerkin Approach	A
3.1	sp Task Force Support	B,C,D

Table 1-1: HY-12 Task Summary

Support for the sp project included Task 4F2 predictive modeling of sorbing tracer transport in the TRUE-1 rock block, and analysis of two kilometer scale geochemical transport pathways for Task 5 .

This report provides a summary of work completed by Golder Associates during HY-12. Technical information about Golder Associates HY-12 support to JNC is provided in the appendices to this report.

2. TASK 2.4.2 DFN - CN PATHWAYS STUDY, LAPLACE TRANSFORM GALERKIN APPROACH

During H-12, Golder Associates assisted JNC through a comparative study of solute transport in discrete fracture network (DFN) and channel network (CN) models for transport based on Laplace Transform Galerkin transport (LTG) methods. The LTG approach in DFN models is potentially the most accurate and powerful method, and is therefore of considerable importance to JNC. This comparison was based on verification cases developed by Golder for JNC during H-11.

The following combination of the processes were evaluated:

- ?? advection + dispersion
- ?? advection + dispersion + matrix diffusion + sorption on fracture surfaces
- ?? advection + dispersion + matrix diffusion + adsorption in matrix
- ?? advection + dispersion + matrix diffusion + adsorption in matrix + decay chain

Analyses were carried out for both simple pipe systems and pipe network. One of the cases simulated is illustrated in Figure 2-1. Breakthrough curves are illustrated in Figures 2-2 through 2-5.

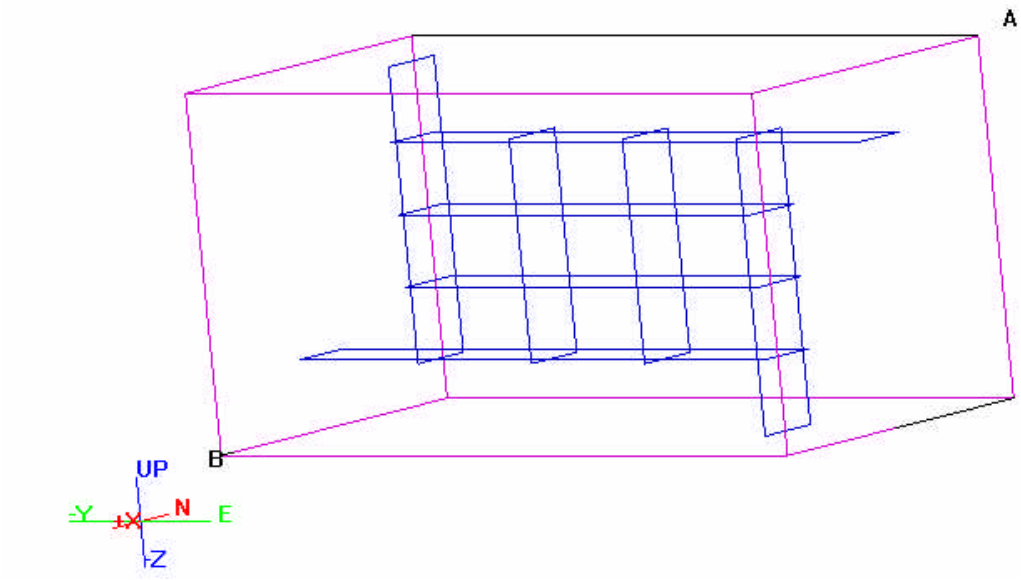

Figure 2-1: LTG Plate vs. LTG Pipe Network Verification Case

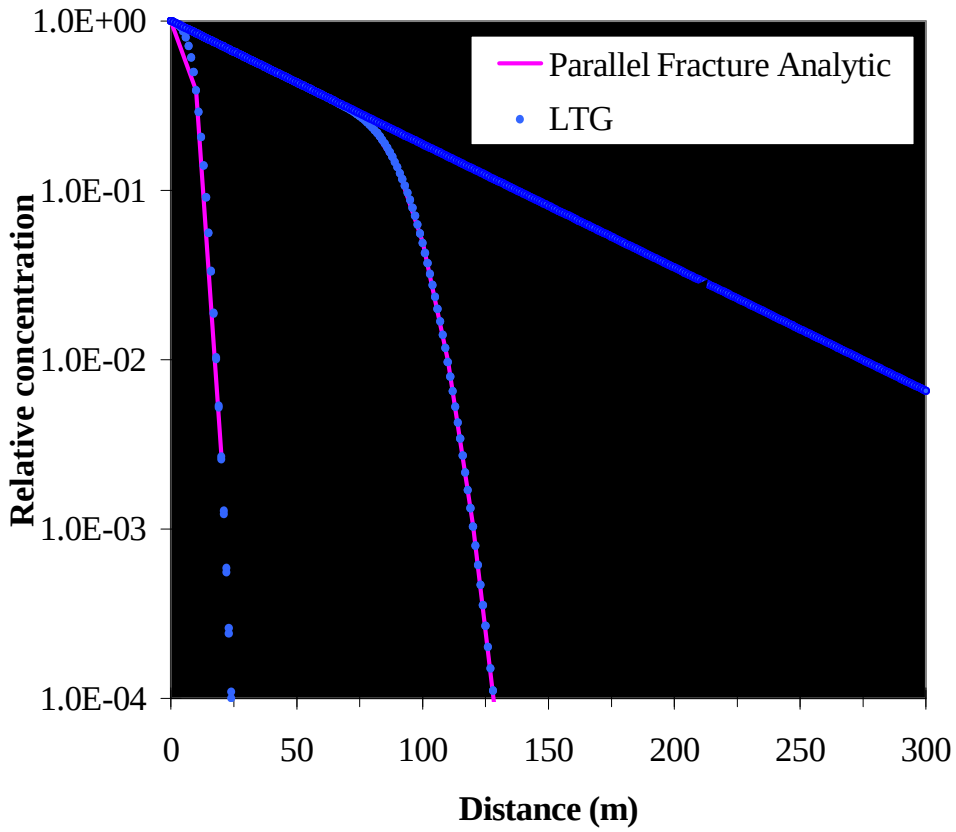

Figure 2-2: Tritium Transport for Verification Test LTG_T3 (log scale)

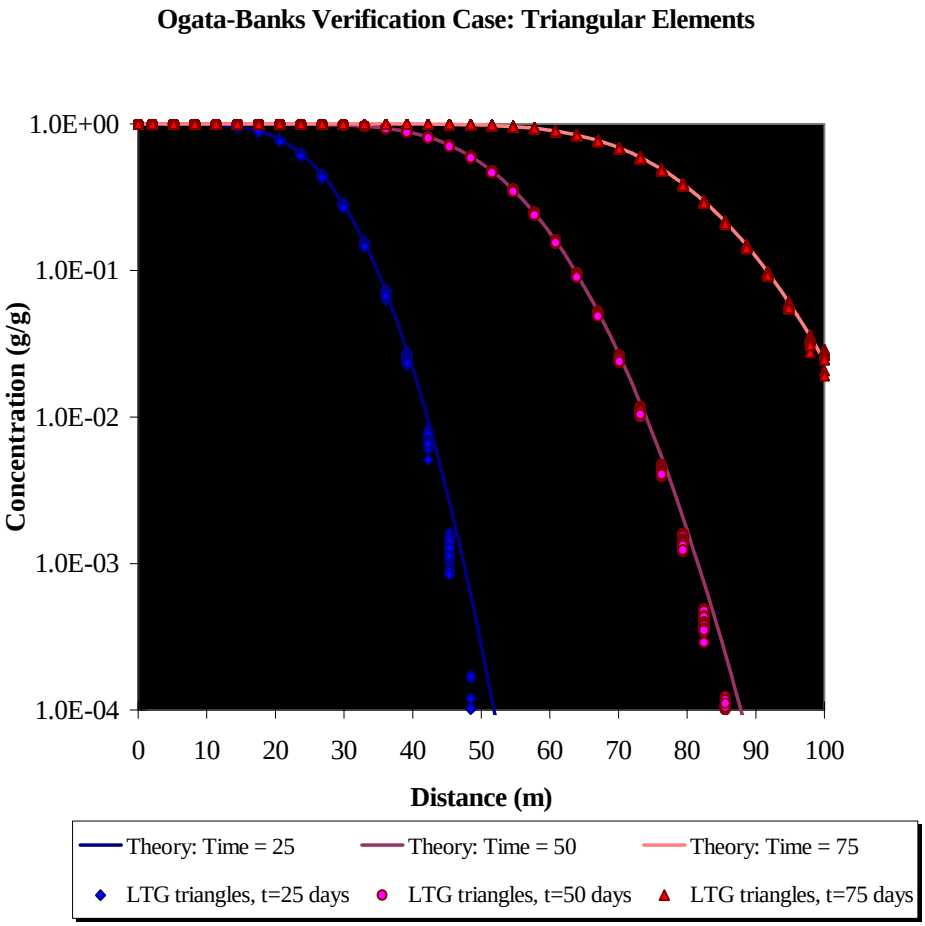

Figure 2-3: LTG and Ogata-Banks Comparison for Verification Test LTG_T2

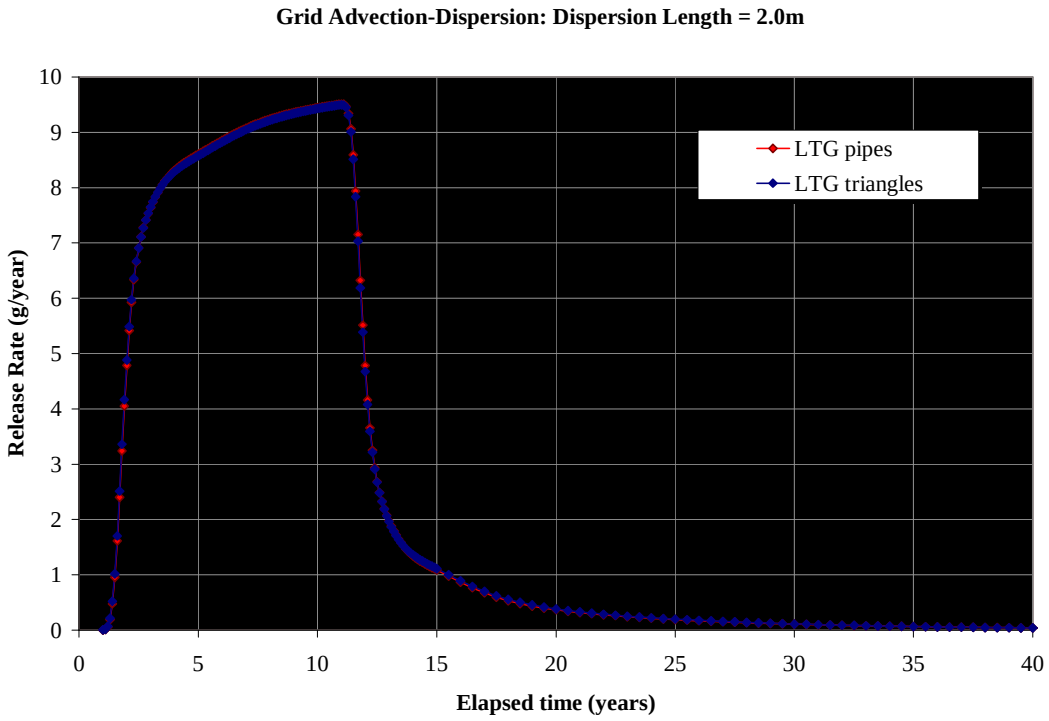

Figure 2-4 LTG Pipe and LTG Plate Breakthrough for Case LTG_GT3 (Disersion=2.0m)

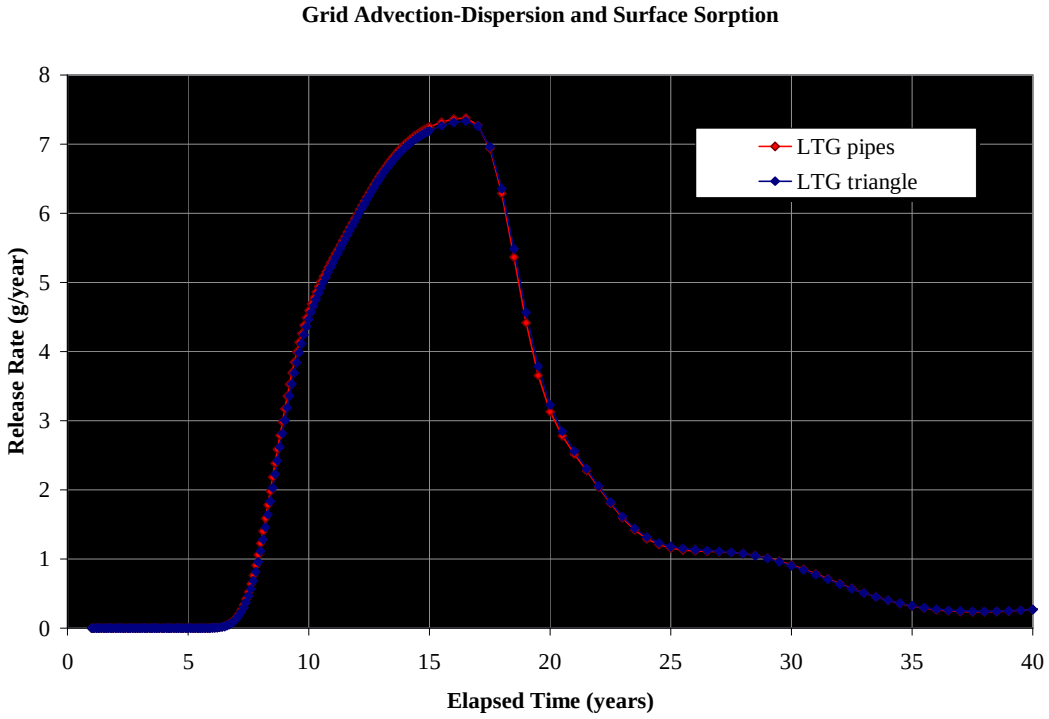

Figure 2-5: LTG Pipe and LTG Plate Breakthrough for Case LTG_GT2

2.1 DFN Transport Equations

The governing transport equations for DFN transport and their implementation using the Laplace Transform Galerkin method are described below. Equations are provided in the time domain, and in the Laplace transform space as they are solved numerically according to the LTG method.

2.1.1 Time-domain Transport Equations

2.1.1.1 Two Dimensional Transport

Assuming steady-state flow and a second-order approach to describe the diffusive mass transfer of a solute between the groundwater in a triangular element and the multiple immobile porosity zones attached to it, the advective-dispersive transport of solute species n in a triangular element network is given by:

$$A\theta R_n(\theta)\frac{\partial C_n}{\partial t} + q\frac{\partial C_n}{\partial x_i} - \frac{\partial}{\partial x_i}D_{i,j_n}\frac{\partial C_n}{\partial x_j} + R_n\lambda_n C_n - R_{n-1}\lambda_{n-1}C_{n-1}\theta = \sum_{im=1}^{IM} V_{im}\lambda_{im}D_{im}\frac{\partial C_n^{im}}{\partial w}\Big|_{w=0} + M(t)\delta(x_i - x_i') + Q(C_n - C_n^*)\delta(x_i - x_i^*)$$

Equation 2-1

where:

n	=	nuclide index [-]
l	=	element index [-]
$x_{i,j}$	=	spatial Cartesian coordinate (i, j = x, z) [L]
im	=	immobile zone class number (note: if desired *im* can equal 0) [-]
IM( )	=	total number of immobile zones attached to triangular element [-]
A( )	=	triangular element cross-sectional area per unit width [L^2]
	=	fracture aperture [L]
R_n( )	=	retardation factor [-]
q ( )	=	specific discharge (= Triangular element velocity v) [L/T]
D_{i,j_n}( )	=	dispersion coefficient [L^2/T]
D_n^{θ}	=	free-solution diffusion coefficient [L^2/T]
λ_n	=	decay constant [1/T]
M (*t*)	=	internal solute mass source/sink [M/T]
Q	=	external fluid source/sink [L^3/T]
δ( )	=	dirac delta [1/L]
δ( )	=	dirac delta [1/L]
V_{im}	=	block surface area per unit volume of matrix and fissures [1/L]
D_{im}	=	matrix effective diffusion coefficient [L^2/T]
θ_{im}	=	immobile zone porosity for immobile zone im
C_n	=	concentration in the flowing zone [M/L^3]
C_n^*	=	concentration of injectate in external fluid source [M/L^3]
C_n^{im}	=	Immobile zone concentration [M/L^3]
	=	Distance along interconnected triangular element network [L]
	=	Location of solute mass source/sink [L]
	=	Location of external fluid source/sink [L]
w	=	Distance perpendicular to plane of fracture [L]
t	=	time [T]

The hydrodynamic dispersion coefficient D_{i,j_n}( ) is given by:

$D_{i,i} = ?_L v_x^2 / |v| + ?_T v_z^2 / |v| + D_n^?$

$D_{j,j} = ?_T v_x^2 / |v| + ?_L v_z^2 / |v| + D_n^?$

$D_{i,j} = (?_L - ?_T) v_x v_z / |v|$

Where

$|v| = (v_x^2 + v_y^2)^{0.5}$

$?_L$ = longitudinal dispersion coefficient [L]

$?_T$ = transverse dispersion coefficient [L]

It should be noted that if there is no flow along a particular triangular element within the network (i.e. $q(\ ) = 0$), then the model allows for diffusive transport through this triangular element. It should also be pointed out that if fluid is withdrawn at a resident concentration $C_n^* = C_n$, then the term involving Q in (2-1) vanishes. If the injectate concentration $C_n^* = 0.0$, then this term accounts for the dilution effect of the injection of solute-free water.

The initial concentrations of all species within the domain are assumed to be zero in the LTG. Boundary conditions may be either of the Dirichlet-type where the input concentration history of each species is a specified function of time, or of the Cauchy-type where the advective input mass flux can be prescribed as a function of time at the origin of a triangular element on the boundary of the domain. Mathematically, these boundary conditions are described by:

Dirichlet: $C_n = C_n^?(t)$ on $?$ Equation 2-2

Cauchy: $A(\ )q(\ )C_n^o(t) ? A(\ )\left?\right.q(\ )C_n(\ ,t) ? D_{\ n}(\ )\frac{?C_n}{?}\left?\right.$ on $?$ Equation 2-3

where $C_n^?(t)$ is the specified concentration for species n. LTG also allows the concentration or flux rate (e.g. mol/yr) to be specified at an interior point.

2.1.1.2 Immobile Zone

In order to represent the diffusive exchange of solute mass between the triangular elements and any on the *im* immobile zones attached to them, LTG uses a second-order approach described by:

$$? _{im} ?im, \ ?R_n^{im} ?im. \ ?\frac{?C_n^{im}}{?t} ? \frac{?}{?w}? _{im} ?im, \ ?D_{im} \frac{?C_n^{im}}{?w}$$
$$? ? _{im} ?im, \ ?R_n^{im} ?im, \ ?? _n C_n^{im} ? ? _{im} ?im, \ ?R_{n?1}^{im} ?im, \ ?? _{n?1} C_{n?1}^{im} ? 0 \qquad \text{Equation 2-4}$$

where:

$?_{im}(im,\ )$	=	Immobile zone porosity for immobile zone *im* attached to triangular element [-]
R_n^{im} (im,)	=	Immobile zone retardation factor for immobile zone im attached to triangular element [-]
C_n^{im}	=	Concentration in matrix [M/L3]
Dim	=	Matrix effective diffusion coefficient [L2/T]
	=	D_n^0 ?
$D_n^?$	=	Free-solution diffusion coefficient [L2/T]
?	=	Tortuosity [-]

If a particular immobile zone is fluid-filled, such as within an immobile water zone attached to a triangular element within a fracture plane, then the immobile zone porosity, $?_{im}$, would equal 1.0.

2.1.2 Laplace-transform Domain Transport Equations

The LTG method (Sudicky, 1989; Sudicky, 1990; Sudicky and McLaren, 1992) is a numerical solution procedure where the Laplace transform is first applied to the governing equation, and the transformed equation is then solved numerically using the Galerkin finite element procedure (or alternatively any other discretization method such as finite differences). Finally, upon a solution for the nodal Laplace-space solution, the time-domain solution is recovered by a numerical inversion of the Laplace transformed nodal solution.

Let the Laplace transform of a function *f(t)* be defined according to:

$$\bar{f}(p) ? \int_0^? f(t) e^{? pt} dt \qquad \text{Equation 2-5}$$

where *p* is the Laplace-transform parameter. Applying this to Equation 2-4 for the *im*th immobile zone and following algebraic manipulations, one obtains:

$$g_n\overline{C}_n - qA\frac{\partial\overline{C}_n}{\partial z} + A\frac{\partial}{\partial z}D_n\frac{\partial\overline{C}_n}{\partial z} + AR_{n-1}\lambda_{n-1}\overline{C}_{n-1} = \sum_{im=1}^{IM}\sum_{k=1}^{n-1}G_{nk}^{im}\overline{C}_n \qquad \text{Equation 2-6}$$

the k summation in Equation 2-6 is summing the nuclide s predecessors, where nuclide 1 is the first species in the chain, and nuclide n-1 is the direct parent.

In Equation 2-6:

VSA = volume per surface area [L]
p = Laplace transform parameter

$$g_n = \left[AR_n(p+\lambda_n) + \sum_{im=1}^{IM}V_{im}\theta_{im}D_{im}\frac{\theta_n^{im2}}{VSA_{im}}B_n^{im}(\theta_n^{im})\right] \qquad \text{Equation 2-7}$$

$$G_{n,k}^{im} = V_{im}\theta_{im}D_{im}\sum_{k}^{n}E_{n,k}^{,im}\frac{\theta^{im2}}{VSA_{im}}B^{im}(\theta^{im}) \qquad \text{Equation 2-8}$$

$$E_{n,k}^{,im} = \frac{\sum_{p=k}^{n-1}(\theta_p R_p^{im})}{\sum_{p=k}^{n}R_p^{im}(p+\lambda_p) + R^{im}(p+\lambda)} \qquad \text{Equation 2-9}$$

$$\theta_n^{im} = \sqrt{\frac{(p+\lambda_n)R_n^{im}}{D_{im}}} \qquad \text{Equation 2-10}$$

$$\theta_n^{im} = \theta_n^{im}VSA_{im} \qquad \text{Equation 2-11}$$

For a "slab" geometry for a matrix block $? \frac{im}{n} (? \frac{im}{n})$ and VSA are defined by:

$$? \frac{im}{n} (? \frac{im}{n}) ? \frac{\tanh(? \frac{im}{n})}{? \frac{im}{n}} \qquad \text{Equation 2-12}$$

VSA, the volume to surface area ratio is equal to half the total slab width, $2d_{max}$.

VSA = d_{max}.

2.2 Numerical Solution Procedure

The numerical solution of the primary governing equation 2-6 is obtained using a standard Galerkin finite element procedure with linear interpolation functions used for each one-dimensional triangular element finite element, and a consistent mass matrix formulation applied to the accumulation terms arising from the Laplace transform of the temporal derivative and decay terms. Details concerning the application of the Galerkin finite element method in the context of the LTG algorithm can be found elsewhere (e.g. Sudicky, 1989; Sudicky, 1990; Sudicky and McLaren, 1992) and will not be repeated here. Inversion of the nodal Laplace-transformed concentrations is achieved using the discrete Fourier series methodology provided by de Hoog et al. (1982) which employs an efficient quotient-difference algorithm to enhance convergence of the inversion process, thus yielding a high degree of accuracy with relatively few discrete $p = p_n$ Laplace p-space vectors. Details concerning the implementation and performance of the de Hoog et al. scheme when applied to the inversion of nodal Laplace-transformed concentrations that arise from an application of the LTG method to solve for transport in fractured geologic media can be found in Sudicky and McLaren (1992).

The matrix equations arising from the LTG algorithm when used in conjunction with the de Hoog et al. (1982) Laplace inversion scheme are complex-valued, and the coefficient matrix is sparsely populated for an arbitrary network of interconnected triangular elements. Thus, the WatSolv iterative sparse-matrix solver library (VanderKwaak et al., 1997) was adapted to handle the complex system of matrix equations. The WatSolv library is based on an ILU factorization of the non-symmetric coefficient matrix with user defined levels of infill (set to zero in LTG). Watsolv also uses a compact ia-ja data storage structure such that only the non-zero terms in the matrix equations are stored and operated on. Further details on the capabilities of WatSolv can be found in VanderKwaak et al. (1997). The WatSolv library is designed to solve systems of equations arising from finite element, finite difference or finite volume discretizations using either single- or double-precision real, or single- or double-precision complex arithmetic.

2.3 Comparison of LTG Plates to LTG Pipes

Table 2-1 summarizes the comparison between LTG Plate and LTG Pipe solutions for eight of the cases studied. Although the average difference between the LTG Plate and LTG Pipe solutions is very small, the maximum difference for the more complex cases can be as high as 4.6%. Figures 2-1 illustrates the geometry of the simple grid cases GT1 through GT4. Figure 2-2 presents the geometry of the network case TN1. Figures 2-3 and 2-4 illustrate the comparison of analytical solutions against LTG Plate solutions for cases LTG_T3 and LTG_T2, respectively. Figure 2-5 shows the comparison of LTG plate and pipe results for case LTG_GT3.

Table 2-1: Comparison of Breakthrough Curves from LTG Plates and LTG Pipes

Case ID	Geometry	Processes	Normalized(1) Max Difference LTG Plates vs. Analytic(2) (%)	Normalized(1) Average Difference LTG Plates vs Analytic(2) (%)
LTG_T1	One-D Pathway	Single-porosity Transport of a Nonreactive Solute (t = 50 days)	-3.99E-02	-6.79E-03
LTG_T2	One-D Pathway	Single-porosity Transport of a Nonreactive Solute (t = 50 days)	-6.53E-01	-8.14E-02
LTG_T3	System of Parallel Fractures	Tritium Transport (t = 10,000 days)	-1.45E-01	-4.04E-02
LTG_T4	Parallel Fractures spaced at 10m	Decay Chain Transport (3 species)	-3.25E-01 -7.08E-01 -2.18E+00	-4.38E-02 -9.00E-02 -7.79E-01
LTG_GT1[2]	Simple Grid	Advection, dispersion length = 1.0 m	1.43E+00	-6.28E-03
LTG_GT2[2]	Simple Grid	Surface Sorption and Advection	1.05E+00	-2.38E-03
LTG_GT3[2]	Simple Grid	Matrix Diffusion and Advection	-8.95E-01	-3.47E-01
LTG_GT4[2]	Simple Grid	Advection-Diffusion, Matrix Diffusion and Decay Chain	-1.74E+00	-4.81E-01

[1] Normalized by the peak analytic release rate

[2] No analytic solution, therefore compared to the pipe solution and normalized to the peak pipe release rate

Table 2-2 summarizes the comparison of memory and CPU time requirements for LTG pipes and LTG plates. In general, the plate solution requires approximately two orders of magnitude more CPU time, and one to two orders of magnitude more memory than the pipe solution. However, the CPU and memory requirements are still quite modest for the simulations included in this study.

Table 2-2: Performance Comparison between LTG Pipes and LTG Plates

Verification Case	**Memory (kB)**		**CPU (seconds)[1]**	
	Triangular	**Pipes**	**Triangular**	**Pipes**
LTG_T1	296	43	0.17	0.05
LTG_T2	3796	43	4.71	0.05
LTG_T3	1205	84	4.96	0.69
LTG_T4	202	7	8.39	0.57
LTG_GT1, D_L=1.0m		12	130.76	2.16
LTG_GT1, D_L=2.0m	829	12	164.01	1.75
LTG_GT1, D_L=5.0m	829	12	236.21	1.47
LTG_GT2	829	12	116.37	2.48
LTG_GT3	829	12	92.60	1.89
LTG_GT4	829	12	86.29	1.87

[1]Measured on a Pentium 600

3 TASK 3. INTERNATIONAL PROGRAMS

3.1 Task 3.1 sp Task Force Support

During HY-12, Golder Associates supported JNC participation in the sp Task Force on Modeling of Groundwater Flow and Transport of Solutes. This support included:

- ?? Simulation, Reporting, Presentation Preparation, and Meeting Attendance for the Task-4F2 Evaluation of Sorbing Tracer Transport at the 10 Meter Scale.
- ?? Development of Scope and Specifications, and Demonstration Simulations for Task-6 Performance Assessment Modeling Using Site Characterization Data (PASC).

In addition, during HY-12, Golder Associates formally submitted reports for sp Task Force Tasks 4CD and 4EF for publication as SKB ICR series reports. Golder Associates prepared and presented a paper summarizing important issues raised by sp Tracer Transport Experiments.

3.1.1 Task 3.1.1: Task 4 TRUE-1 Sorbing Tracer Transport Experiments

From 1996 through 2000, SKB carried out a series of hydrologic and transport experiments in a mylonitic structure, Feature A within the TRUE-1 rock block of sp island, at the north east edge of the sp Hard Rock Laboratory. This work was completed and reported during HY-12. Golder Associates major effort for this task during HY-12 included:

- ?? Simulations to address remaining uncertainties regarding the appropriate parameters and conceptual models for flow and transport in single fractures like Feature A . (Appendix B).
- ?? Preparation of Final Reports for Task 4CD and Task 4EF, for publication as SKB ICR series reports.
- ?? Preparation of a Paper Summarizing JNC s contributions for the AMTF within Task 4F (Appendix C).

Figures 3-1 through 3-4 illustrate matches between JNC/FracMan-PAWorks solute transport models with Task 4F2 sorbing/decaying solute transport experimental measurements.

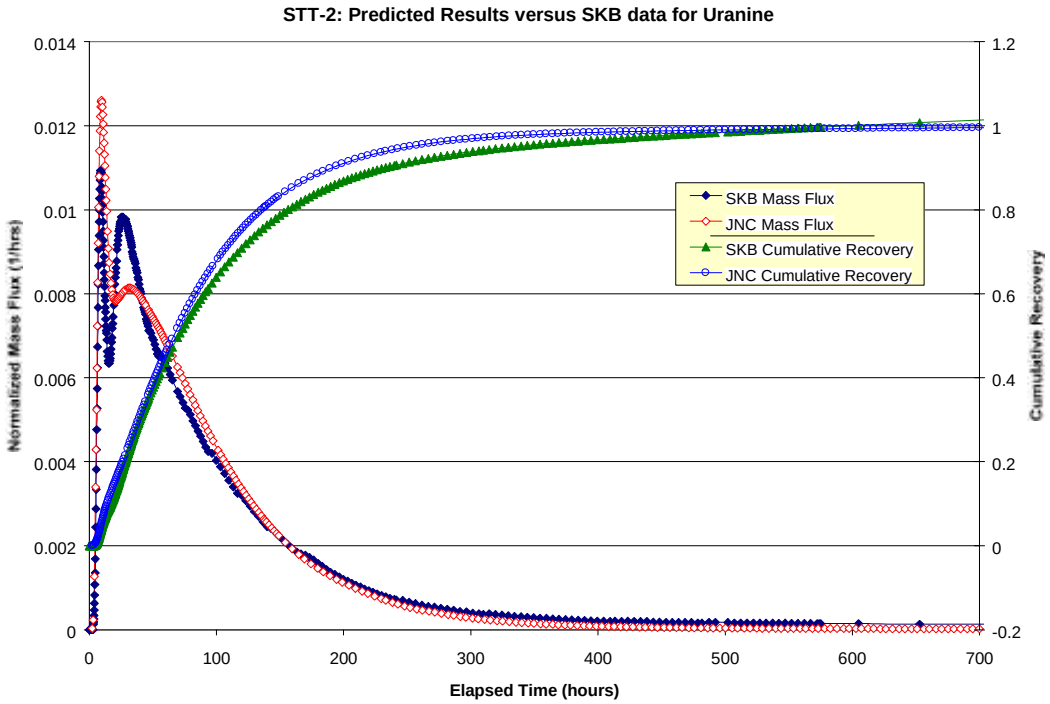

Figure 3-1: Uranine Transport Model and Measurement

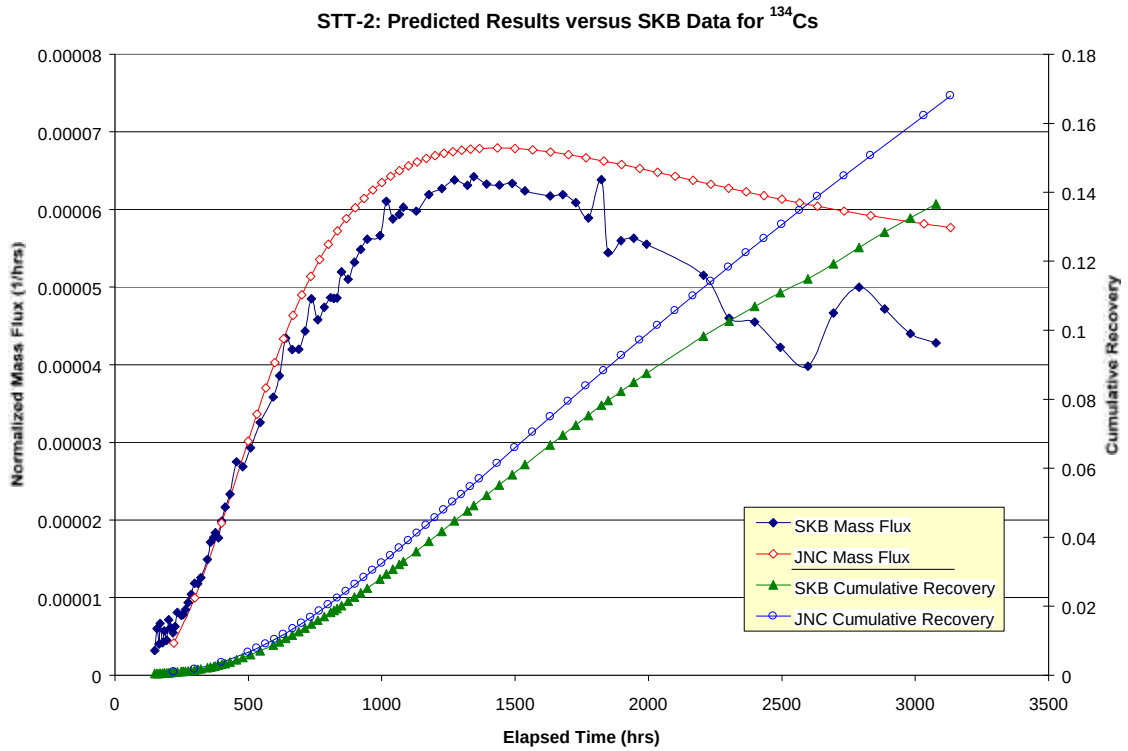

Figure 3-2: Cesium Transport Model and Measurement

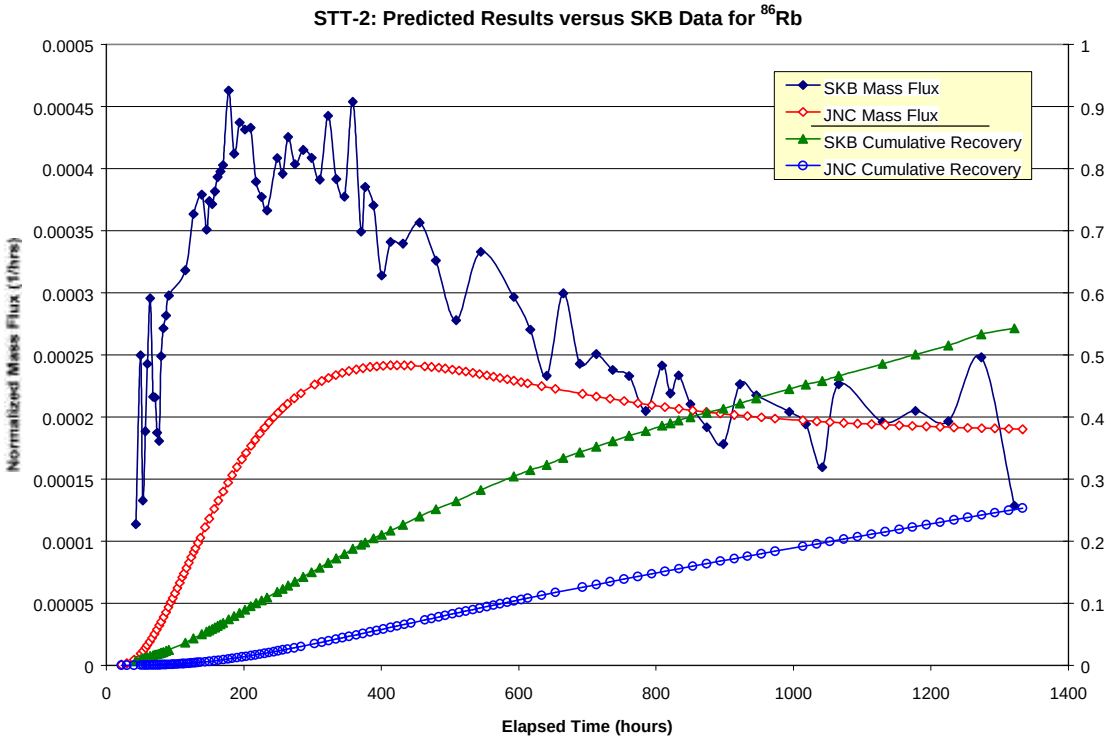

Figure 3-3: Rubidium Transport Model and Measurement

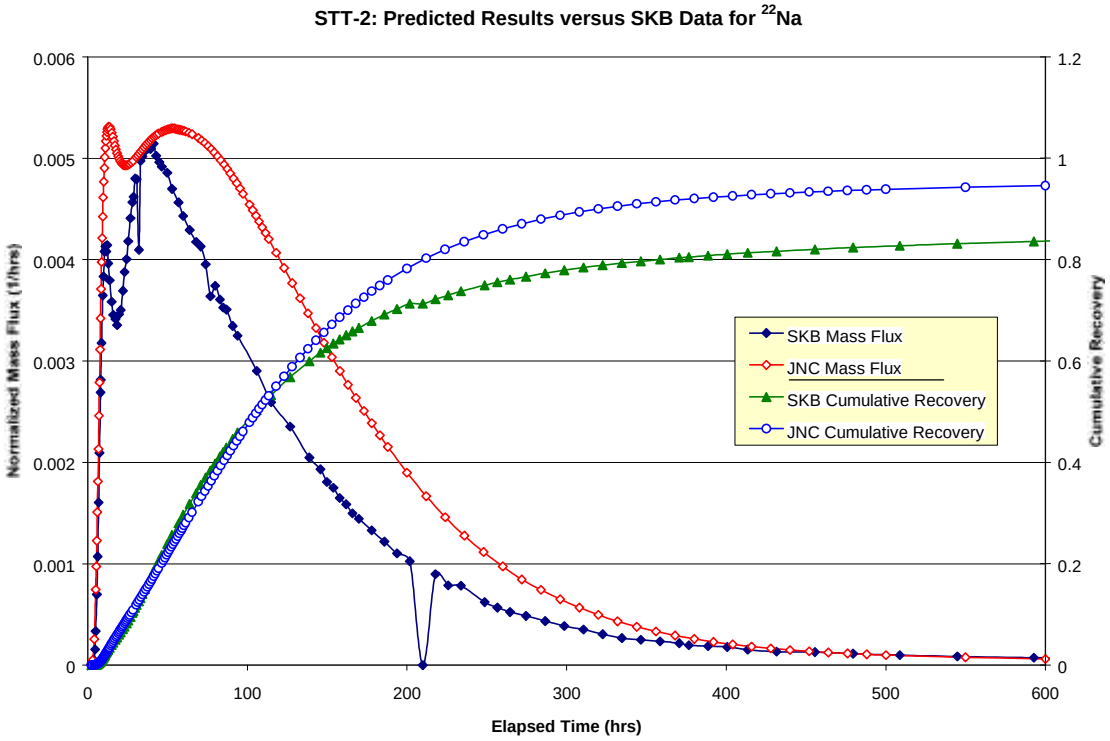

Figure 3-4: Sodium Transport Model and Measurement

3.1.2 Task6: Performance Assessment Modeling Using Site Characterization Data (PASC)

Solute transport is a key aspect of both performance assessment and repository site characterization. During HY-12, Golder supported JNC in working with SKB to develop a specification for an sp Modeling Task Force activity to provide a bridge between site characterization (SC) and performance assessment (PA) approaches to solute transport in fractured rock. Task 6 will address both site characterization and performance assessment modeling focused on the 50 to 100m scale which is critical to PA according to many repository programs.

Task 6 is developed in the context of arguments concerning the usefulness of *in situ* tracer experiments for PA, as discussed at the 1st GEOTRAP workshop held at Cologne in 1996. PA requires an understanding of slower processes, which are sometimes difficult to observe during short duration tracer experiments; *in situ* tracer experiments are dominated by rather faster processes. At the same time, PA models are generally simpler and physically less realistic than SC models[1].

Task 6 tries to bridge the gap between PA and SC models by applying both approaches for the same tracer experiment, and also for PA boundary conditions. In other word, this exercise will try to look at ***how far in-situ tracer experiments can constrain PA models***. It is hoped this will help to identify the relevant conceptualizations (in processes/structures) for longer-term PA predictions and identify site characterization data requirements to support PA calculations.

- ?? Task 6 combines the use of PA and SC models for both PA and SC boundary conditions.
- ?? All modelers should first implement their models such that they can reproduce the results from relevant sp *in situ* tracer experiments.
- ?? Modelers can make appropriate assumptions for PA modeling, while continuing to honor the *in situ* tracer experiment result.

Task 6 is phased from simple to complex, and includes sensitivity studies to maximize the amount of information obtained from the task to support both site characterization and performance assessment efforts.

[1] PA model refers to a Performance Assessment model that typically is based on a number of simplifications concerning geometrical description and treatment of processes. A site characterisation, or process, model is more rigorous in description of primarily processes. However, the latter type of model typically describes a smaller or less complex system than a PA model does.

It is emphasized that up-scaling is not a primary objective of Task 6; this is a change of focus as compared to the presentation of Task 6 at the 13th Task Force meeting in Carlsbad. Up-scaling is now assumed to be an implicit part of the model approaches, whereas the goal of the exercise is to apply PA and SC models to sp data.

3.1.2.1 Objectives

The general objectives of Task 6 is to assess simplifications used in PA models, to assess the constraining power of tracer experiments for PA models, and to provide input for site characterization programs from a PA perspective. The objectives may be elaborated as follows:

1. Identify key assumptions needed for long term prediction in PA and identify less important assumptions in PA.
2. Identify the most significant PA model components of the site.
3. Prioritize assumptions in PA modeling and demonstrate a rationale for simplifications in PA-models by parallel application of PA models of varying degree of simplification.
4. Understand the capability of in-situ tracer experiments to constrain PA models.
5. Understand the site-specific flow and transport behavior at different scales using SC models.
6. Provide a benchmark for comparison of PA and SC models in terms of PA measures for radionuclide transport at PA temporal and spatial scales.
7. Establish how to transfer SC models using site characterization data to PA models.
8. Provide support for site characterization program design and execution aimed at delivering needed data for PA.

3.1.2.2 Framework and proposed site

The objectives will be met by adopting a step-by-step process of model implementation, calibration to in situ experiments, PA type simulations, and sensitivity studies.
Task 6 will focus on the 50 to 100 meter scale, which is frequently the critical scale for geosphere retention. However, in order to allow for a more direct comparison, initial simulations will be carried out on the TRUE-1 block at the 5-meter scale:

?? Single fracture scale: the TRUE-1 block will be modeled. The purpose of the modeling study is to assess how different conceptualizations of a single fracture compare to each other.

?? Fracture network scale: a synthetic block based on the Prototype Repository, TRUE Block Scale, TRUE-1 and FCC features. The purpose of the modeling study is to assess how different conceptualizations of a fracture network compare to each other.

Flow and transport at the two scales will be addressed in the following two steps by applying SC-type models and/or PA-type models:

?? Traditional tracer experiment (SC time scale): the selected sets of TRUE-1 tracer experiment will be modeled. The purpose of the modeling study is to provide constraints to all the models before invoking assumptions for PA time scale predictions.

?? PA time scale prediction: Nuclide transport or sorbing tracer transport with PA type boundary conditions will be performed. Modelers can make any assumptions as long as they honor the material properties used for TRUE-1 tracer transport modeling.

Flow and transport will be analyzed for both current boundary conditions and for PA relevant time scales. Transport is considered from a virtual canister emplacement location in the sp HRL rock mass to a structural feature at a specified distance (starting from a few meters to 50-100 m). As an option, the addressed scale may be extended to the site scale (i.e., canister to biosphere). For this option, geochemical data may also be utilized similar to Task 5.

It is acknowledged that the distinction between SC and PA models may be somewhat ambiguous. However, it is stressed that all simplifications utilized when going from SC (tracer experiment) time scales to PA time scales and up-scaling procedures utilized when going from the single fracture scale to the network scale needs to be clearly stated by the modeling teams.

It is also foreseen that SC-type approaches and visualization techniques be used to understand the nature of flow and transport of radionuclides at PA spatial scales. It is anticipated that different groups will provide visualizations of transport pathways and processes using a variety of tools including pathway analysis, velocity distributions, spatial distributions of F- and ? factors, etc.

3.1.2.3 Scope

The specific tasks to be performed are:

Task 6A. Model and reproduce selected TRUE-1 tests with a PA model and/or a SC model. This task provides a common reference platform for all SC-type and PA-type modeling to be carried out as the project progresses. This ensures a common basis for future comparison.

Task 6B. Model selected PA cases in the TRUE-1 site with new PA relevant (long term/base case) boundary conditions and temporal scales. This task serves as a means to understand the differences between the use of SC-type and PA-type models, and the influence of various assumptions made for PA calculations for extrapolation in time.

Task 6C. Develop a 50-100m scale synthesized structural model using data from the Prototype Repository, TRUE Block Scale, TRUE-1 and FCC. The structural model should also be complemented with a hydraulic parameterization. It is suggested that a deterministic rather than a stochastic model be constructed so that the differences between models will be results of variations in assumptions, simplifications, and implementation rather than in the structural framework. The structural model will include sufficient elements of the TRUE Block Scale experiment to make it possible to reproduce a TRUE Block Scale tracer experiment as part of Task 6D. It is also suggested that Task 6C be performed by a single group led by SKB.

Task 6D. Task 6D is similar to Task 6A, using the synthetic structural model and a 50 to 100 m scale TRUE-Block Scale tracer experiment. The flow and transport simulations will be carried out using both SC-type and PA-type models. The task will provide an improved understanding of how these approaches compare at in situ tracer test time and distance scales.

Task 6E. Task 6E extends the Task 6D transport calculations to a reference set of PA time scales and boundary conditions. In the first part of Task 6E, a basic set of PA and SC assumptions and simplifications should be used. These can be extended to alternative assumptions as part of the sensitivity study part of Task 6E.

Modelers are encouraged to apply different conceptual models of varying degrees of simplification. The possible range of simplifications could be from simple 1D uniform streamtubes to a 3D representation of the internal structure of the fracture, stagnant pools, in-plane heterogeneity of aperture distribution etc for Tasks 6A and 6B. However, it is noted that if a modeling group uses a PA model, they should also provide interim modeling assumptions and results to provide a platform for model comparison. For example, if a 1D PA model is going to be used, model assumptions (such as transmissivity, boundary conditions) and drawdown match of an interim model, e.g. a stochastic continuum flow model used for deriving streamlines, should be reported. For Task 6D and 6E, modeling groups are encouraged to apply various conceptual models which addresses network effects such as dilution, branching (dispersion at fracture intersections) or flow/transport along FIZs (fracture intersection zone).

4 CONCLUSIONS

During HY-12, Golder major accomplishments in support of JNC/Tokai including the following:

- ?? Feasibility demonstration for Laplace Transform Galerkin transport in fracture network (DFN) models using triangular elements;
- ?? Evaluation of sorbing solute transport parameters and processes for transport in as single fracture, within the context of the sp Task Force on Modeling; and
- ?? Assistance in Development of sp Task 6, performance assessment modeling using site characterization data (PASC).

5 REFERENCES

de Hoog, F.R., Knight, J.H. and Stokes, A.N., 1982. An improved method for numerical inversion of Laplace transforms, SIAM J. Sci. Stat. Comput., 3(3), 357-366.

Sudicky, E.A. and McLaren, R.G., 1992. The Laplace transform Galerkin technique for large-scale simulation of mass transport in discretely fractured porous formations, Water Resour. Res., 28(2), 499-514.

Sudicky, E.A., 1990. The Laplace transform Galerkin technique for efficient time-continuous solution of solute transport in double-porosity media, Geoderma, 46, 209-232.

Sudicky, E.A., 1989. The Laplace transform Galerkin technique: A time-continuous finite element theory and application to mass transport in groundwater. Water Resour. Res., 25(8) ,1833-1846.

VanderKwaak, J.E., Forsyth, P.A., MacQuarrie, K.T.B. and Sudicky, E.A., 1997. WatSolv: Sparse Matrix Iterative Solver, User s Guide for Version 2.16, Groundwater Simulations Group, Waterloo, Ontario, Canada.

APPENDIX A

COMPARISON OF LTG TRANSPORT IN PIPE (CN) AND PLATE (DFN) FRACTURE NETWORKS

Comparison of LTG Transport in Pipe (CN) and Plate (DFN) Fracture Network

Version 0.2

Prepared for JNC, Tokai Japan

Dawn Shuttle
Glori Lee

TABLE OF CONTENTS Page No.

1. INTRODUCTION 1

2. 1D VERIFICATION CASES 2

2.1 LTG_T1 Single-porosity Case: Transport of a Nonreactive Solute 2
2.2 LTG_T2: Single-porosity Case: Transport of a Nonreactive Solute 4
2.3 LTG_T3: Transport of Tritium in a System of Parallel Fractures 5
2.4 LTG_T4: Decay Chain Transport in Parallel Fractures spaced at 10m 7

3. GRID VERIFICATION CASES 10

3.1 LTG_GT1 – Grid Advective Flow 11
3.2 LTG_GT2 –Grid Surface Sorption and Advective Flow 15
3.3 LTG_GT3 –Grid Matrix Diffusion and Advective Flow 17
3.4 LTG_GT4 –Grid Advection-Diffusion, Matrix Diffusion and Decay Chain 18

4. PERFORMANCE MEASURES 20

5. REFERENCES 21

LIST OF TABLES Page No.

Table 2-1 Ogata-Banks Analytic Results for Verification Test LTG_T1 2
Table 2-2 LTG Results for Verification Test LTG_T1 3
Table 2-3 Analytic Results for Verification Test LTG_T3 5
Table 2-4 LTG Results for Verification Test LTG_T3 6
Table 2-5 Analytic Solution for Verification Test LTG_T4 8
Table 2-6 LTG Solution for Verification Test LTG_T4 8
Table 3-1 Flow Solution Properties for Pipe Elements in LTG_GT1 12
Table 3-2 Release Rates for Dispersion Length of 1.0 m 15
Table 3-3 Release Rates for Dispersion Length of 2.0 m 15
Table 3-4 Release Rates for Dispersion Length of 5.0 m 15
Table 3-5 Release Rates for Advection, Dispersion and Surface Sorption 16
Table 3-6 Release Rates for Advection, Dispersion and Matrix Diffusion 17
Table 3-7 Release Rates for Advection, Dispersion, Matrix Diffusion and Decay 19
Table 4-1 Memory requirement and speed for 1-D verification cases 20
Table 4-2 Memory requirement and speed for Grid verification cases 20

LIST OF FIGURES Page No.

Figure 2-1 LTG and Ogata-Banks Comparison for Verification Test LTG_T1 3
Figure 2-2 LTG and Ogata-Banks Comparison for Verification Test LTG_T2 4
Figure 2-3 Tritium Transport for Verification Test LTG_T3 6
Figure 2-4 Tritium Transport for Verification Test LTG_T3 (log scale) 7
Figure 2-5 Decay Chain Transport for Verification Test LTG_T4 9
Figure 3-1 Fracture Network for LTG_GT Verification Cases 10
Figure 3-2 Transmissivity of Fractures for LTG_GT Cases 10
Figure 3-3 Pipe Numbering for LTG_GT1 11
Figure 3-4 Comparison of Mass Release Rate for Dispersion Length of 1.0 m 13
Figure 3-5 Comparison of Mass Release Rate for Dispersion Length of 2.0 m 14
Figure 3-6 Comparison of Mass Release Rate for Dispersion Length of 5.0 m 14
Figure 3-7 Comparison of Mass Release Rate for Advection and Surface Sorption 16
Figure 3-8 Comparison of Mass Release Rate for Advection and Matrix Diffusion 17
Figure 3-9 Comparison of Mass Release Rate for Advection, Matrix Diffusion and Decay 18

1. INTRODUCTION

A new version of LTG, LTG V3.0, was developed during HY-12. The previous version of LTG, LTG V2.00, used pipe elements to model the discrete fracture network. The extended code, LTG V3.0, has the capabilities of the original code, plus it is also able to represent the discrete fracture network using triangular plate elements. In this document, only the capabilities of the code relating to plate triangular elements are considered.

The input parameters for plate triangular elements are read from two files: the FracMan restart.maf format file, and a new format input file with extension .rdt.

The original pipe LTG read the pipes from the user-generated input file called LTG.DAT, or PAWorks generated the input files for full FracMan DFN networks. Although not discussed in this report, LTG V3.0 continues to read input files for pipe elements, using minor modifications from the original file formats.

Sections 2 and 3 of the report are dedicated to verification cases for the triangular element option in LTG. The tests fall into two distinct categories: comparison with analytical solutions and cross-verification with published results for LTG pipe elements. The cross-verification allows a greater range of features to be tested, as analytical solution to problems incorporating diffusion and retardation in both the flowing fracture and immobile zones are rare.

Section 4 discusses the relative performance of LTG for triangular plates and pipe elements.

2. 1D VERIFICATION CASES

The four 1-D test problems described in the following sections are designed to check that LTG correctly solves the governing equations using triangular plate elements.

The verification problems involve transport along a one-dimensional flow path. The simulations have been set up by constructing the restart.maf file explicitly, unless otherwise stated. This allows the LTG solver to be tested for uniform mesh construction prior to investigating the effect of the finite element mesh on the accuracy of the solution. The test problems were designed to test a hierarchy of transport processes represented in LTG, and range in complexity from strictly one-dimensional advective-dispersive transport of a single, nonreactive solute, to cross verification of the migration of a three-member decay chain with the pipe LTG solute solution.

The user may rerun the following verifications using the defined input parameters. For all problems the analytic solutions are documented in the associated tables.

2.1 LTG_T1 Single-porosity Case: Transport of a Nonreactive Solute

2.1.1 Definition

In this test the following component of LTG is tested:

- LTG advective dispersion algorithm

This problem consists of the transport of a single nonreactive solute (retardation R = 1.0, decay constant λ = 0.0) by advection and dispersion in a single-porosity domain. The input Darcy flux, q, is 1.0 m/day, the flowing cross-sectional area of the fracture, A, equals 1 m^2, and the longitudinal dispersivity, α, is 1.0 m. Diffusion along the flow direction is neglected for simplicity. The domain is 100m in length and the spatial discretization is 1.0 m in the flow direction giving a Peclet number of 1.0.

A Dirichlet boundary condition equal to 1.0 Ci/m^3 was specified at the inflow.

2.1.2 Criteria

A subset of the well known Ogata-Banks analytic results are presented in Table 2-1.

Table 2-1 Ogata-Banks Analytic Results for Verification Test LTG_T1

Distance along Fracture (m)	**Conc. (Ci/m^3) 25 days**	**Conc. (Ci/m^3) 50 days**	**Conc. (Ci/m^3) 75 days**
20	0.8079	0.9993	1.0000
40	0.0215	0.8679	0.9986
60	0.0000	0.1805	0.9066
80	0.0000	0.0017	0.3704

2.1.3 Results

A subset of LTG results is presented in Table 2-2. The match is excellent with the criteria above.

Table 2-2 LTG Results for Verification Test LTG_T1

Distance along Fracture (m)	Conc. (Ci/m³) 25 days	Conc. (Ci/m³) 50 days	Conc. (Ci/m³) 75 days
20	0.8076	0.9992	1.0000
40	0.0212	0.8676	0.9985
60	0.0000	0.1807	0.9064
80	0.0000	0.0016	0.3705

A log scale plot of LTG results is shown on Figure 2-1 for transport times equal to 25, 50, and 75 days. These results are compared to those obtained with the Ogata-Banks analytic solution.

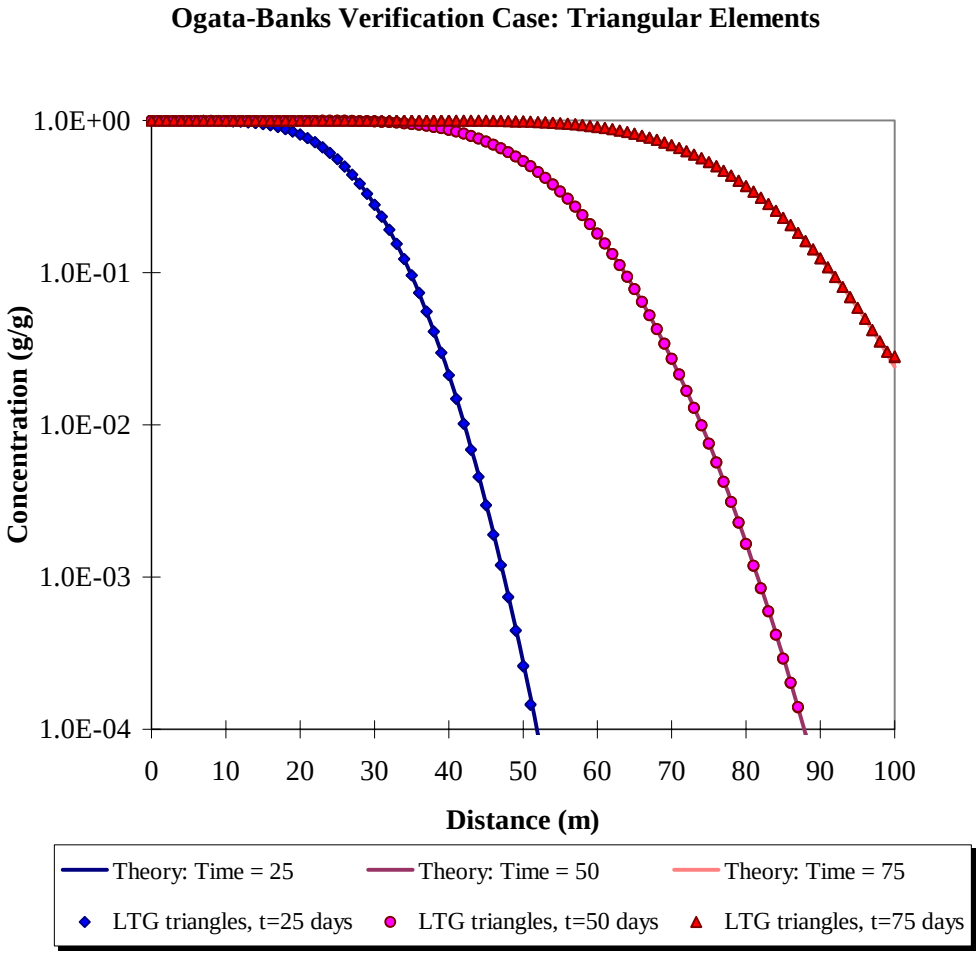

Figure 2-1 LTG and Ogata-Banks Comparison for Verification Test LTG_T1

2.2 LTG_T2: Single-porosity Case: Transport of a Nonreactive Solute

2.2.1 Definition

In this test the following components of LTG are tested:

- LTG advective dispersion algorithm
- Sensitivity of results to finite element mesh generation

This problem is essentially identical to LTG_T1. It consists of the transport of a single nonreactive solute (retardation R = 1.0, decay constant λ = 0.0) by advection and dispersion in a single-porosity domain. The input Darcy flux, q, is 1.0 m/day, the aperture, e, is equal to 5 x 10^{-3} m, the fracture width, W, equals 200 m, and the longitudinal dispersivity, α, is 1.0 m. Diffusion along the flow direction is neglected for simplicity. The domain is 100m in length and the spatial discretization is 1.0 m in the flow direction giving a Peclet number of 1.0.

A Dirichlet boundary condition equal to 1.0 Ci/m^3 was specified at the inflow.

2.2.2 Criteria

A subset of the analytic results was presented in Table 2-1.

2.2.3 Results

A plot of LTG results are shown in Figure 2-2 on a log scale for transport times equal to 25, 50, and 75 days. The results are compared to those obtained with the Ogata-Banks analytic solution.

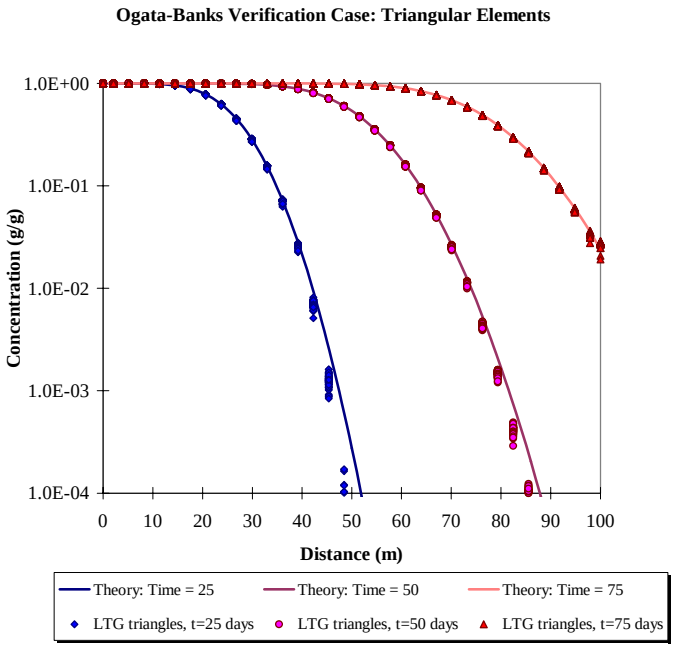

Figure 2-2 LTG and Ogata-Banks Comparison for Verification Test LTG_T2

2.3 LTG_T3: Transport of Tritium in a System of Parallel Fractures

2.3.1 Definition

In this test the following components of LTG are tested:

- LTG advective dispersion algorithm
- LTG diffusion into matrix immobile zones
- LTG radioactive decay

This problem models the transport of a decaying, non-sorbing (i.e., $R = 1.0$) solute in a double-porosity system comprised of parallel fractures embedded in low-permeability, low-porosity rock matrix. The solute is tritium which has a half-life of 12.35 years ($\lambda = 1.54 \times 10^{-4}$ days^{-1}). The flow system is 300 m in length and the aperture of the parallel fractures, spaced at 0.1 m, is 100 μm. With this setting, the flowing cross-sectional area of the fracture, A, is equal to 10^{-4} m^2. The Darcy flux, q, is 0.1 m/day in the fractures and the longitudinal dispersivity of the fractures, α_L, is 0.1 m. The free-solution diffusion coefficient for tritium, D^o, equals 1.38×10^{-4} m^2/day. The matrix porosity, θ_m, and tortuosity, τ, are 0.01 and 0.1, respectively. A maximum diffusion distance, d, equal to the half-spacing of the fractures (0.05 m) was used. The mesh spacing used is 10.0 m which yields a grid Pe number equal to about 100. The concentration was fixed at 1.0 at the inlet boundary.

2.3.2 Criteria

Table 2-3 presents the analytical solution of Sudicky and Frind (1982) at times 1,000 days, 10,000 days, and 100,000 days (equal to steady state) at intervals along the fracture pathway.

Table 2-3 Analytic Results for Verification Test LTG_T3

Distance along Fracture (m)	**Rel. Conc. 1,000 days**	**Rel. Conc. 10,000 days**	**Rel. Conc. 100,000 days**
10	0.3894	0.8465	0.8445
50	0.0000	0.4332	0.4305
100	0.0000	0.0494	0.1865
150	0.0000	0.0000	0.0808
200	0.0000	0.0000	0.0351

2.3.3 Results

Table 2-4 presents the LTG solution at times 1,000 days, 10,000 days, and steady state at intervals along the fracture pathway. The results at the two nodes at the same Y distance along the fracture are not always identical. Therefore the X=0.0 result is quoted.

Table 2-4 LTG Results for Verification Test LTG_T3

Distance along Fracture (m)	Rel. Conc. 1,000 days	Rel. Conc. 10,000 days	Rel. Conc. steady state
10	0.3890	0.8450	0.8461
50	0.0000	0.4318	0.4318
100	0.0000	0.0488	0.1868
150	0.0000	0.0000	0.0808
200	0.0000	0.0000	0.0349

Figure 2-3 compares example LTG results with those obtained with the analytic solution of Sudicky and Frind (1982) at times equal to 1,000 days, 10,000 days and at steady-state. The same results plotted with a log scale for the concentration are shown on Figure 2-4. The figures indicate good agreement between the LTG and analytic solutions.

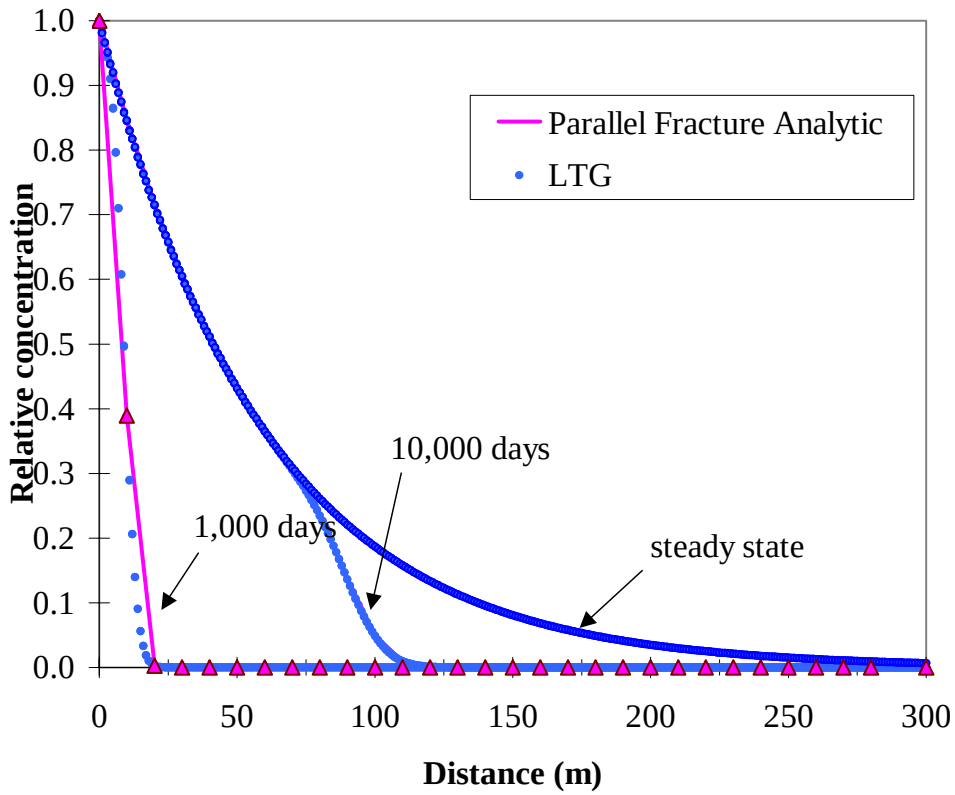

Figure 2-3 Tritium Transport for Verification Test LTG_T3

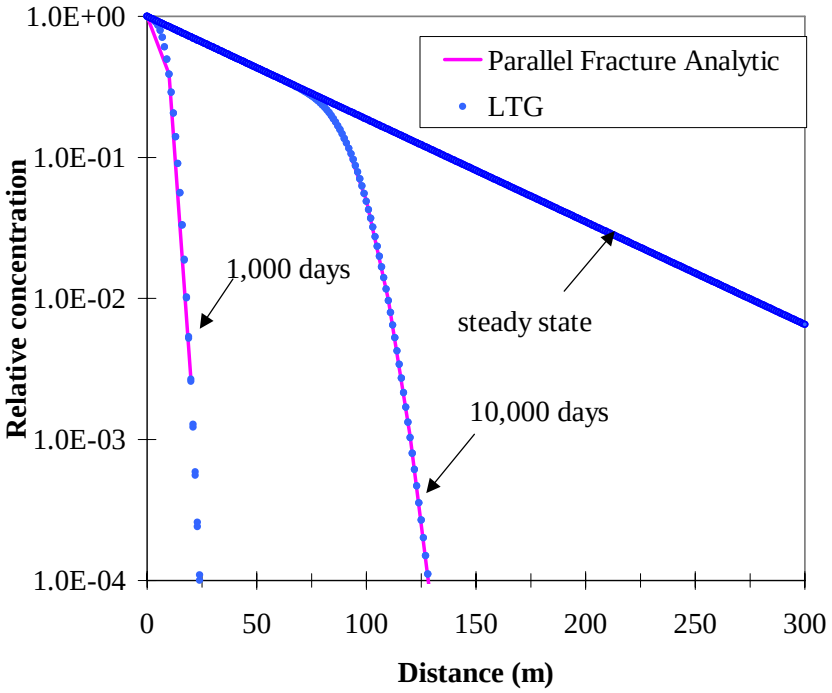

Figure 2-4 Tritium Transport for Verification Test LTG_T3 (log scale)

2.4 LTG_T4: Decay Chain Transport in Parallel Fractures spaced at 10m

2.4.1 Definition

In this test the following components of PAWorks are tested:

- decay chain transport for large diffusion distances

The final analytic comparison involves the transport of the decay chain Uranium 234 → Thorium 230 → Radium 226 in a system of parallel fractures and is designed to verify an accurate solution is obtained for large maximum diffusion distances.

For this example the Darcy flux, q, in the fractures is 100 m/year and the longitudinal dispersivity of the fractures, α, is 10.0 m. The flow system is 500 m in length, with a maximum diffusion distance of 5m. The fracture aperture is 10^{-4} m, and the matrix porosity is 0.01. The matrix rock density was 2500 km/m^3. The partition coefficients (Kd values) for chain Uranium 234, Thorium 230, and Radium 226 are 0.057196, 0.2 and 0.002 respectively. These parameters result in matrix (i.e., immobile zone) retardation factors for U^{234}, Th^{230} and Ra^{226} equal to 1.43×10^4, 5.00×10^4 and 5.00×10^2.

The decay constants were equal 2.83×10^{-6}, 9.00×10^{-6} and 4.33×10^{-6} year^{-1}, respectively. For simplicity, retardation on the surfaces of the fractures was neglected. Tortuosity in the matrix was set to 0.1 and the diffusion

coefficients for each of the species, D^o, were assigned identical values equal to 3.154×10^{-2} m^2/year. A prescribed concentration of 1.0 mol/m^3 was assigned for U^{234} at the fracture inlet, but 0.0 mol/m^3 was used as the inlet concentration for Th^{230} and Ra^{226}.

2.4.2 Criteria

The analytic solution of Hodgkinson and Maul (1985) at a time equal to 100,000 years is given in Table 2-5.

Table 2-5 Analytic Solution for Verification Test LTG_T4

Distance	Concentration (mol/m^3)		
	U-234	Th-230	Ra-226
10	7.66E-01	1.21E-02	1.89E-02
50	2.17E-01	7.62E-03	4.15E-02
100	2.95E-02	8.85E-04	2.80E-02
200	1.66E-04	2.96E-06	8.07E-03
400	1.00E-10	0.00E+00	4.48E-04

2.4.3 Results

The LTG solution at a time equal to 100,000 years is given in Table 2-6.

Table 2-6 LTG Solution for Verification Test LTG_T4

Distance	Concentration (mol/m^3)		
	U-234	Th-230	Ra-226
10	7.64E-01	1.21E-02	1.88E-02
50	2.14E-01	7.53E-03	4.08E-02
100	2.89E-02	8.66E-04	2.71E-02
200	1.60E-04	2.85E-06	7.63E-03
400	1.27E-10	0.00E+00	4.22E-04

Figure 2-5 compares example LTG results to those obtained with the analytic solution of Hodgkinson and Maul (1985) at a time equal to 100,000 years. It can be seen from the results that LTG is capable of accurately representing the transport of a reactive decay chain in a double porosity-medium where the maximum diffusion distance is large.

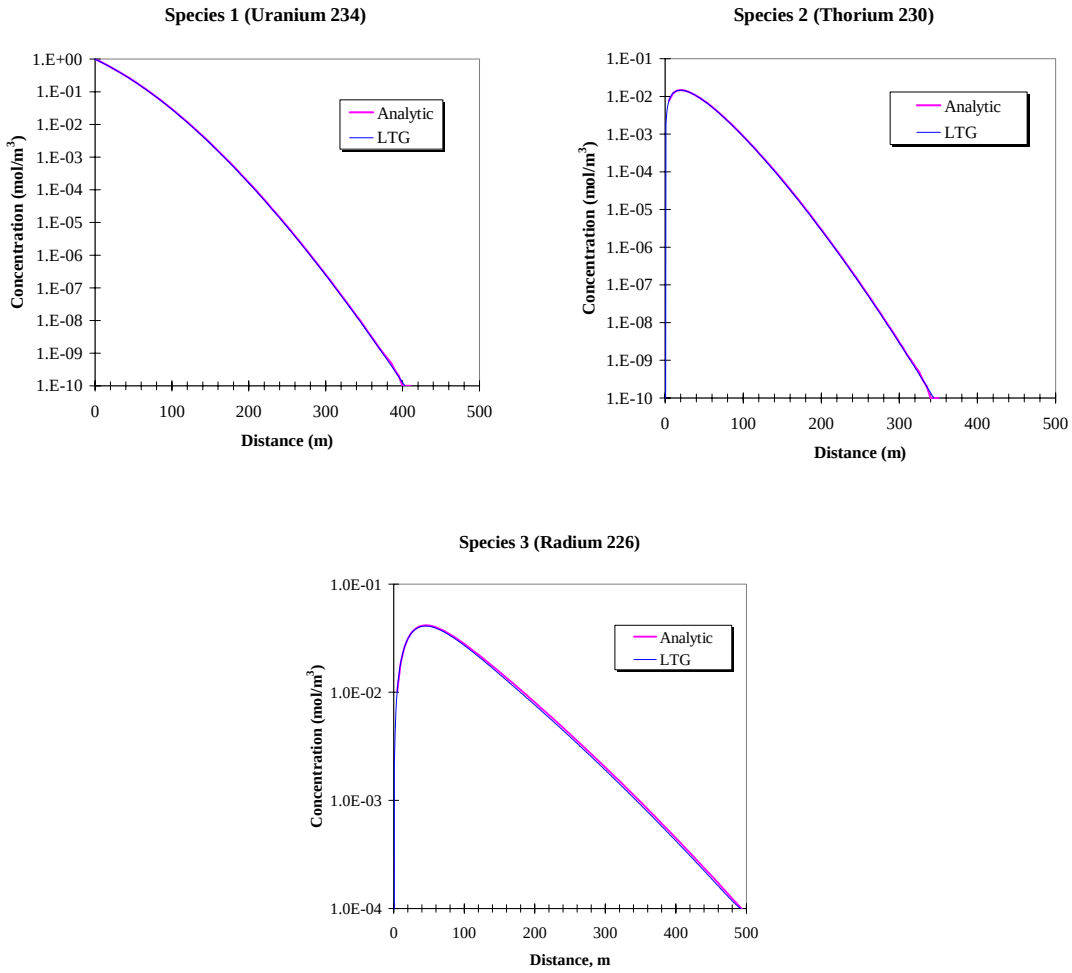

Figure 2-5 Decay Chain Transport for Verification Test LTG_T4

3. GRID VERIFICATION CASES

The three verification cases presented in this section are based on the H11 LTG verification cases. These cases use a simple grid of 8 fractures, arranged as shown in Figure 3-1.

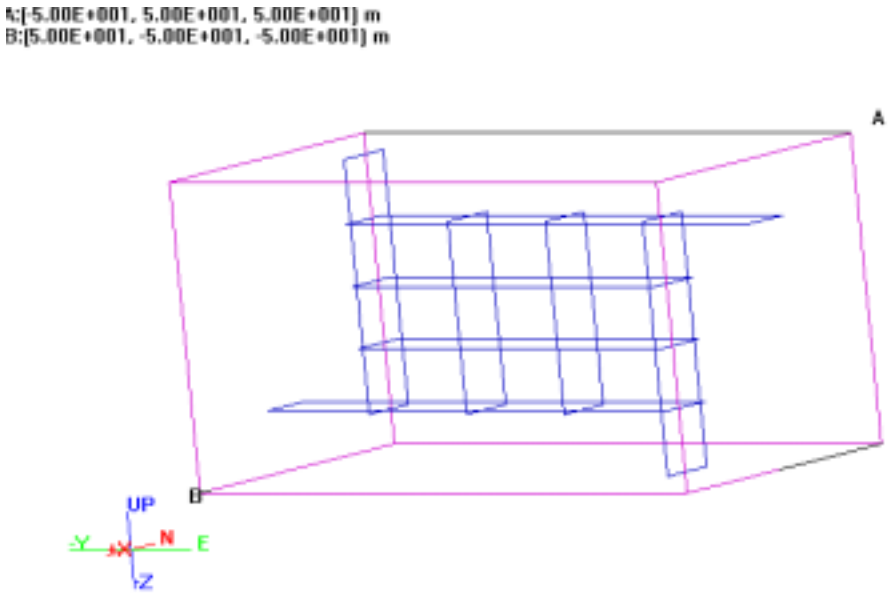

Figure 3-1 Fracture Network for LTG_GT Verification Cases

The width of all fractures in Figure 3-1 is 20 m. The transmissivity of the fractures is shown in Figure 3-2. Aperture is related to transmissivity by the equation aperture = 2 $T^{0.5}$.

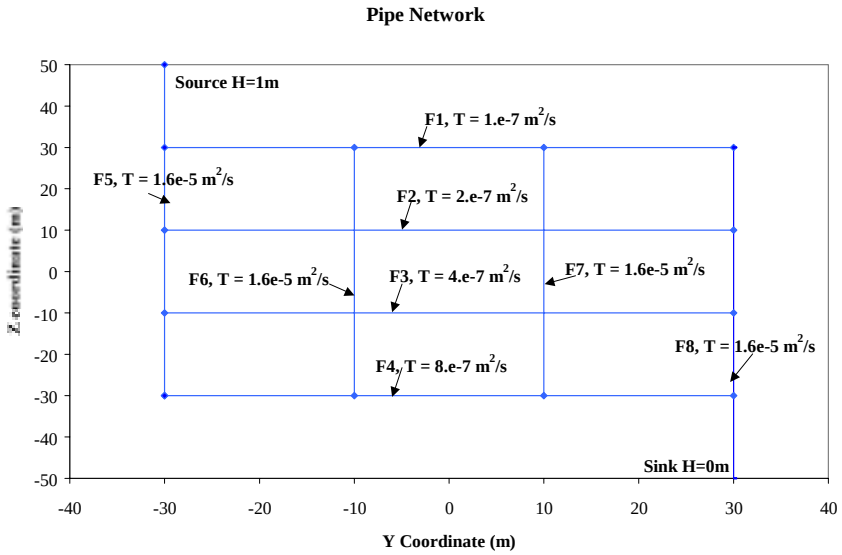

Figure 3-2 Transmissivity of Fractures for LTG_GT Cases

For consistency, the code version used to produce the pipe solutions for comparison with the triangular plate solution is also LTG V3.0.

3.1 LTG_GT1 – Grid Advective Flow

A simple purely advective network was used as the baseline problem.

A head flow boundary condition was used, with a head at the source of 1.0 m, and a sink head of 0.0 m. For these boundary conditions the velocity, flow area, and flow rate distribution for the pipe elements is presented in Table 3-1. The pipe numbers are shown in Figure 3-3.

The mass release boundary condition at the source is defined as a uniform release of 10g/yr for the first 10 years, then zero release for the remainder of the simulation.

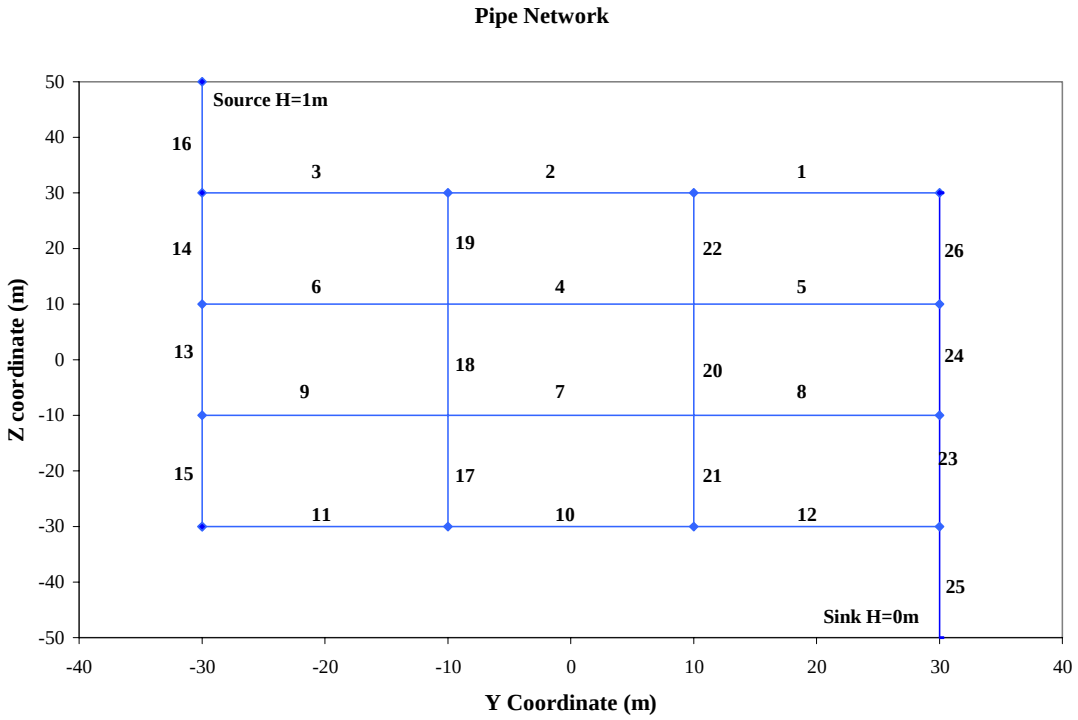

Figure 3-3 Pipe Numbering for LTG_GT1

Table 3-1 Flow Solution Properties for Pipe Elements in LTG_GT1

pipe	velocity (m/yr)	area (m^2)	Flow (m^3/yr)	Travel Time (yr)
1	7.40E+01	1.27E-02	0.9367	2.70E-01
2	7.08E+01	1.27E-02	0.8962	2.82E-01
3	8.58E+01	1.27E-02	1.0854	2.33E-01
4	1.05E+02	1.79E-02	1.8720	1.91E-01
5	1.01E+02	1.79E-02	1.8030	1.98E-01
6	1.12E+02	1.79E-02	2.0109	1.78E-01
7	1.48E+02	2.53E-02	3.7395	1.35E-01
8	1.45E+02	2.53E-02	3.6708	1.38E-01
9	1.48E+02	2.53E-02	3.7560	1.35E-01
10	2.00E+02	3.58E-02	7.1687	9.98E-02
11	2.09E+02	3.58E-02	7.4728	9.58E-02
12	2.14E+02	3.58E-02	7.6511	9.35E-02
13	6.83E+01	1.60E-01	10.9245	2.93E-01
14	8.08E+01	1.60E-01	12.9356	2.47E-01
15	4.48E+01	1.60E-01	7.1689	4.46E-01
16	8.76E+01	1.60E-01	14.0212	2.28E-01
17	1.80E+00	1.60E-01	0.2878	1.11E+01
18	9.28E-01	1.60E-01	0.1485	2.16E+01
19	1.90E+00	1.60E-01	0.3040	1.05E+01
20	6.82E-01	1.60E-01	0.1091	2.93E+01
21	2.56E-01	1.60E-01	0.0409	7.82E+01
22	1.12E+00	1.60E-01	0.1787	1.79E+01
23	3.98E+01	1.60E-01	6.3699	5.02E-01
24	1.69E+01	1.60E-01	2.6992	1.19E+00
25	8.76E+01	1.60E-01	14.0210	2.28E-01
26	5.60E+00	1.60E-01	0.8962	3.57E+00

To indicate the effect of dispersion on the fit between the LTG pipe and plate solutions, three different longitudinal dispersion length values were used; 1.0 m, 2.0 m, and 5.0 m. The transverse dispersion length was set at nominal small value of 0.1m for all cases.

A comparison of the results for these three cases is presented graphically in Figure 3-4 to Figure 3-6. A summary of the results is given in Table 3-2 to Table 3-4 for dispersion lengths of 1.0 m, 2.0 m and 5.0 m respectively.

The results show that for the smallest dispersion length of 1.0 m the maximum difference between the pipe and plate idealisation is approximately 1.7%. This difference increases to 11% for a dispersion length of 5.0m. However, at the peak release rates, occurring at times between approximately 3 an 12 years elapsed time, the error is typically less than 0.5%.

The only erroneous result occurs for the pipe elements and a dispersion length of 5.0m. At a time of approximately 4 years the results are not smooth close to T_{max} (the time used for the Laplace inversion).

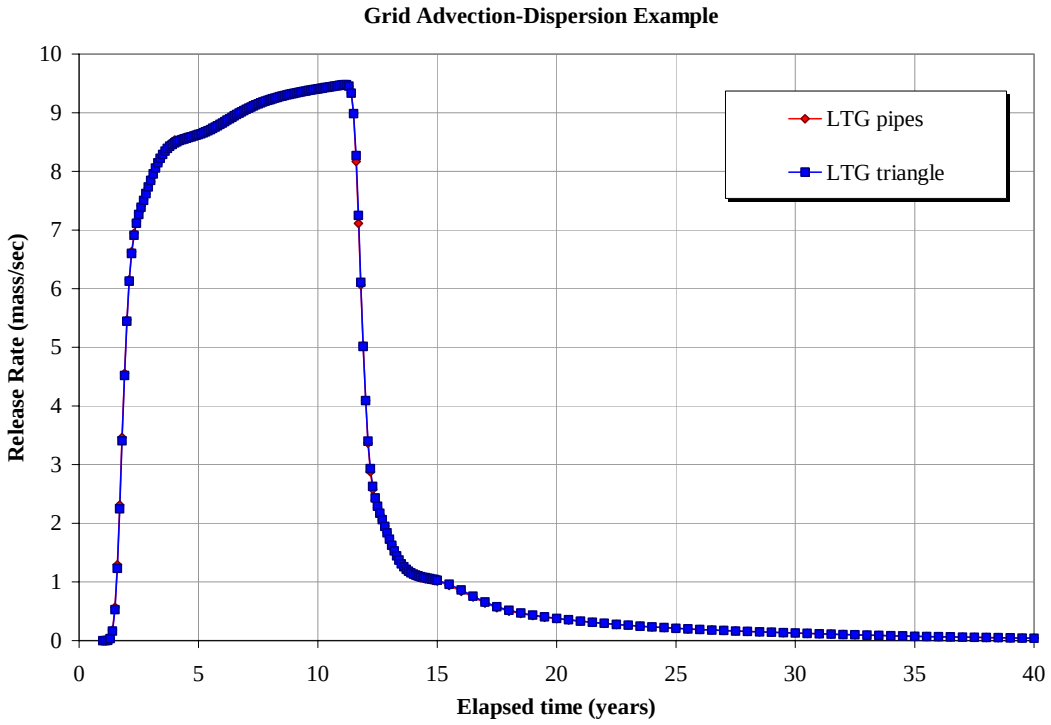

Figure 3-4 Comparison of Mass Release Rate for Dispersion Length of 1.0 m

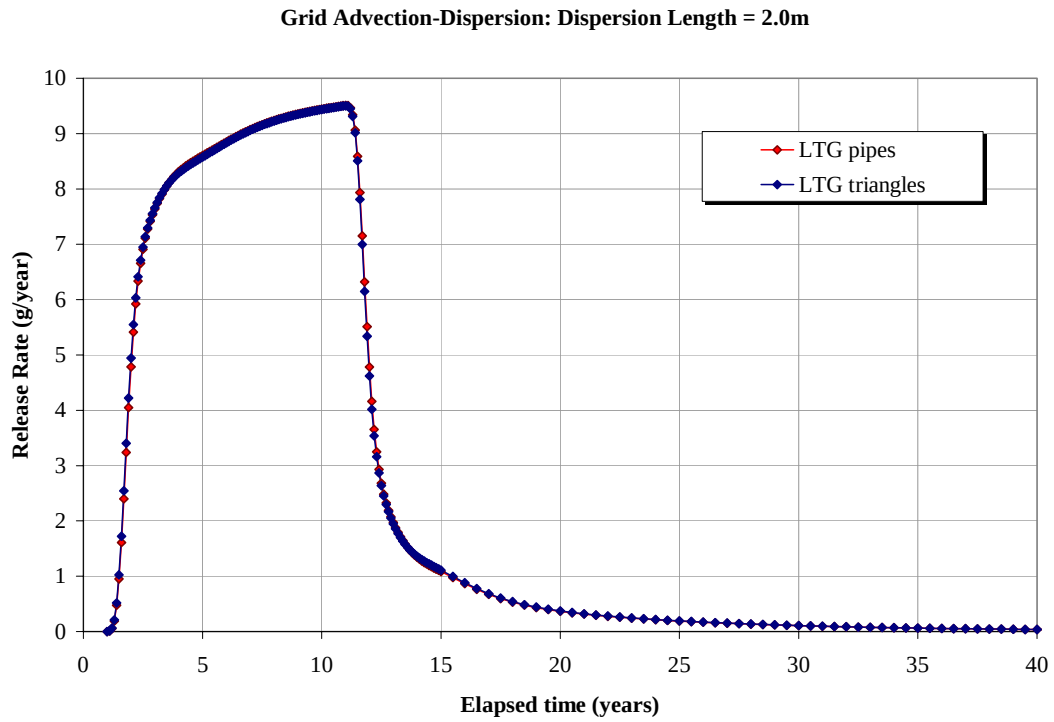

Figure 3-5 Comparison of Mass Release Rate for Dispersion Length of 2.0 m

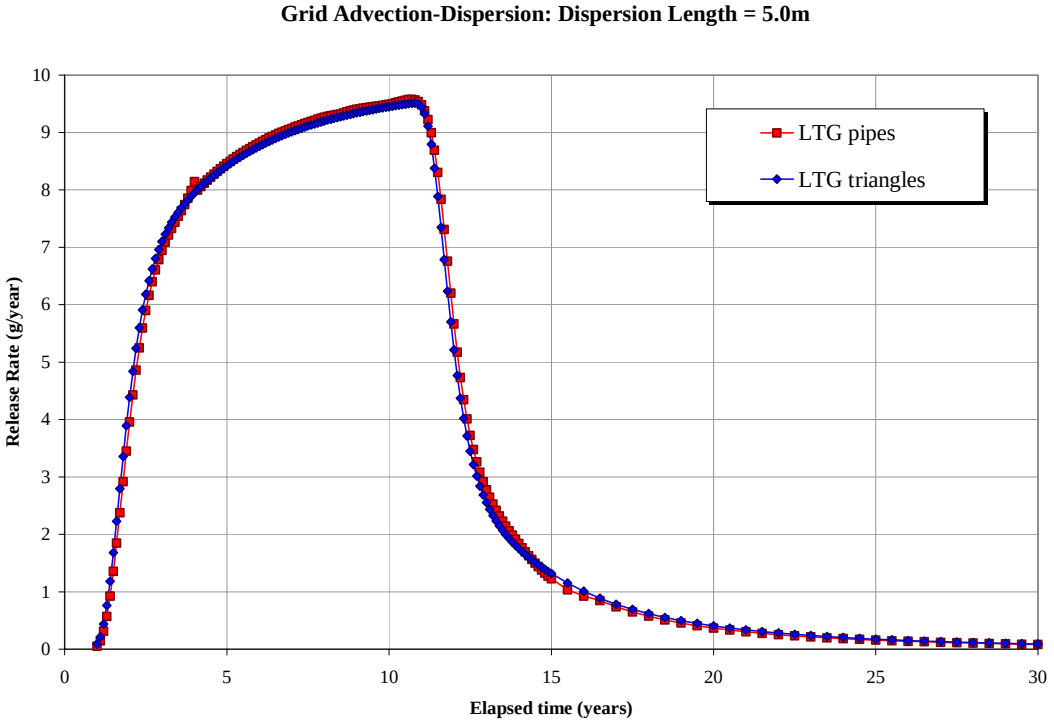

Figure 3-6 Comparison of Mass Release Rate for Dispersion Length of 5.0 m

Table 3-2 Release Rates for Dispersion Length of 1.0 m

Elapsed Time (years)	Release Rate (g/year)		
	LTG pipe	LTG triangle	Difference (%)
2	5.47E+00	5.44E+00	0.42
5	8.64E+00	8.63E+00	0.17
7	9.08E+00	9.06E+00	0.20
10	9.41E+00	9.41E+00	0.03
15	1.01E+00	1.03E+00	-1.67
20	3.75E-01	3.78E-01	-1.02

Table 3-3 Release Rates for Dispersion Length of 2.0 m

Elapsed Time (years)	Release Rate (g/year)		
	LTG pipe	LTG triangle	Difference (%)
2	4.78E+00	4.94E+00	-3.36
5	8.60E+00	8.57E+00	0.35
7	9.07E+00	9.06E+00	0.15
10	9.44E+00	9.44E+00	0.09
15	1.08E+00	1.11E+00	-2.47
20	3.66E-01	3.74E-01	-2.04

Table 3-4 Release Rates for Dispersion Length of 5.0 m

Elapsed Time (years)	Release Rate (g/year)		
	LTG pipe	LTG triangle	Difference (%)
2	3.96E+00	4.39E+00	-10.89
5	8.45E+00	8.42E+00	0.42
7	9.07E+00	9.01E+00	0.65
10	9.49E+00	9.45E+00	0.44
15	1.22E+00	1.32E+00	-7.45
20	3.67E-01	4.05E-01	-10.30

3.2 LTG_GT2 –Grid Surface Sorption and Advective Flow

This verification case is an extension of LTG_GT1. The grid geometry and material properties are essentially the properties used in LTG_GT1 for a longitudinal dispersion length of 1.0m but in this verification case surface sorption has been added.

The surface sorption is defined by a Ka of 0.01m for all fractures for the triangular plate elements. In PAWorks/LTG the conversion from Kd to Ka is given by:

Ka = Kd * rock density * infill thickness

Therefore to define the properties for the pipe elements a Kd of 0.004 m^3/kg, a rock density of 2500 kg/m^3 and an infill thickness of 1mm was used.

The resulting mass release rate for both triangular plates and pipes is shown graphically in Figure 3-7. A summary of the results is given in Table 3-5. The results show a very good match between the pipe and plate elements.

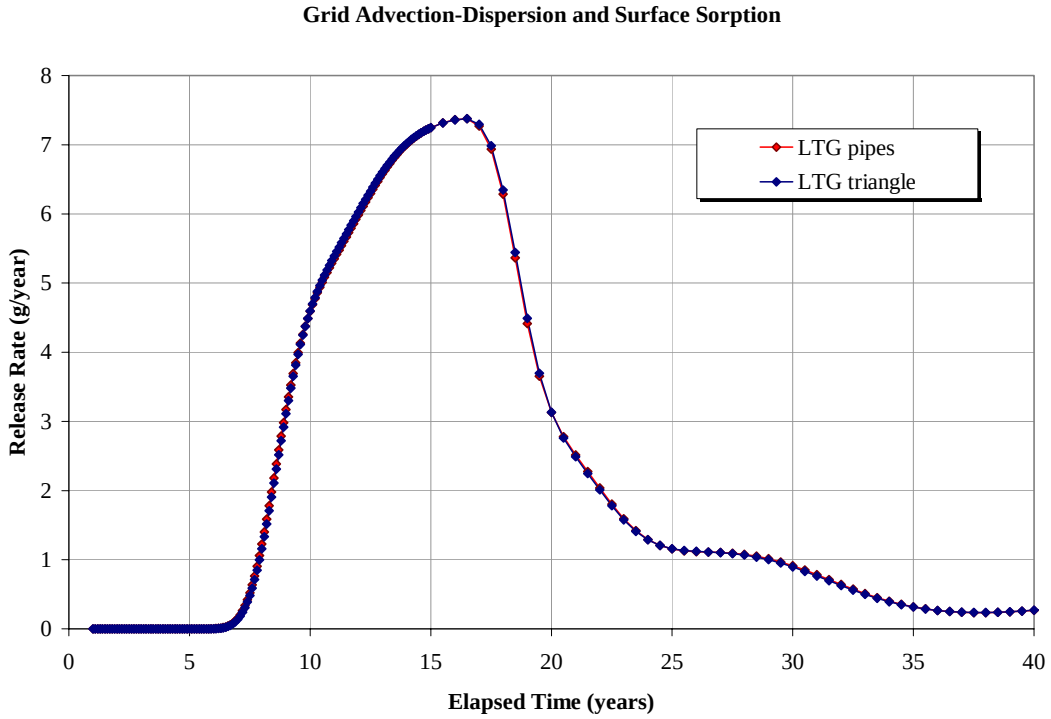

Figure 3-7 Comparison of Mass Release Rate for Advection and Surface Sorption

Table 3-5 Release Rates for Advection, Dispersion and Surface Sorption

Elapsed Time (years)	Release Rate (g/year)		
	LTG pipe	LTG triangle	Difference (%)
10	4.59E+00	4.597E+00	-0.13
15	7.25E+00	7.248E+00	0.00
20	3.13E+00	3.133E+00	-0.12
25	1.16E+00	1.157E+00	-0.12
30	9.13E-01	8.952E-01	1.93
35	3.19E-01	3.155E-01	0.99

3.3 LTG_GT3 –Grid Matrix Diffusion and Advective Flow

This verification case is also an extension of LTG_GT1. The grid geometry and advective-dispersive flow properties are the same as used in LTG_GT1 with a longitudinal dispersion length of 1.0m. In addition matrix diffusion has been added. Matrix diffusion is defined by the following material properties: a Kd of 0.001 m^3/kg, a rock density of 2500 kg/m^3 and a matrix porosity of 0.1.

The resulting mass release rate for both triangular plates and pipes is shown graphically in Figure 3-8. A summary of the results is given in Table 3-6. The results show a reasonable match between the pipe and plate elements, although the release for the triangular elements is slightly lower.

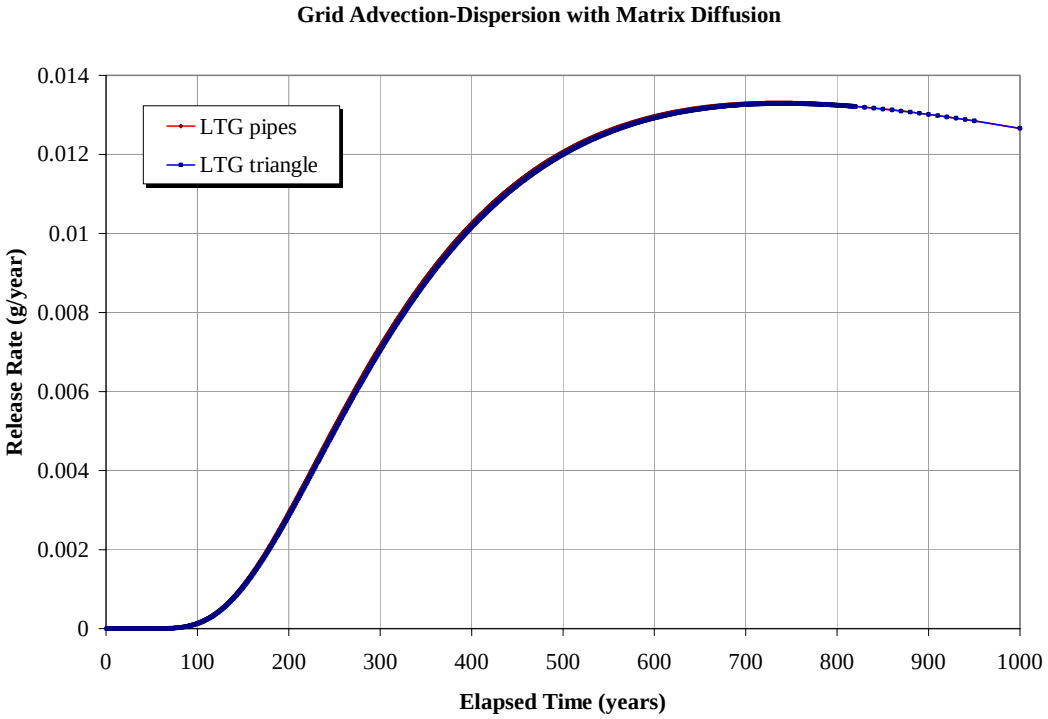

Figure 3-8 Comparison of Mass Release Rate for Advection and Matrix Diffusion

Table 3-6 Release Rates for Advection, Dispersion and Matrix Diffusion

Elapsed Time (years)	Release Rate (g/year)		
	LTG pipe	LTG triangle	Difference (%)
200	2.94E-03	2.85E-03	3.10
400	1.03E-02	1.02E-02	0.96
600	1.30E-02	1.29E-02	0.32

Elapsed Time (years)	Release Rate (g/year)		
	LTG pipe	LTG triangle	Difference (%)
800	1.33E-02	1.32E-02	0.07
1000	1.27E-02	1.27E-02	-0.04

3.4 LTG_GT4 –Grid Advection-Diffusion, Matrix Diffusion and Decay Chain

The final grid verification case is case LTG_GT3 with nuclide decay included. The decay rate used is 1×10^{-10} 1/s, equivalent to 3.15576×10^{-3} 1/yr.

The resulting mass release rate for both triangular plates and pipes is shown graphically in Figure 3-9. A summary of the results is given in Table 3-7. Again the results show a reasonable match between the pipe and plate elements, but with the triangular elements showing lower releases at all times. The difference between the results being typically below 4%.

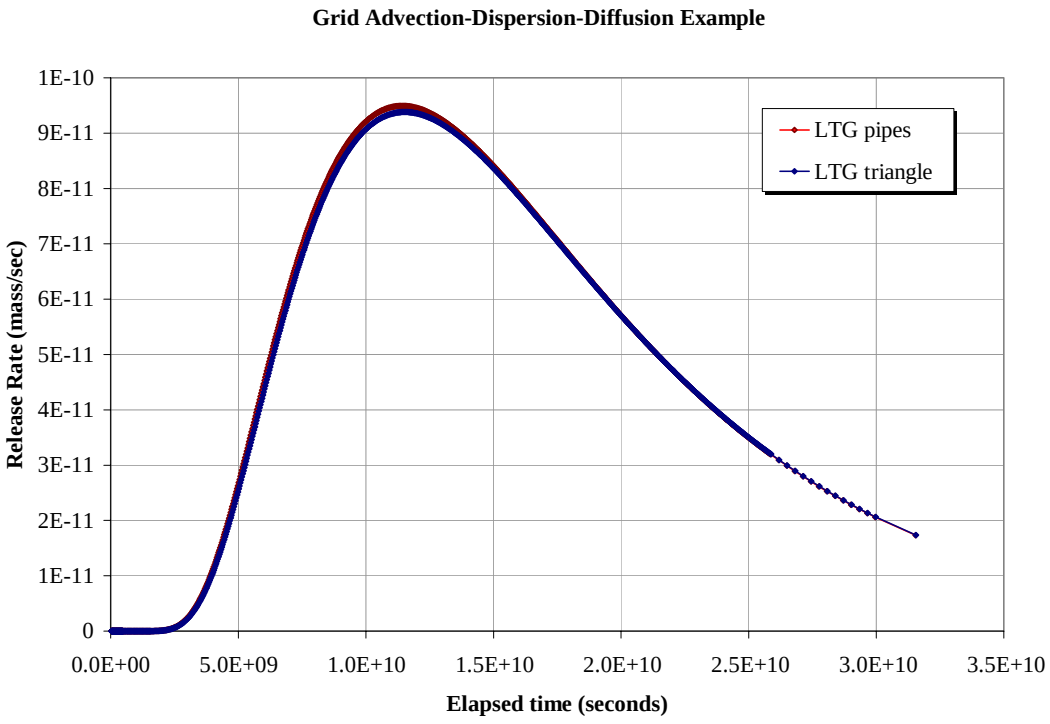

Figure 3-9 Comparison of Mass Release Rate for Advection, Matrix Diffusion and Decay

Table 3-7 Release Rates for Advection, Dispersion, Matrix Diffusion and Decay

Elapsed Time (years)	Release Rate (g/year)		
	LTG pipe	LTG triangle	Difference (%)
200	1.590E-03	1.54E-03	3.06
400	2.946E-03	2.92E-03	0.88
600	1.981E-03	1.98E-03	0.20
800	1.077E-03	1.08E-03	-0.09
1000	5.468E-04	5.48E-04	-0.24

4. PERFORMANCE MEASURES

The relative performance for LTG V3.0 pipes versus triangular elements is reported in this section. Performance is measured in two, inter-related ways: the speed of computation and the accuracy of the solution.

The verification cases are typically small and will not give a good representation of the speed and memory requirement of pipes versus triangular plates. However, for completeness this information is given in Table 4-1.

Table 4-1 Memory requirement and speed for 1-D verification cases

Verification Case	Memory (kB)		CPU (seconds)[1]	
	Triangular	Pipes	Triangular	Pipes
LTG_T1	296	43	0.17	0.05
LTG_T2	3796	43	4.71	0.05
LTG_T3	1205	84	4.96	0.69
LTG_T4	202	7	8.39	0.57

[1]Measured on a Pentium 600

In addition, one mesh geometry has been considered; the grid geometry used for verification cases LTG_TG1 to LTG_TG3. The memory requirements are summarized in Table 4-2.

Table 4-2 Memory requirement and speed for Grid verification cases

Verification Case	Memory (kB)		CPU (seconds)[1]	
	Triangular	Pipes	Triangular	Pipes
LTG_TG1, D_L=1.0m	829	12	130.76	2.16
LTG_TG1, D_L=2.0m	829	12	164.01	1.75
LTG_TG1, D_L=5.0m	829	12	236.21	1.47
LTG_TG2	829	12	116.37	2.48
LTG_TG3	829	12	92.60	1.89
LTG_TG4	829	12	86.29	1.87

[1]Measured on a Pentium 600

5. REFERENCES

Barten, W. (1996) PICNIC-I test cases: Fracture Case, Paul Scherrer Institut

de Hoog, F.R., Knight, J.H. and Stokes, A.N., 1982. An improved method for numerical inversion of Laplace transforms, SIAM J. Sci. Stat. Comput., 3(3), 357-366.

Dershowitz, W., G. Lee, J. Geier, T. Foxford, P. LaPointe, and A. Thomas, 1995. FracMan Interactive Discrete Fracture Data Analysis, Geometric Modeling, and Exploration Simulation. User Documentation. Version 2.5. Golder Associates Inc, Seattle.

Grobner & Hofreiter (1949,1950) W. Grobner & N. Hofreiter, "Integraltafel", Springer, Vienna, Vol.1, 1949, Vol.2 1950.

Hodgkinson, D.P. and Maul, P.R., 1985. Harwell Laboratory of the United Kingdom Atomic Energy Authority report “One-dimensional modeling of radionuclide migration through permeable and fractured rock for arbitrary length decay chains using numerical inversion of Laplace transforms”, September, 1985.

Dershowitz, W., T. Foxford, E. Sudicky, D.A. Shuttle, and Th. Eiben, 1998. PAWorks Pathway Analysis for Discrete Fracture Networks with LTG Solute Transport. User Documentation, Version 1.5. Golder Associates Inc, Seattle.

Miller, I, G. Lee, W. Dershowitz, and G. Sharp, 1994. MAFIC Matrix/Fracture Interaction Code with Solute Transport. User Documentation, Version 1.5. Golder Associates Inc. Report 923-1089. Golder Associates Inc, Seattle.

Ogata, A. & R.B. Banks (1961) "A solution of the differential equation of longitudinal dispersion in porous media". U.S. Geol. Survey, Professional Paper 411-A.

Sudicky, E.A. and McLaren, R.G., 1992. The Laplace transform Galerkin technique for large-scale simulation of mass transport in discretely fractured porous formations, Water Resour. Res., 28(2), 499-514.

Sudicky, E.A., 1990. The Laplace transform Galerkin technique for efficient time-continuous solution of solute transport in double-porosity media, Geoderma, 46, 209-232.

Sudicky, E.A., 1989. The Laplace transform Galerkin technique: A time-continuous finite element theory and application to mass transport in groundwater. Water Resour. Res., 25(8) ,1833-1846.

Sudicky, E.A. and Frind, E.O., 1982. Contaminant transport in fractured porous media: Analytical solutions for a system of parallel fractures. Water Resour. Res., 18(3), 1634-1642.

van der Vorst, H., 1992. Bi-CGSTAB: A fast and smoothly converging variant of Bi-CG for the solution of nonsymmetric linear systems, SIAM J. Sci. Stat. Comput., 13, 631-644.

VanderKwaak, J.E., Forsyth, P.A., MacQuarrie, K.T.B. and Sudicky, E.A., 1997. WatSolv: Sparse Matrix Iterative Solver, User’s Guide for Version 2.16, Groundwater Simulations Group, Waterloo, Ontario, Canada.

APPENDIX B

SP TASK 4F2
CALIBRATION OF DFN TRANSPORT MODELING
AT THE 10 M SCALE

APPENDIX B

UNDERSTANDING OF SORBING TRACER TRANSPORT IN FRACTURE NETWORKS AT THE 10 METER SCALE

William S. Dershowitz[1]
Aaron Fox[1]
Masahiro Uchida[2]

[1]Golder Associates, Inc., Redmond, WA, USA
[2]JNC Japan Nuclear Cycle Development Institute, Tokai, Japan

June 2000

EXECUTIVE SUMMARY

Solute transport in fractured rock is controlled by unique combinations of transport properties, transport pathway geometry, and the hydraulic head field. Minor changes in the head field can radically alter the transport pathways, producing completely different transport results. The JNC/Golder team developed and calibrated Discrete Fracture Network (DFN) and Channel Network (CN) models for a series of sorbing tracer experiments carried out at the 450-meter level of the Äspö Hard Rock Laboratory in Äspö, Sweden. This calibrated model was used to predict sorbing transport along a pathway, which had previously seen only conservative tracer transport. This experiment is designated "STT-2."

The predictions for STT-2 compared surprisingly well with in situ measurements. This report describes an investigation of the possibilities to improve the match between measurements and simulations, based on our understanding of the internal structure of the discrete feature "Feature A" and the calibrated transport properties.

TABLE OF CONTENTS

1. INTRODUCTION AND BACKGROUND 1

2. STT-2 PREDICTIVE MODELING 2

3. EVALUATION OF STT-2 PREDICTIONS 8

   3.1 Uranine Calibration 8
   3.2 Cesium Calibration 14
   3.3 Rubidium Calibration 14
   3.4 Strontium Calibration 14

4. FEATURE A INTERNAL STRUCTURE 21

   4.1 Multiple Transport Pathways 21
   4.2 Transport Aperture 22
   4.3 Immobile Zone Porosity 23
   4.4 Sorption Processes and Values 23
   4.5 Pathway Width 24

5. CONCLUSIONS 25

6. REFERENCES 26

LIST OF TABLES

Table 2-1: Retardation values for tracers 5
Table 2-2: Transport parameters (sorptions) used for STT-2 5
Table 2-3: Comparison of retardations used in STT-1b and STT-2 5
Table 3-1: Strontium Calibration 9

LIST OF FIGURES

Figure 2-1: PAWorks/LTG conceptual model of transport processes 2
Figure 2-2: Feature A Pathway 3
Figure 2-3: Network Topography 4
Figure 2-4: STT-2 injection curves 4
Figure 2-5: STT-2 mass flux curves to 100 hours 6
Figure 2-6: STT-2 predicted breakthrough curves, to 3000 hours 6
Figure 2-7: STT-2 predictions, log-log plot 7
Figure 2-8: STT-2 predictions, cumulative mass arrival at extraction well (see appendix for official scale plots) 7
Figure 3-1: Uranine Cumulative Recovery 10
Figure 3-2: Uranine Injection 10
Figure 3-3: Uranine Prediction 11
Figure 3-4: Uranine Mass Flux Comparison by Pathway 11
Figure 3-5 Uranine Cumulative Breakthrough by Pathway 12
Figure 3-6: Uranine Pathway Velocity Calibration 12
Figure 3-7: Uranine Pathway Calibration 13
Figure 3-8: Cs-134 Mass Flux Injection Curve 15
Figure 3-9: Cesium Prediction 15
Figure 3-10: Cesium Calibration, Normalized Mass Flux 16
Figure 3-11: Cesium Calibration 16
Figure 3-12: Rubidium Injection Curve Injection 17
Figure 3-13: Rubidium Prediction 17

Figure 3-14: Rubidium Calibration 18
Figure 3-15: Rubidium Calibration Normalized Mass Flux 18
Figure 3-16: Strontium Injection 19
Figure 3-17: Strontium Calibration 19
Figure 3-18: Strontium Calibration, Normalized Mass Flux 20
Figure 4-1: Feature A Geological Structure Model 22
Figure 4-2: Intersecting Background Fractures 22
Figure 4-3. Conceptual Microstructure Model For Feature A (After Winberg et al., 2000) 23

1. INTRODUCTION AND BACKGROUND

The Tracer Retention Understanding Experiments (TRUE) are part of a research program at Äspö, the Swedish Hard Rock Laboratory, designed to study the transport of radionuclides in crystalline rock. A series of tracer tests (TRUE-1) have been performed on a single fracture or fracture zone known as Feature A. The primary goal of the STT-2 sorbing tracer test carried out during 1998 was to further investigate the effects of matrix diffusion by the use of a lower pumping rate. A secondary goal was to demonstrate the modeling of decay by using tracers with relatively short half lives. Golder Associates carried out a "blind" prediction of this tracer test during 1999.

Throughout the TRUE-1 experiment the JNC/GOLDER modeling group has used stochastic discrete feature network (DFN) models to make predictions. Initially, for PDT-3 and STT-1, the DFN models were based upon multiple stochastic DFN realizations of a geologic conceptual model. This DFN model included three deterministic features, Feature A, Feature A', and Feature NW-2, as well as background fractures. Flow simulations of the DFN models provided simulated drawdowns and, via particle tracking, simulated non-sorbing tracer breakthrough curves. Acceptable models were chosen by comparing the measured drawdowns and breakthrough curves of PDT-2 to the model results. Accepted models were then used to predict STT-2 by calculating a retardation factor for each sorbing tracer. The tracers chosen for STT-2 included both conservative tracers, HTO, Uranine, and Br-82, and sorbing tracers, Na-22, Ca-47, Sr-85, Ba-131, Ba-133, Rb-134, and Cs-134.

In this report, the results of the STT-2 blind prediction (STT-1b) are evaluated to determine whether the transport processes are properly being modeled, and how the DFN transport model can be improved.

2. STT-2 PREDICTIVE MODELING

JNC's goal in participating in the TRUE-1 project was to improve understanding of transport in fractures and fracture networks, not to demonstrate the predictive abilities of DFN approaches. Nevertheless, it is worthwhile to note that the calibrated DFN models demonstrate a certain degree of predictive power. The calibration process itself was instructive, since it showed to what extent model parameters needed to be adjusted to provide a match to transport experiments.

The transport model used is illustrated in Figure 2-1. The JNC/Golder team has used a combination of discrete feature network flow modeling and Laplace Transform Galerkin (LTG) transport modeling (Dershowitz et al., 1998). The processes considered in these predictive models are:

- Multiple stochastic pathways;
- Advective transport;
- Dispersion within fracture planes;
- Surface sorption;
- Diffusive exchange between mobile and immobile zones;
- Matrix diffusion; and
- Matrix sorption.

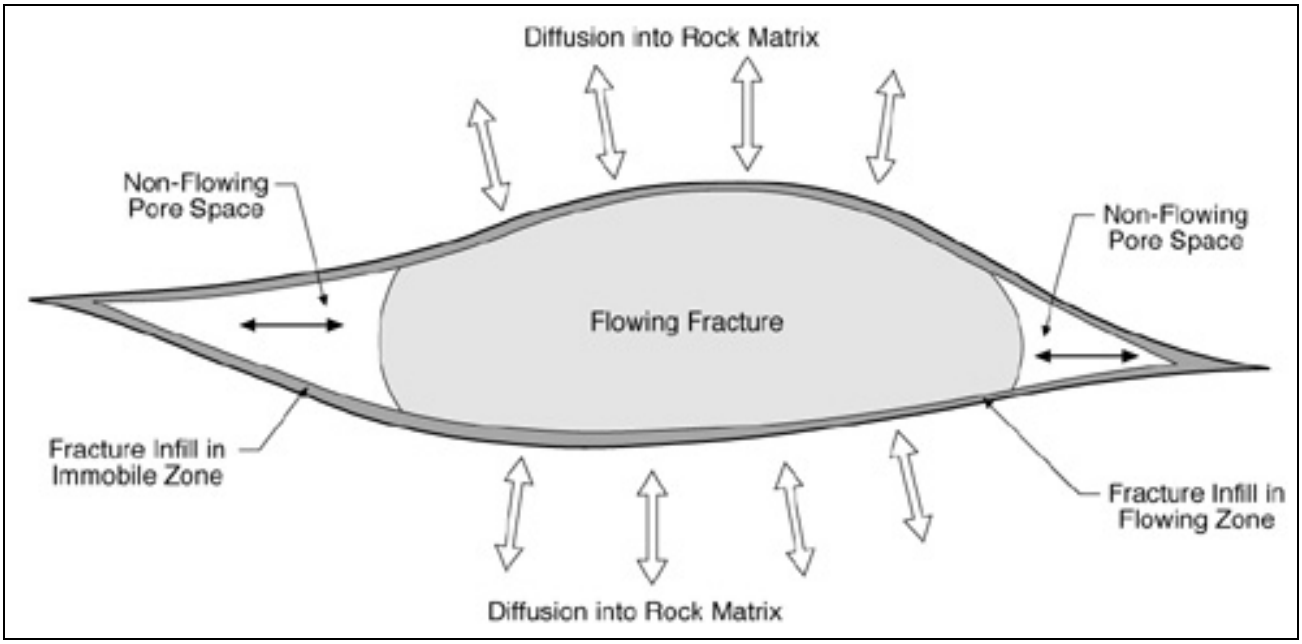

Figure 2-1: PAWorks/LTG conceptual model of transport processes

Over the course of four years JNC/Golder used a series of increasingly refined DFN models to predict tracer breakthrough in "Feature A." These experiments progressed from the initial radially converging tests RC-1 and RC-2, through the dipole tests DP-1 through DP-4, and finally to sorbing tracer experiments of the tracer retention experiment STT-1, STT-2, and

STT-1b. The accuracy of calibrations and predictions improved continuously over this period and in the end the prediction of STT-2 and STT-1b was quite accurate.

The STT-2 Tracer transport experiment pathway is illustrated in Figure 2-2. This figure shows the borehole intersections on the plane of "Feature A." The actual pipe network topology used for the transport modeling is illustrated in Figure 2-3. Figure 2-4 shows the STT-2 injection time history. Predicted breakthroughs are shown in Figures 2-5 through 2-8. These predictions were made using sorption parameters derived from laboratory values, but calibrated to STT-1b breakthroughs. Tables 2-1, 2-2 and 2-3 present the sorption values from laboratory tests and from calibration for STT-2 and STT-1b.

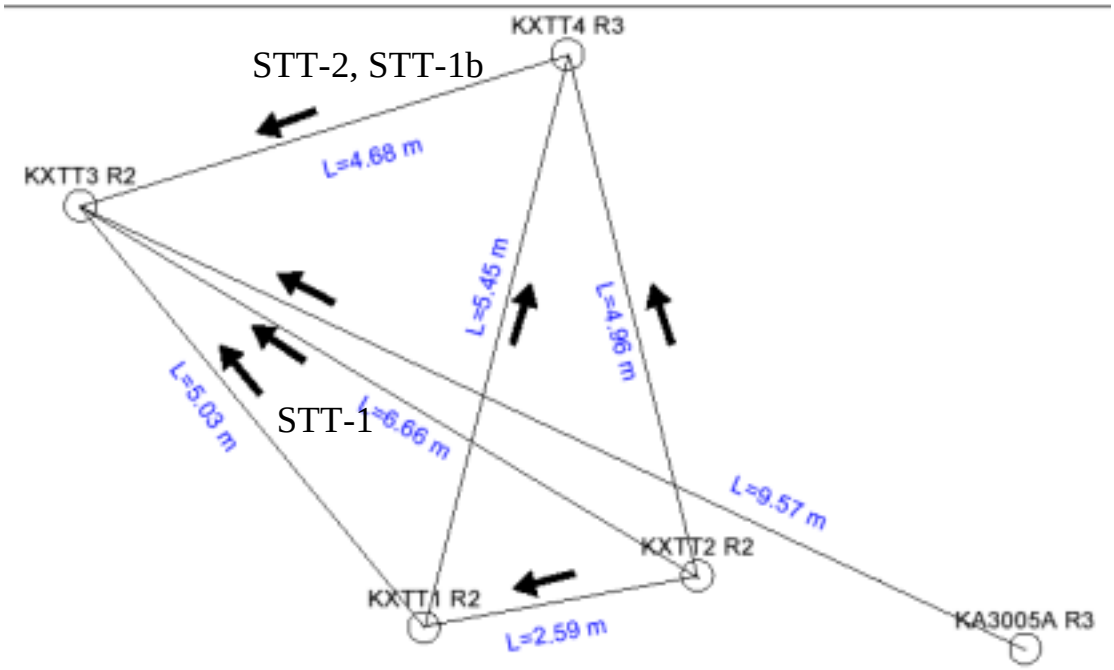

Figure 2-2: Feature A Pathway

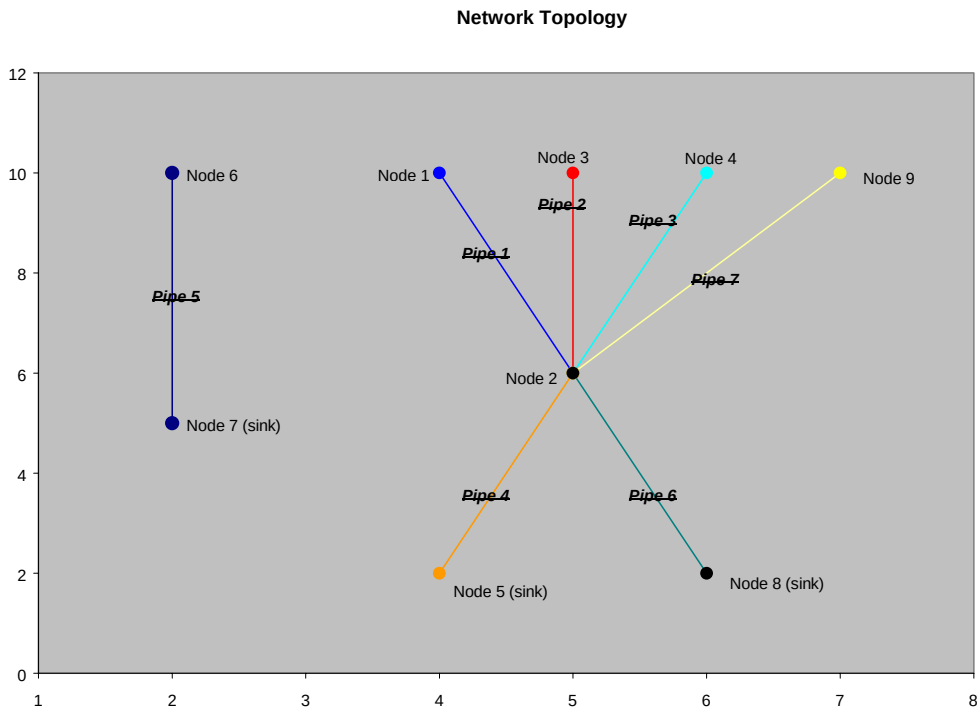

Figure 2-3: Network Topography

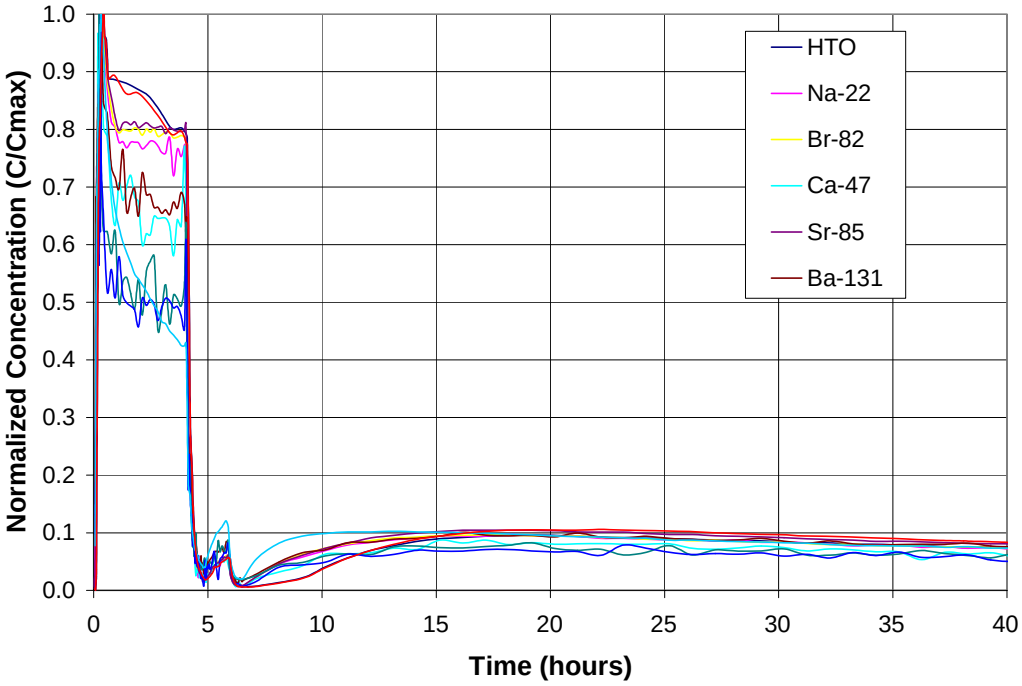

Figure 2-4: STT-2 injection curves

Table 2-1: Retardation values for tracers

Tracer	Surface Sorption, Ka (m)	Diffusivity (m/yr)	Half-Life	Source
Uranine	0	0.032	NA	HRL 97-07
HTO	0	0.076	12.3 y	HRL 97-07
Na-22	1.3E-05	0.042	2.6 y	STT1b
Ca-47	3.0E-05	0.025	4.5 d	HRL 97-07
Br-82	0	0.032	35 h	HRL 97-07
Sr-85	5.0E-05	0.025	65 d	STT1b
Ba-131	6.0E-04	0.026	12 d	Ohlsson &
Ba-133	6.0E-04	0.026	10.5 y	Neretnieks
Rb-96	2.5E-03	0.064	19 d	STT1b
Cs-134	4.0E-03	0.064	2.1 y	HRL 97-07

Table 2-2: Transport parameters (sorptions) used for STT-2

	Ka (m)	**Kd (m^3/kg) = 150*(Ka/ρn)**	**Surface retardation e = 0.29 mm**	**Matrix retardation n = 3%**
Ur, HTO, Br	0	0	1	1
Na-22	1.3E-05	2.7E-05	1.09	3.25
Ca-47	3.0E-05	6.3E-05	1.21	6.2
Sr-85	5.0E-05	1.0E-04	1.34	9.7
Ba-131 -133	6.0E-04	1.3E-03	5.1	105
Rb-96	1.0E-03	2.0E-03	7.6	168
Cs-134	4.0E-03	8.3E-03	28	693

Table 2-3: Comparison of retardations used in STT-1b and STT-2

Tracer and Test	Ka (m)	Kd (m3/kg)	Surface retardation	Matrix retardation
Na-22 STT-2*	1.3E-05	2.7E-05	1.09	3.25
Na-22 STT-1b**	5.0E-06	2.8E-05	1.04	2.00
Sr-85 STT-2	5.0E-05	1.0E-04	1.34	9.7
Sr-85 STT-1b	2.0E-05	2.3E-04	1.14	12
Rb-96 STT-2	2.5E-03	5.2E-03	18.1	434
Rb-96 STT-1b	1.0E-03	1.4E-03	8.1	20

* STT-2 retardations based on nine path models, e=0.29 mm, n=3%

**STT-1b based on one path models, e=4 mm, n=10%

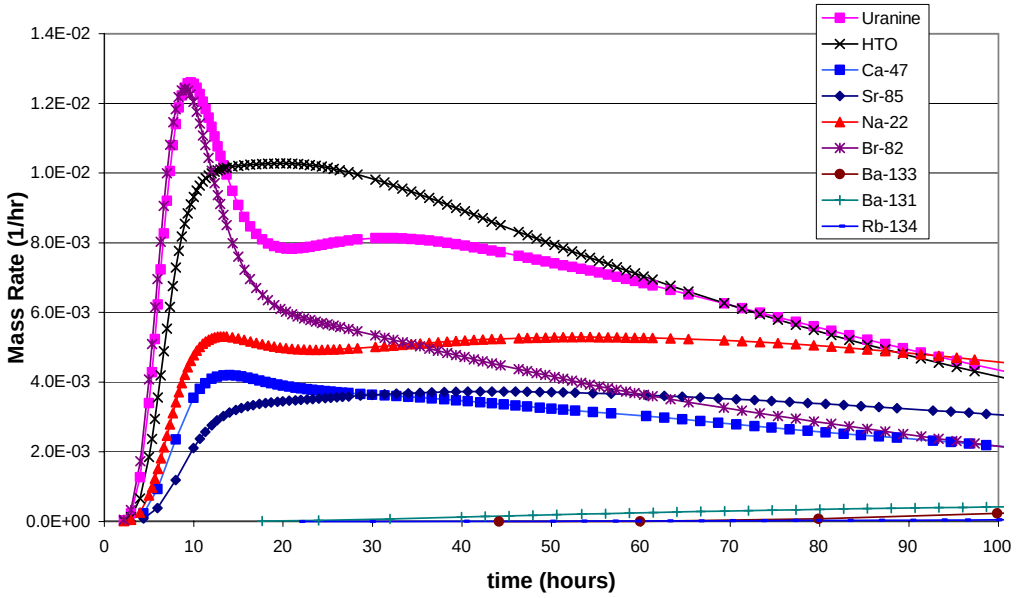

Figure 2-5: STT-2 mass flux curves to 100 hours

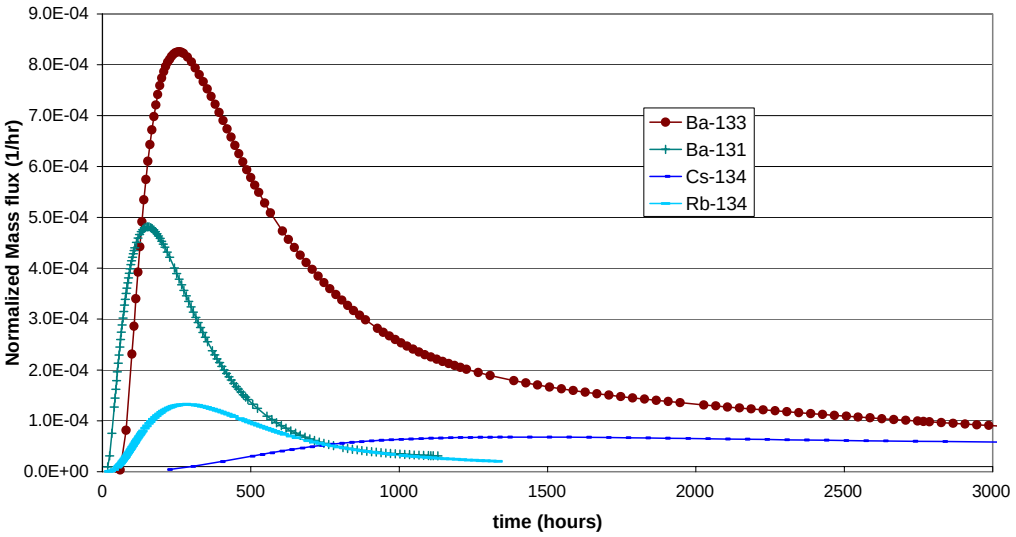

Figure 2-6: STT-2 predicted breakthrough curves, to 3000 hours

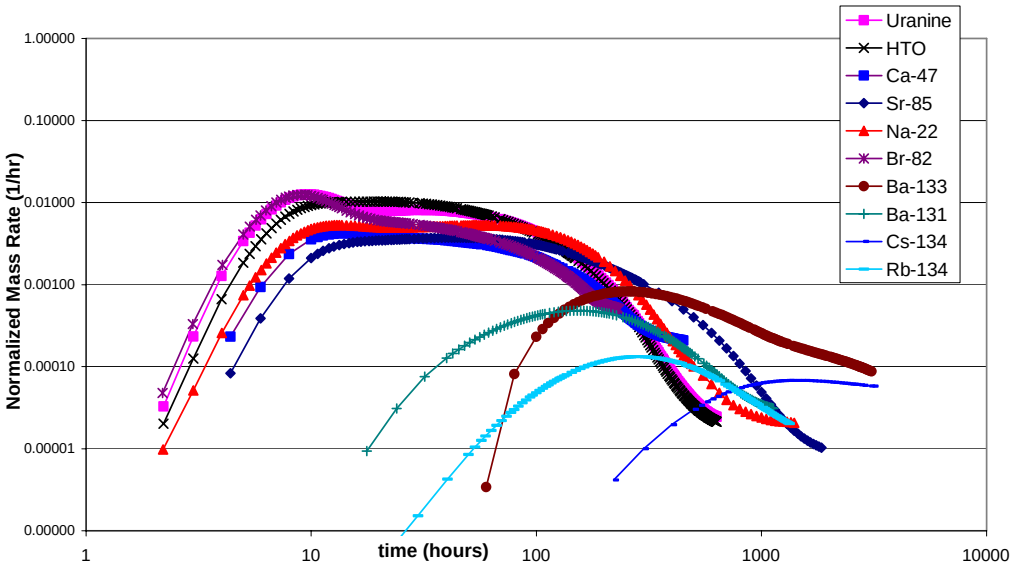

Figure 2-7: STT-2 predictions, log-log plot

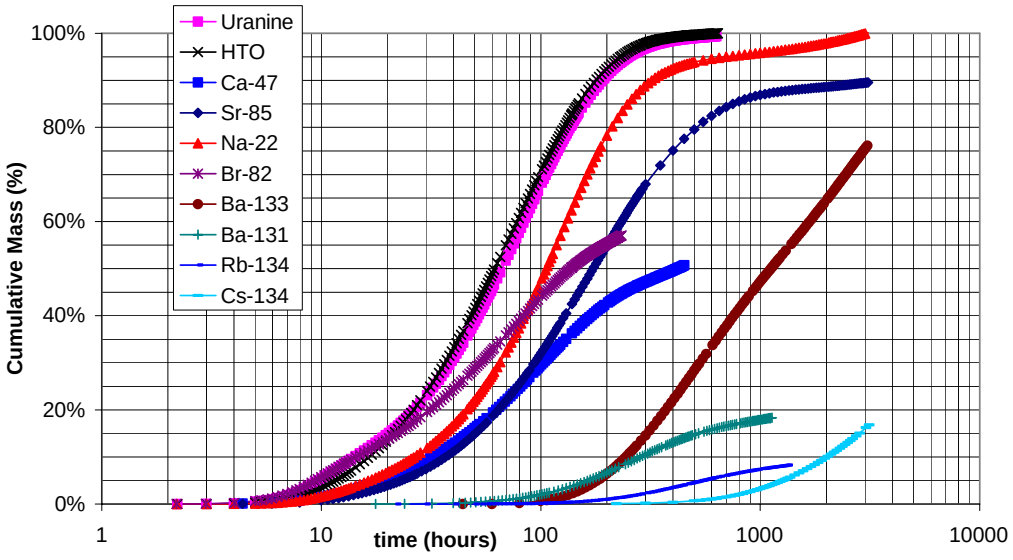

Figure 2-8: STT-2 predictions, cumulative mass arrival at extraction well (see appendix for official scale plots)

3. EVALUATION OF STT-2 PREDICTIONS

Table 3-1 presents a comparison of STT-2 blind predictions to measurements. The comparison shows that, in general, the calibrated model used for prediction produced matches to field measurements, which are better than could reasonably be expected. These matches reflect high levels of matrix diffusion and sorption.

3.1 Uranine Calibration

Figure 3-1 presents a comparison of predictions and measured cumulative breakthrough curves for the conservative tracer Uranine. The cumulative breakthrough curve proves a very good match for the measurement, except near the peak, and the inability to match greater than 100% recovery at large time. This problem with the measurement reflects the difficulty in calculating the actual mass injection from the convolution of flux measurements and the injection curve (Figure 3-2). Figure 3-3 presents a comparison of mass flux for the predictions and measurements. Both the tracer breakthrough prediction and the measurement clearly show two peaks. There has been considerable discussion (Winberg et al., 2000) that these two peaks may be merely a reflection of the two peaks in the injection curve (Figure 3-2). However, the two peaks in the breakthrough curve are of comparable magnitude, while first peaks in the injection curve is approximately ten times greater than the second peak in the injection curve. This increased relative strength of the first peak of the injection curve is directly reflected in the stronger first peak of the prediction (Figure 3-3).

To improve the match between predicted and measured Uranine breakthroughs, it is necessary to strengthen the second peak relative to the first peak. In the FracMan/PAWorks predictive model, this can be done by adjusting the relative amount of tracer mass applied to each pathway in the DFN model. Figures 3-4 and 3-5 shows the contribution to breakthrough from three pathways in the FracMan/PAWorks model. Clearly, Path 4 provides a much larger contribution to the breakthrough than the other pathways. This corresponds directly to the two-peak injection curve.

Figure 3-6 presents a sensitivity study attempting to improve the match of the two peaks of the breakthrough curve. Increasing the velocity and area of pathways 5 and 6 reduces rather than increasing the relative strength of the second peak. Reducing the dispersion to 0.75 m also increases the relative strength of the first peak. Figure 3-7 shows an attempt to improve the match by moving mass between node 7 (pathway 1) and node 5 (pathway 2) or node 8 (pathway 3). These tweaks do provide a marginal improvement to the match. However, none of these calibrations produces a convincing result.

Table 3-1: Strontium Calibration

	Comparison of **Prediction** against *Measurement*			
Tracer	***t5 (h)***	***t50 (h)***	***t95 (h)***	***% Recovery***
Uranin	★ **9.7** *10.58*	★ **65.3** *69.50*	★ **247.9** *329.42*	★ **100** *110.8*
HTO	★ **11.3** *12.50*	**61.3** *79.83*	★ **229.5** *n/a*	★ **100** *90.0*
Na-22	★ **16.3** *16.00*	★ **105.3** *93.83*	★ **650** *n/a*	★ **100** *88.4*
Ca-47	★ **18.7** *23.00*	**414.5** *126.83*	★ **n/a** *346.58*	**50.7** *109.13*
Br-82	★ **9.4** *11.00*	**135.3** *70.83*	★ **n/a** *n/a*	**57.1** *91.96*
Sr-85	★ **22.7** *28.00*	★ **170.6** *157.83*	★ **n/a** *n/a*	★ **89.6** *85.64*
Ba-131	**162.7** *76.83*	★ **1130.7** *736.83*	★ **n/a** *n/a*	**18.3** *61.17*
Ba-133	**180.1** *73.83*	★ **1106.6** *712.83*	★ **n/a** *n/a*	★ **76.1** *72.38*
Rb-86	**n/a** *126.83*	**n/a** *1129.33*	★ **n/a** *n/a*	**0** *54.28*
Cs-134	★ **533.5** *1345.33*	★ **n/a** *n/a*	★ **n/a** *n/a*	★ **8.3** *13.66*

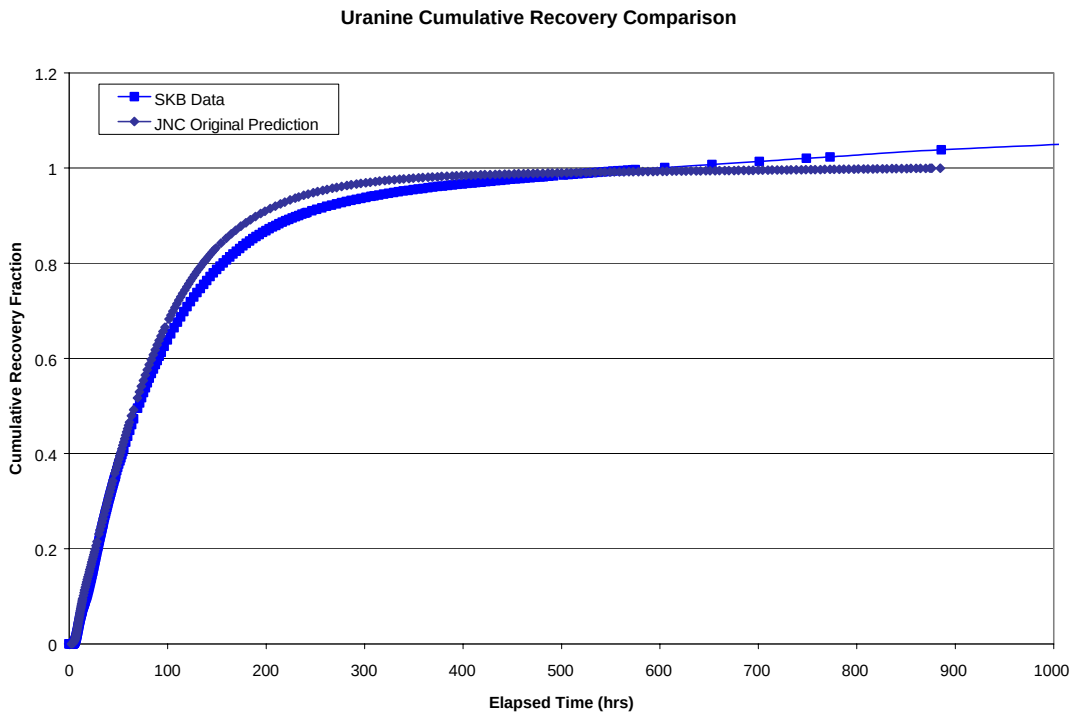

Figure 3-1: Uranine Cumulative Recovery

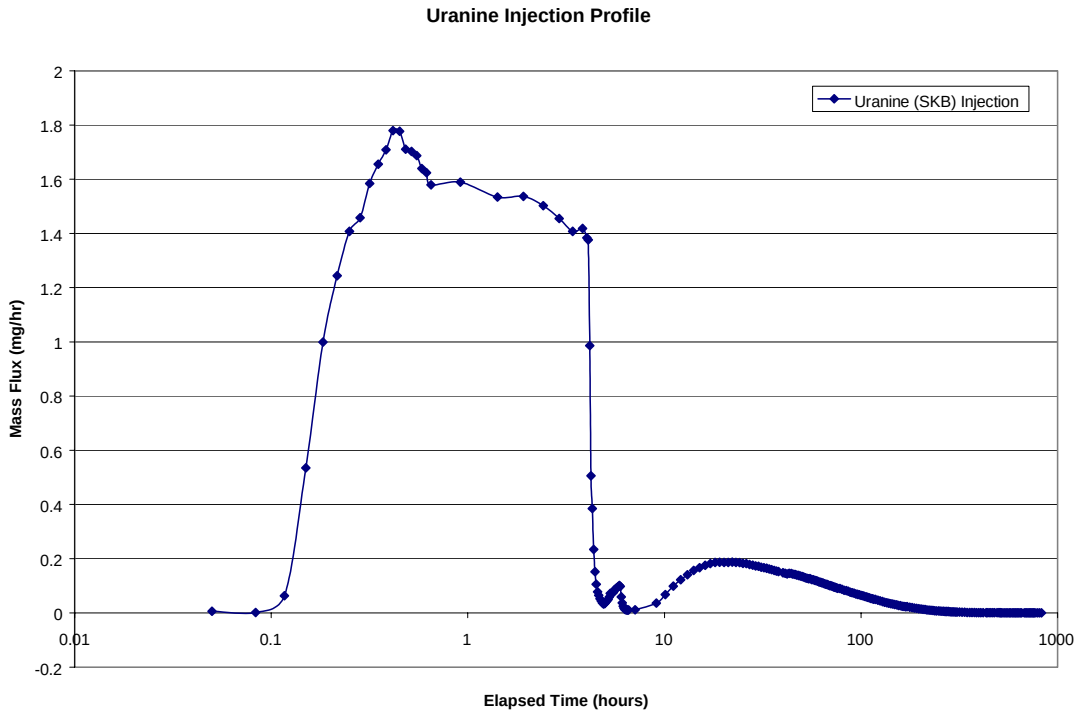

Figure 3-2: Uranine Injection

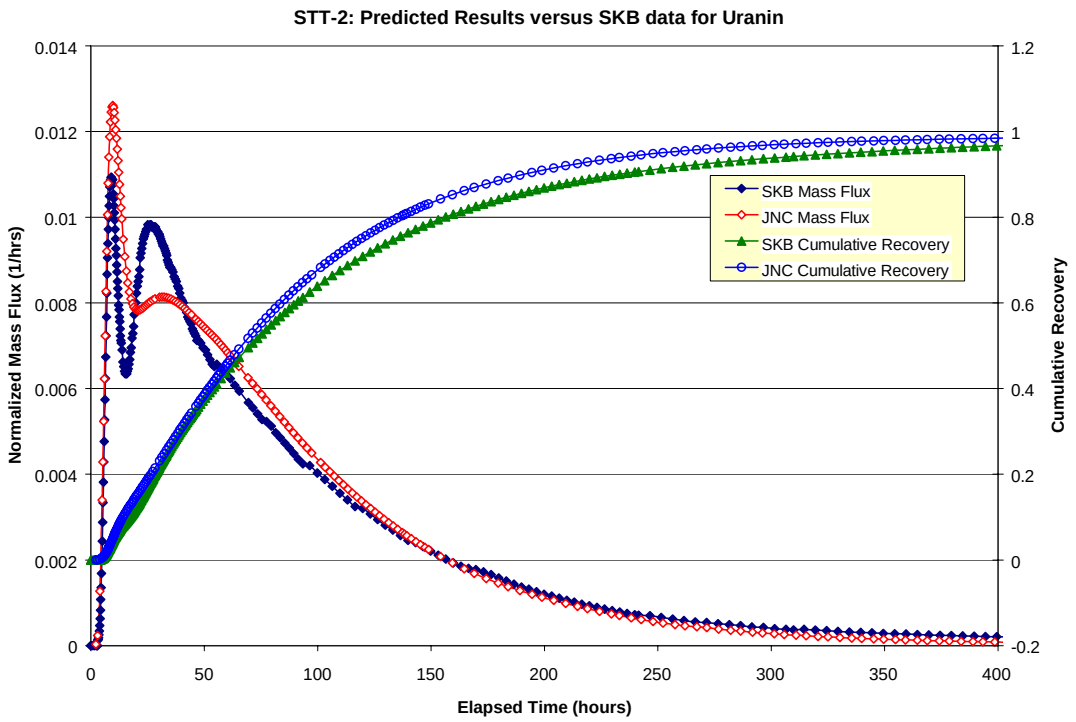

Figure 3-3: Uranine Prediction

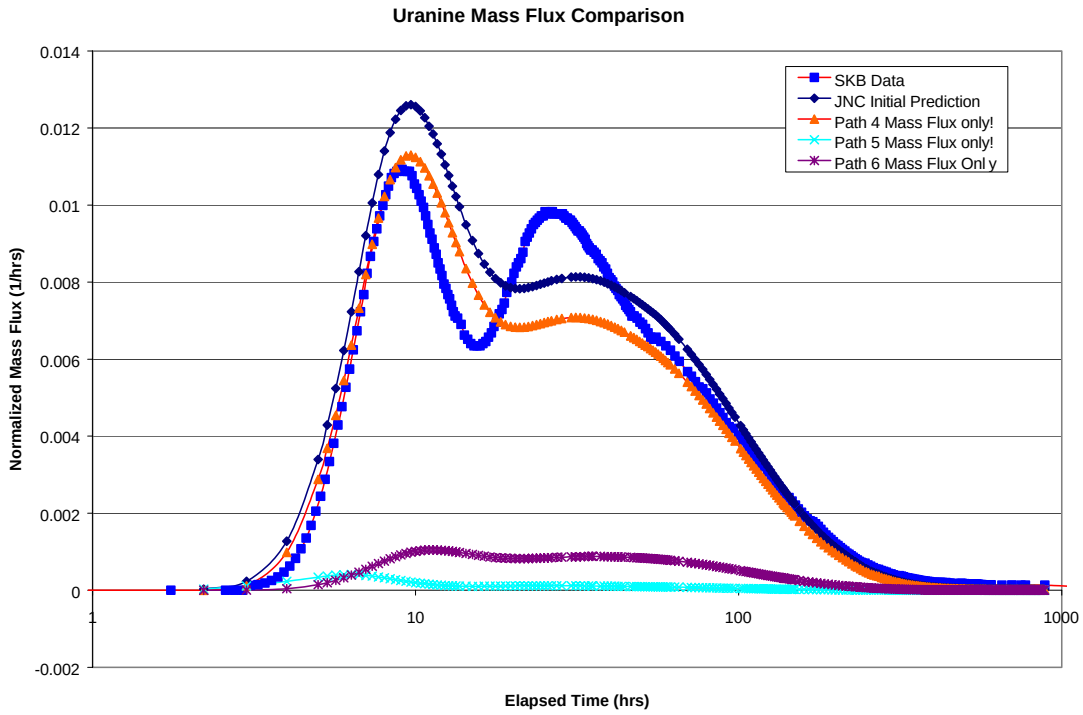

Figure 3-4: Uranine Mass Flux Comparison by Pathway

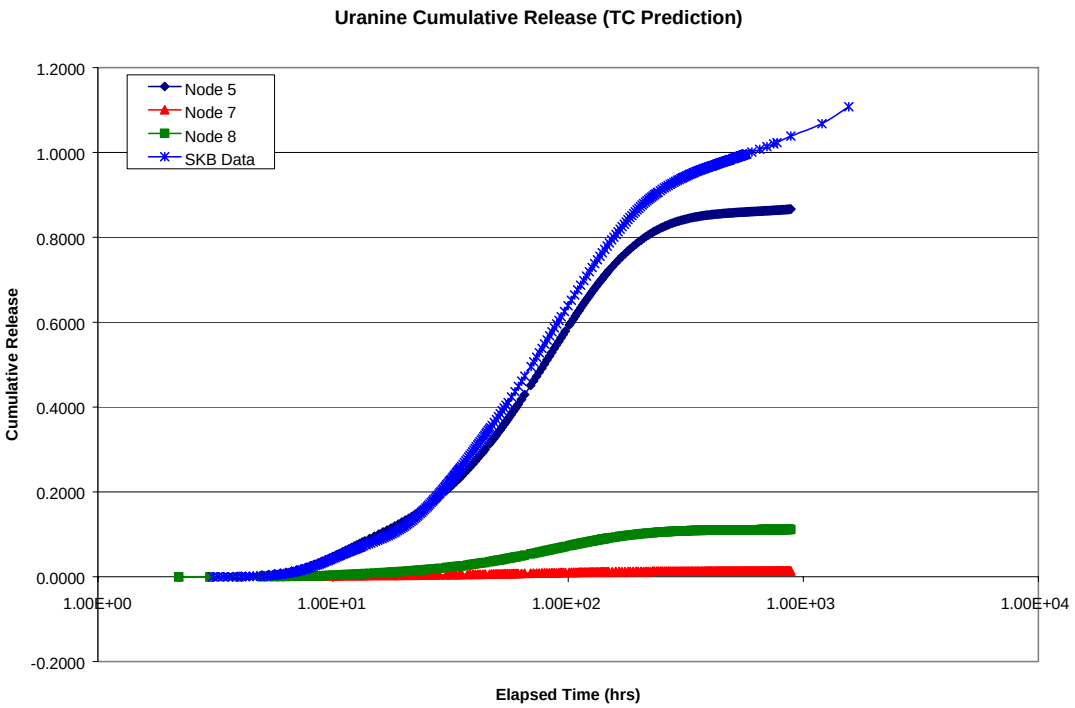

Figure 3-5 Uranine Cumulative Breakthrough by Pathway

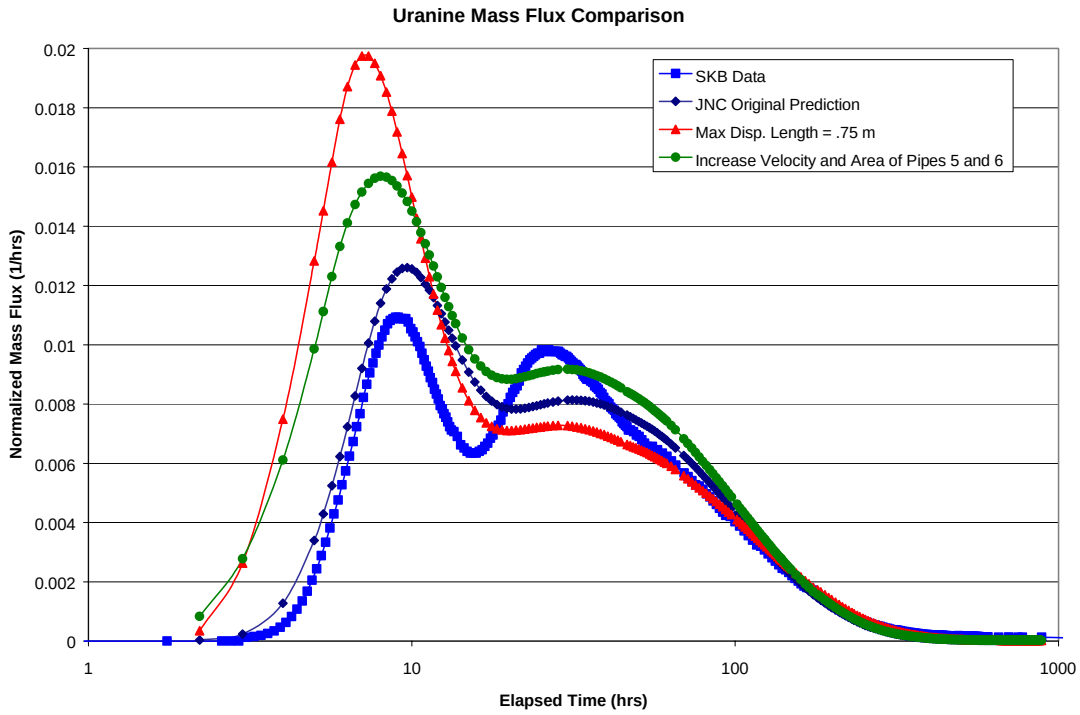

Figure 3-6: Uranine Pathway Velocity Calibration

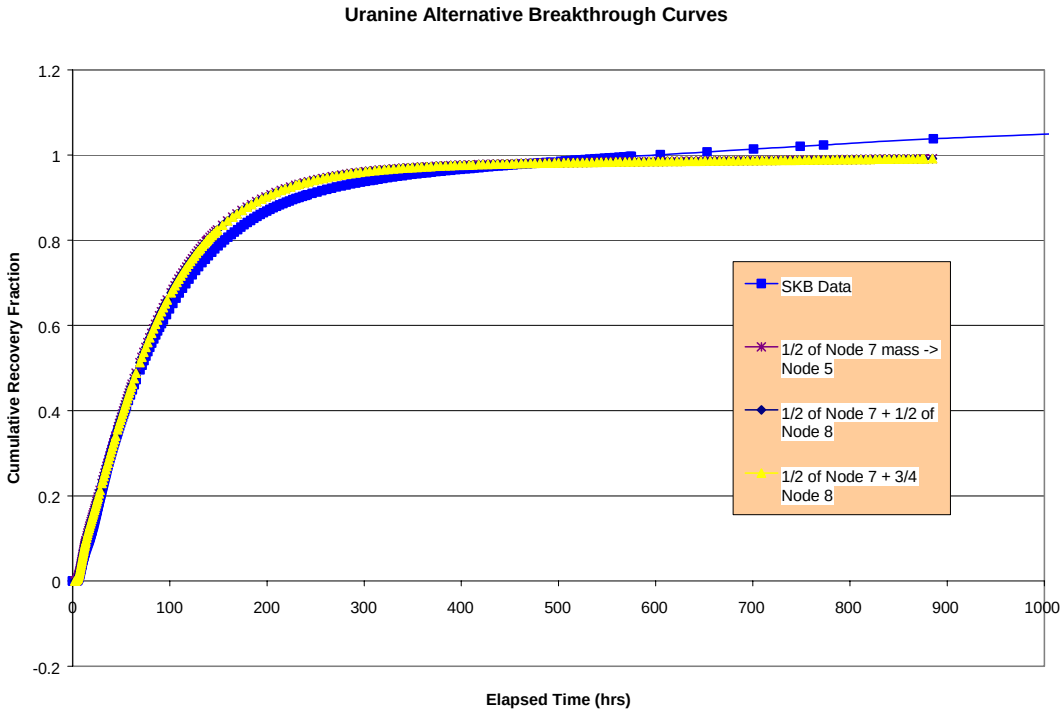

Figure 3-7: Uranine Pathway Calibration

3.2 Cesium Calibration

Figure 3-8 shows the injection curve for the sorbing tracer Cesium, which also exhibits multiple peaks. Figure 3-9 presents a comparison of predictions and measured cumulative breakthrough curves for Cesium. No second peak is visible, which may be due to apparent dispersion produced by matrix diffusion enhanced by matrix sorption. The measured cumulative recovery for Cesium is slightly below that for the prediction.

Figures 3-10 shows a series of simulations attempting to obtain a better match to the exact shape of the Cesium breakthrough measurements.

- Tweak 1: increasing diffusion distance from 1 cm to 2 cm
- Tweak 2: as tweak 1, also increasing pipe 4 diameter by 50%
- Tweak 3: as tweak 1, also reductive pipe 4 diameter by 20%
- Tweak 4: as tweak 3, also increasing Kd sorption by 10%

None of the minor changes studied produced a better match to measurements than that in the original prediction. All the changes studied increased the apparent dispersion in the breakthrough curve, without producing the observed more rapid drop off in the tail. Tweak 3 clearly does produce some improvement to the match between the simulation and measurement, as shown in Figure 3-11. It is expected that further calibration of the relative strength of pathways and the amount of surface and matrix sorption could improve this match.

3.3 Rubidium Calibration

Figure 3-12 shows the injection curve for the sorbing tracer Rubidium. Figure 3-13 presents a comparison of predictions and measured cumulative breakthrough curves for Rubidium. While Cesium recovery was slightly over-predicted, Rubidium recovery is significantly larger than predicted. Since the Rubidium breakthrough shows only one peak, changes in the calibration simulations were made to all pipes simultaneously. Figure 3-14 shown two simulations reducing the strength of retention mechanisms to achieve a better match between measurements and simulations. While these calibrations did not lead to the level of recovery achieved in situ, the it was possible to calibrate normalized mass flux (Figure 3-15) very well by reducing matrix porosity, surface sorption Ka and matrix sorption Kd.

3.4 Strontium Calibration

Figure 3-16 shows the injection curve for the sorbing tracer Strontium. Multiple peaks are again clearly visible in the injection curve, but are not apparent in the measured breakthrough curves (Figure 3-17 and 3-18). Because the shape of the breakthrough curve for Strontium was well predicted, even though the total mass recovery was over predicted, the calibration shown in Figures 3-17 and 3-18 focused on slight increases in retention mechanisms. Increasing both surface sorption (by increasing pipe perimeter) and matrix sorption (by increasing diffusion depth) provided an excellent match to normalized mass flux (Figure 3-18). However, this reduced the recovery too much, as shown in Figure 3-17. A better match to the cumulative recovery (an a worse match to the peak) is obtained by enhancing only matrix sorption, while leaving surface sorption as in the predictive simulations (Figure 3-17).

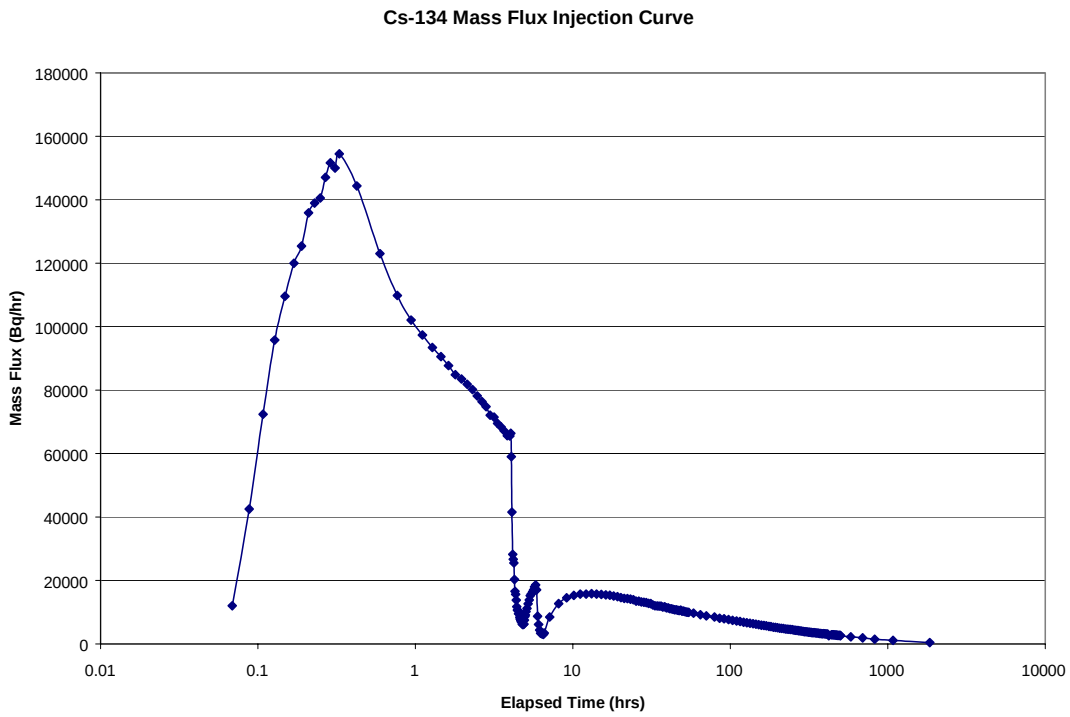

Figure 3-8: Cs-134 Mass Flux Injection Curve

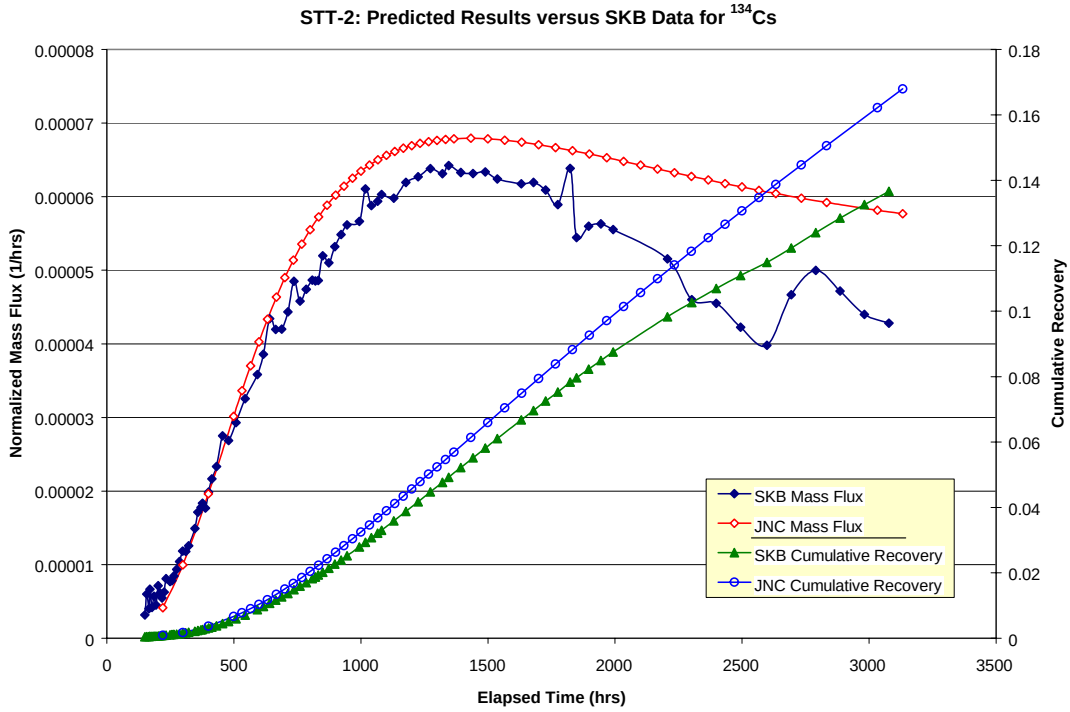

Figure 3-9: Cesium Prediction

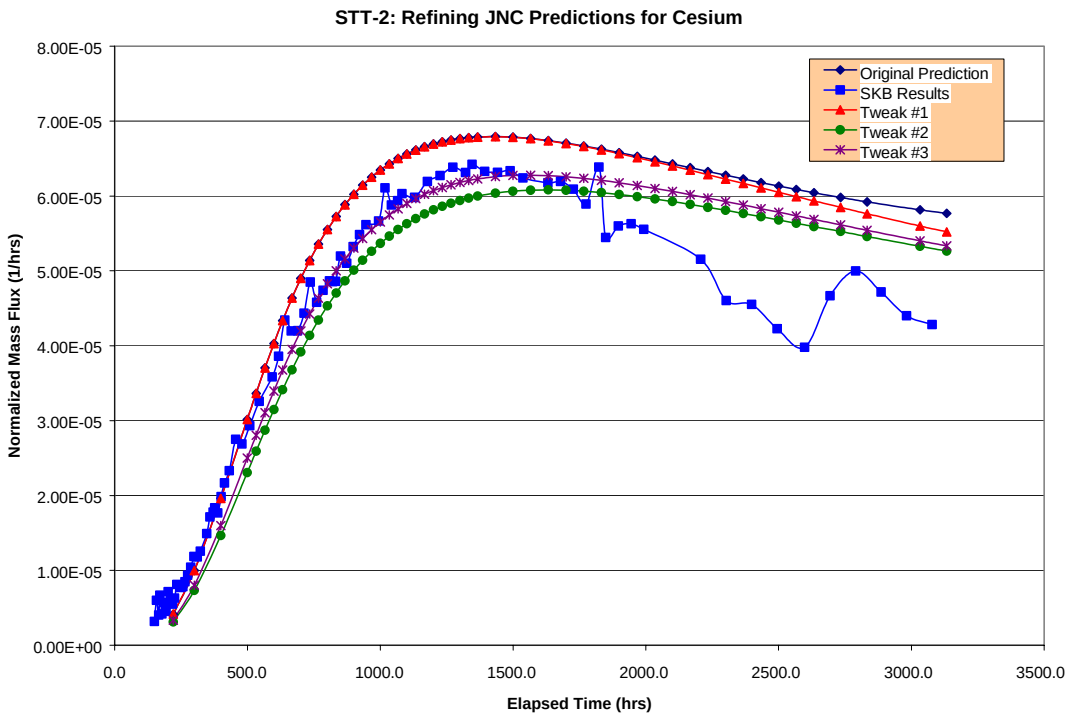

Figure 3-10: Cesium Calibration, Normalized Mass Flux

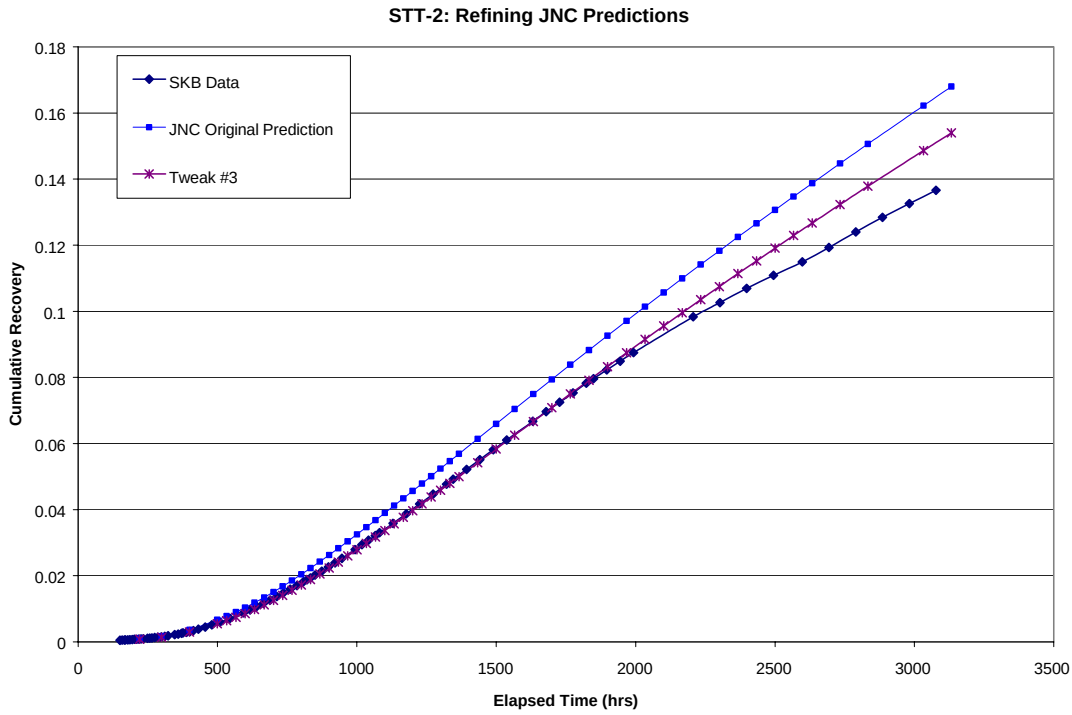

Figure 3-11: Cesium Calibration

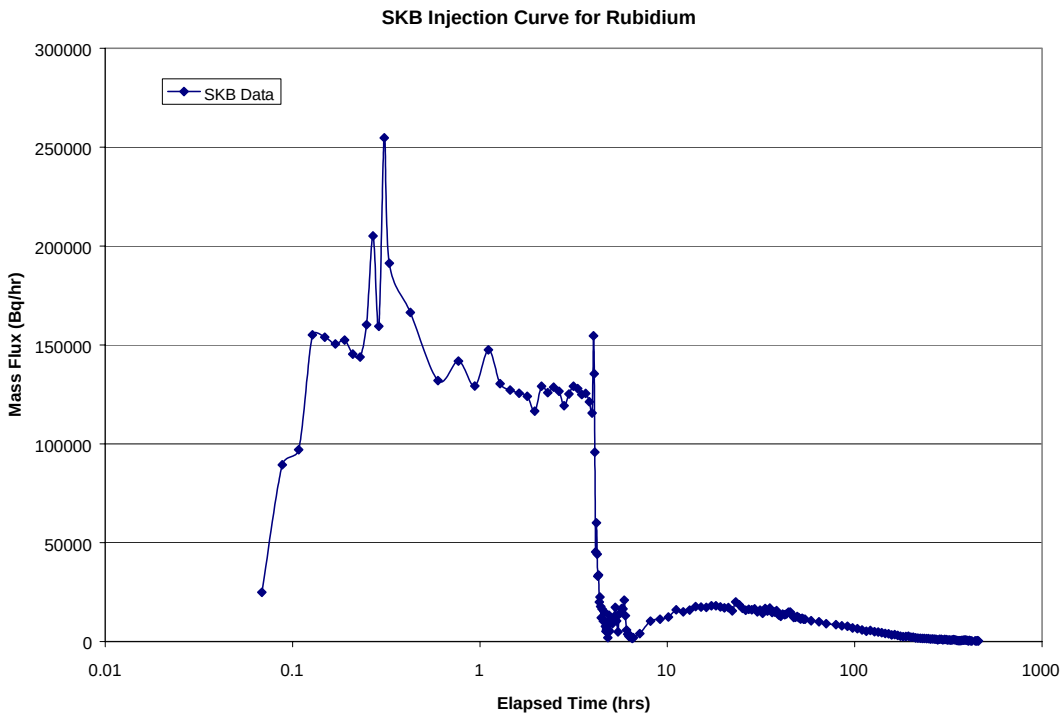

Figure 3-12: Rubidium Injection Curve Injection

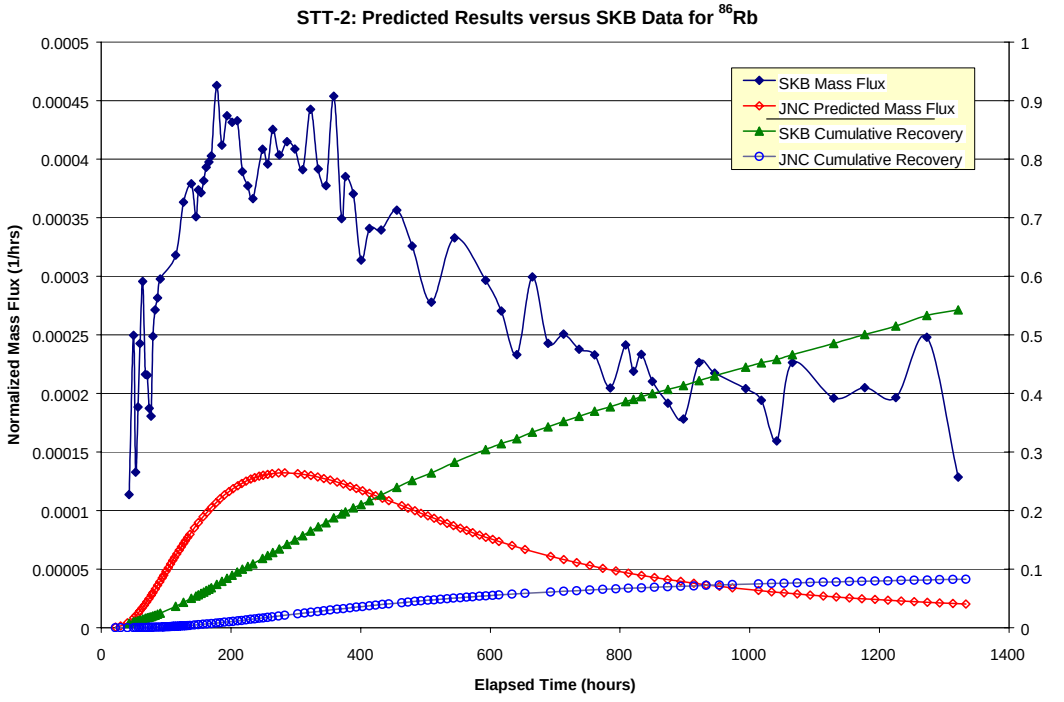

Figure 3-13: Rubidium Prediction

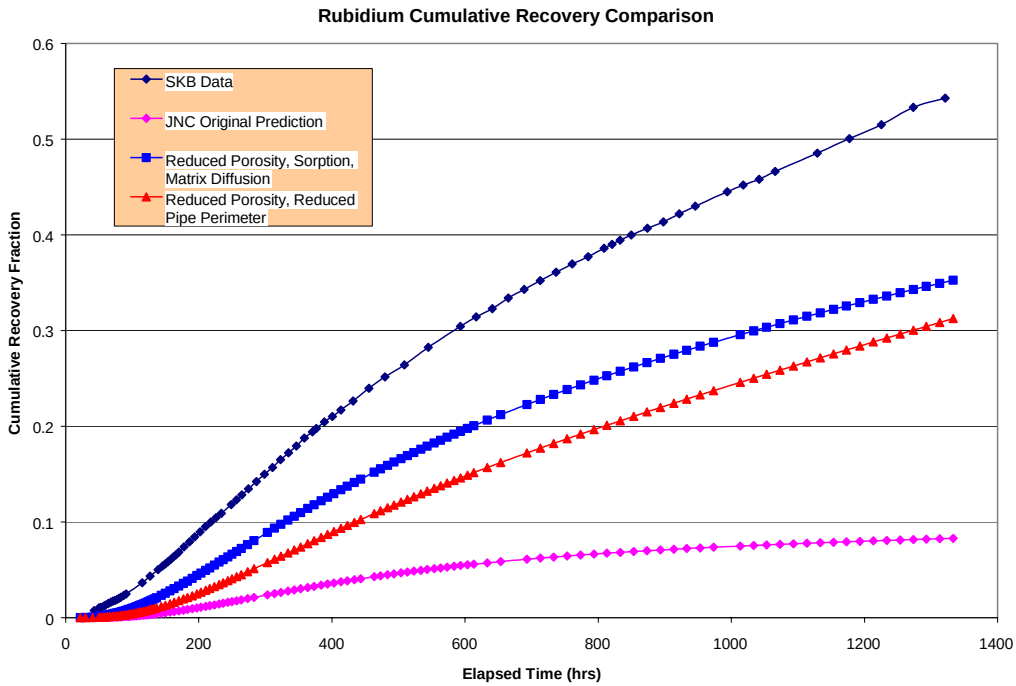

Figure 3-14: Rubidium Calibration

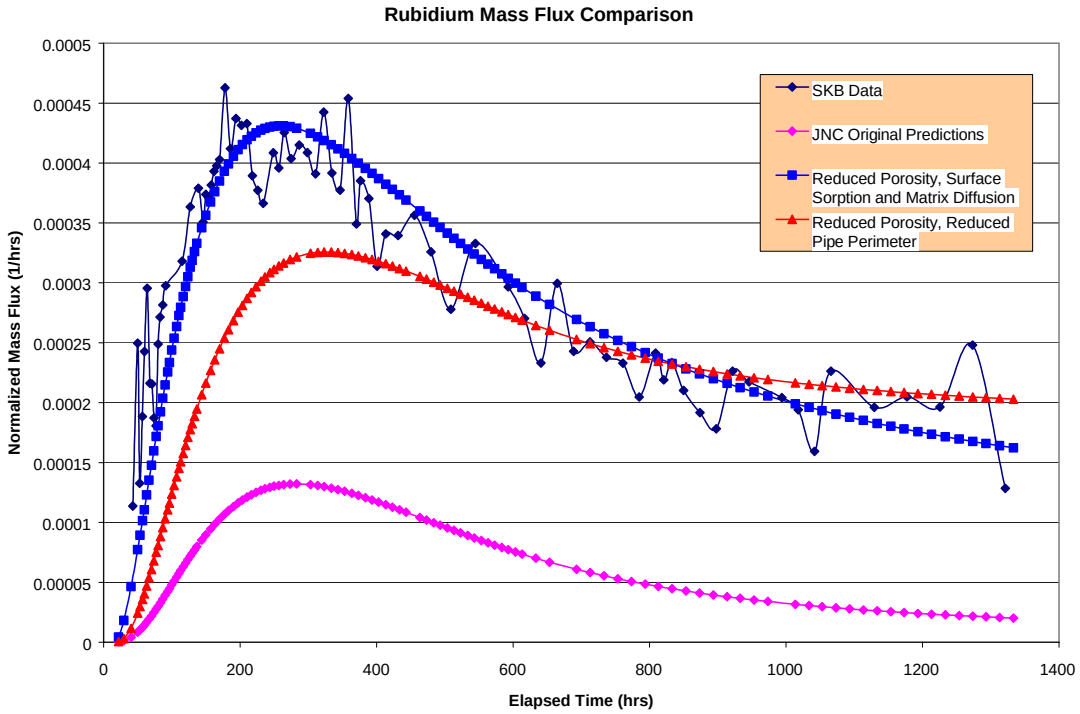

Figure 3-15: Rubidium Calibration Normalized Mass Flux

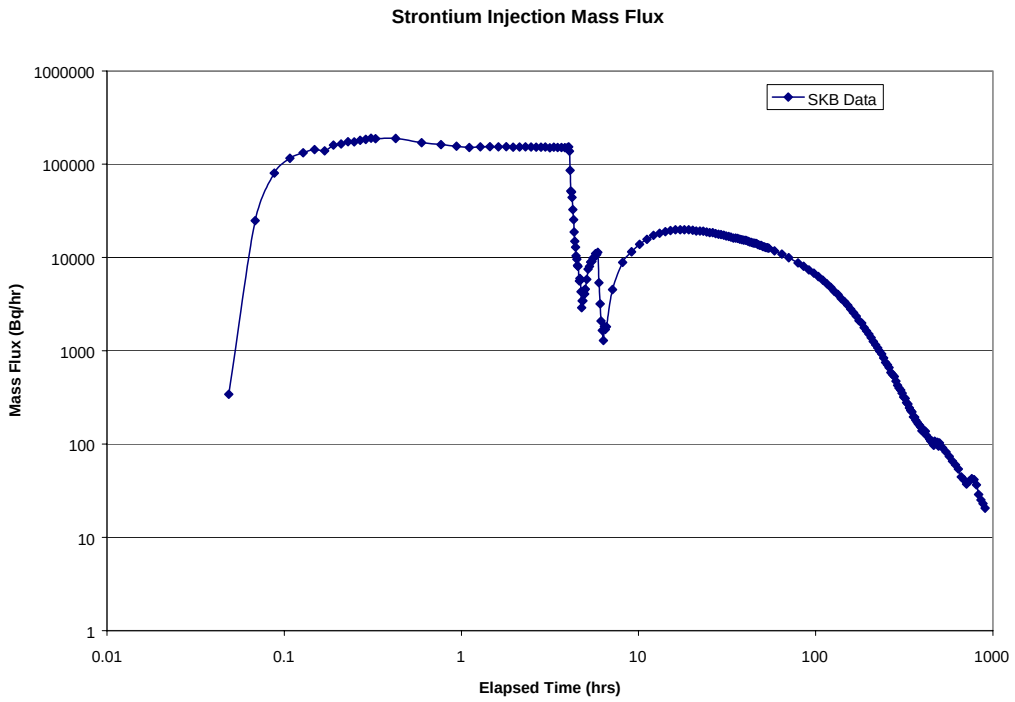

Figure 3-16: Strontium Injection

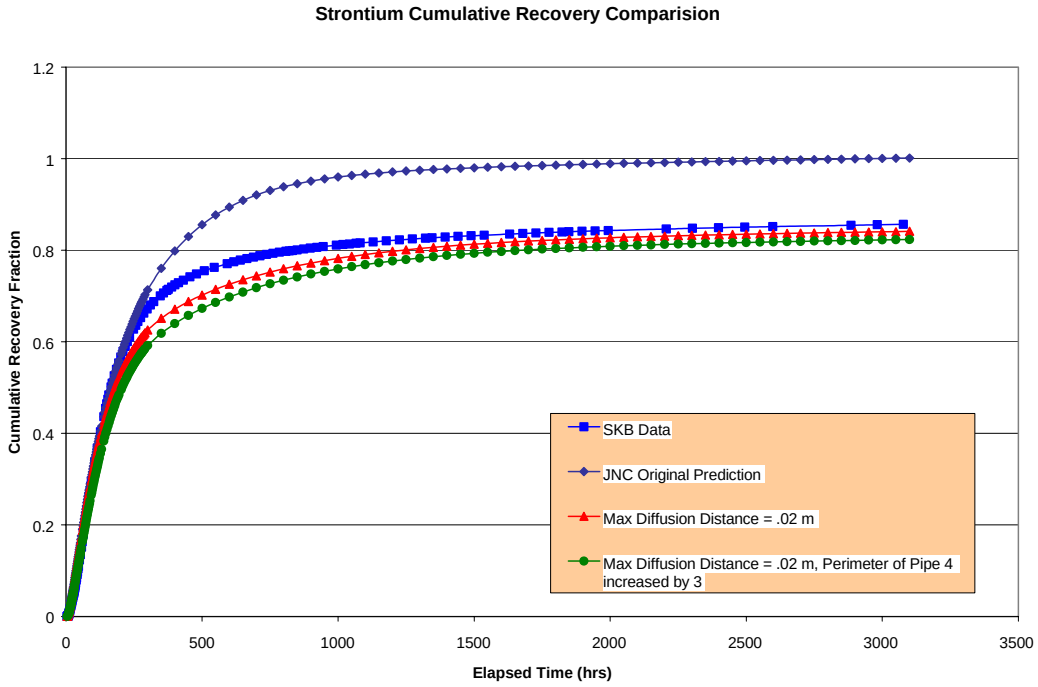

Figure 3-17: Strontium Calibration

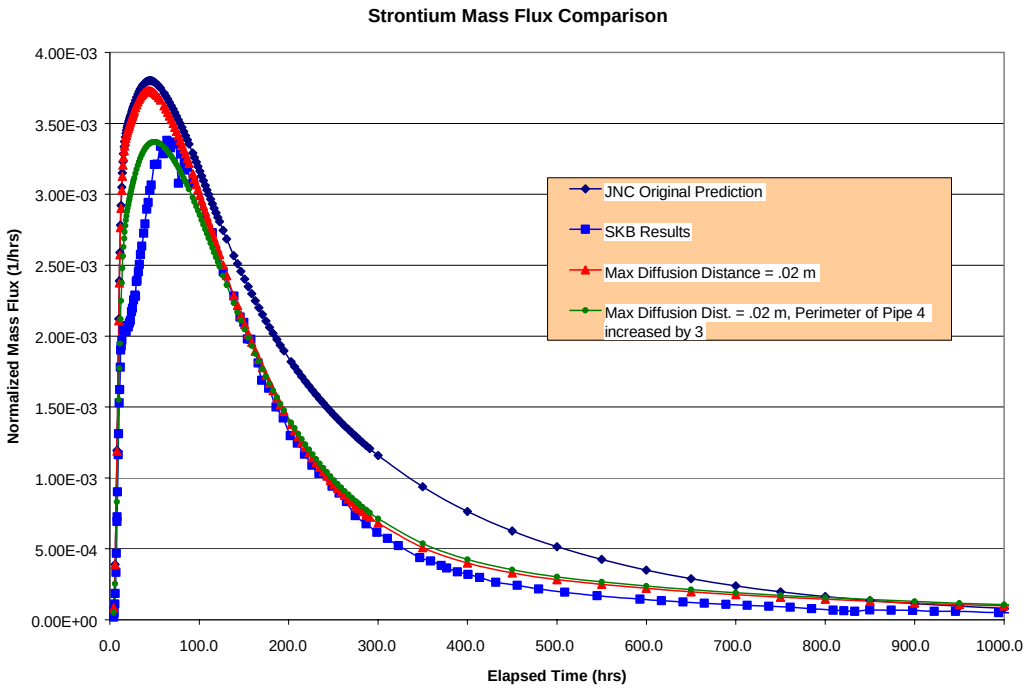

Figure 3-18: Strontium Calibration, Normalized Mass Flux

4. FEATURE A INTERNAL STRUCTURE

The calibration simulations for the STT-2 prediction assumed that the pathways and sorption properties for each tracer could be calibrated separately. However, none of the calibrations considered produced a result significantly better than that obtained in the calibrations to STT-1 and STT-1b that formed the basis for the STT-2 predictions. Clearly, the model used for the successful prediction is not unique – a wide variety of combinations of parameters could explain the observed transport behavior. However, the accurancy of the prediction indicates that there may be at least some degree of validity to the conceptual model used for the predictions. In addition, none of the calibrations resulted indicated a need for significant changes to the underlying model parameters – the prediction quality is generally within the measurement accuracy and experimental uncertainty. The salient points of this model are:

- Multiple transport pathways consisting of a combination of a single major pathway with one or more minor pathways;
- Transport aperture 0.3 mm;
- Immobile porosity defined as a material of effective porosity on the order of 3%, with a thickness of 1 cm to 2 cm;
- Both surface and matrix sorption active, with effective sorption values similar to laboratory values (generally within one half order of magnitude); and
- Path width on the order of 1.5 meters, with some path widths as high as 5 m.

The question, which then arises, is whether these values are consistent with what is actually occurring within feature A. The consistency is assessed in Sections 4.1 through 4.5.

4.1 Multiple Transport Pathways

Multiple transport pathways are explained as either channels developed on the surface of Feature A due to local heterogeneity or mylonitization, or pathways formed by intersecting fractures. Feature A is conceptualized as a planar structure oriented at N29W/79E. However, the orientations measured at the various borehole intercepts vary by 5 to 10 degrees, with slightly different geological properties. The project geologists have proposed the concept the Feature A may indeed be made up of multiple fractures which form a thin zone rather than a single discrete fracture (Winberg et al., 2000). This by itself could result in multiple pathways. The borehole intercepts are characterized geologically by the presence of a reactivated mylonitic structure along one, or alternatively two sub-parallel fault planes (Winberg et al., 2000). This geological interpretation also supports the possibility of multiple transport pathways within Feature A (Figure 4-1). In the predictive simulations, it was assumed that the multiple pathways were a consequence of the discrete fractures intersecting feature A (Figure 4-2). The hypothesis of multiple transport pathways is thus consistent with the structural model, complex fracture internal structure.

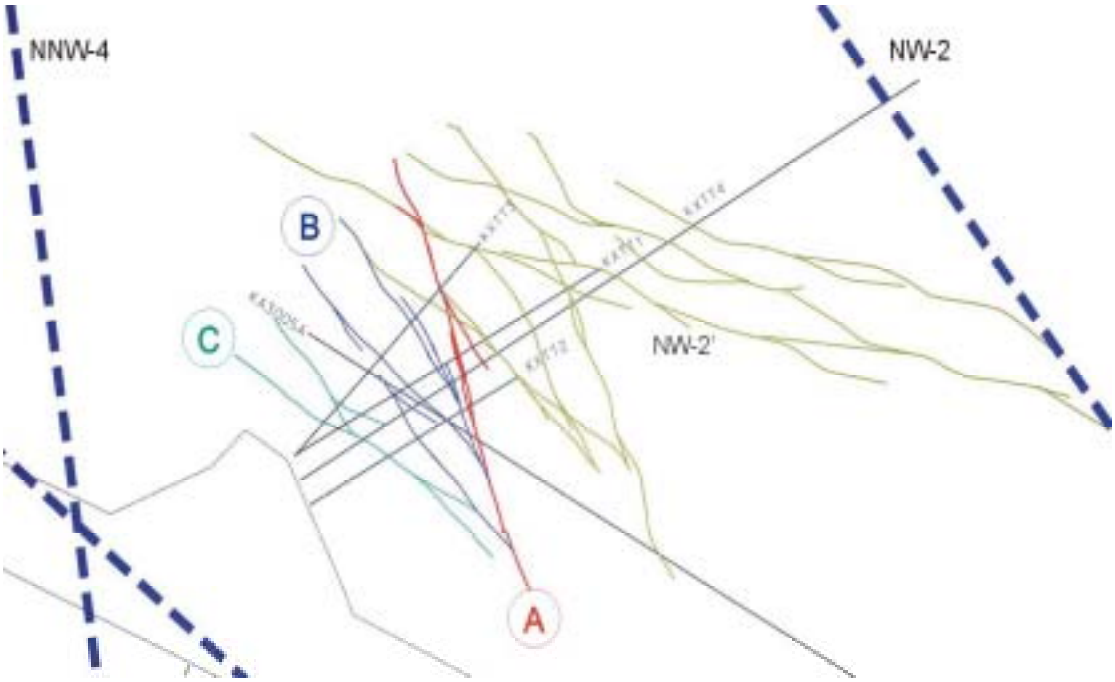

Figure 4-1: Feature A Geological Structure Model

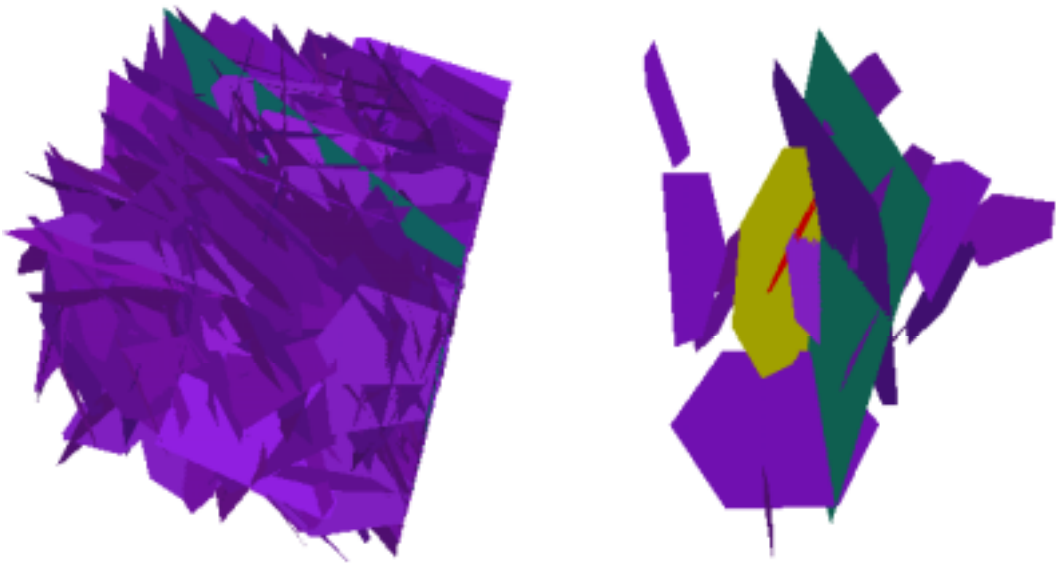

Figure 4-2: Intersecting Background Fractures

4.2 Transport Aperture

The internal structure of Feature A is believed to be a reactivated mylonite which has been exposed to brittle deformation (Winberg et al., 2000). The total thickness of Feature A is estimated by the geologists to be50 to 90 mm (Winberg et al., 2000), with a mechanical aperture on the order of 1 to 3 mm. This is consistent with the calibrated transport aperture of 0.3 mm, considering that effective transport apertures are generally significantly less

than mechanical apertures, particularly with the presence of mylonite, and the potential presence of fault deformation related materials such as gouge and breccia.

4.3 Immobile Zone Porosity

The calibrated immobile zone porosity of 3% is much greater than the measured rock porosities of 0.1% and even the altered rock porosities on the order of 0.5%. The maximum diffusion depth of 1 to 2 cm, on the other hand, is considerably lower than the measured thickness of the altered Äspö diorite halo of 5 to 9 cm. It can therefore be supposed that the primary immobile zone interacting with tracer along the transport pathway is made up of the fracture infillings (Figure 4-3). These fracture infillings have measured porosities as high as 30%. The main fracture infilling minerals are calcite, fluorite, quartz, k-feldspar, and pyrite. There is also some evidence of clay minerals as an outer rim of the fracture mineral coating, and geologists have speculated that this indicates the presence of clay gouge material within Feature A. Investigations by Winberg (2000) using triple tube techniques do show fault gouge in structures similar to Feature A, even though the more disturbed samples taken from Feature A did not show gouge.

This conceptual model for fracture infilling materials is consistent with the calibrated porosities and thicknesses: the porosity for gouge, breccia, and fractural minerals are generally on the order of 1 to 20%, and the thickness of these materials among multiple fractures could easily approach 1 to 2 cm.

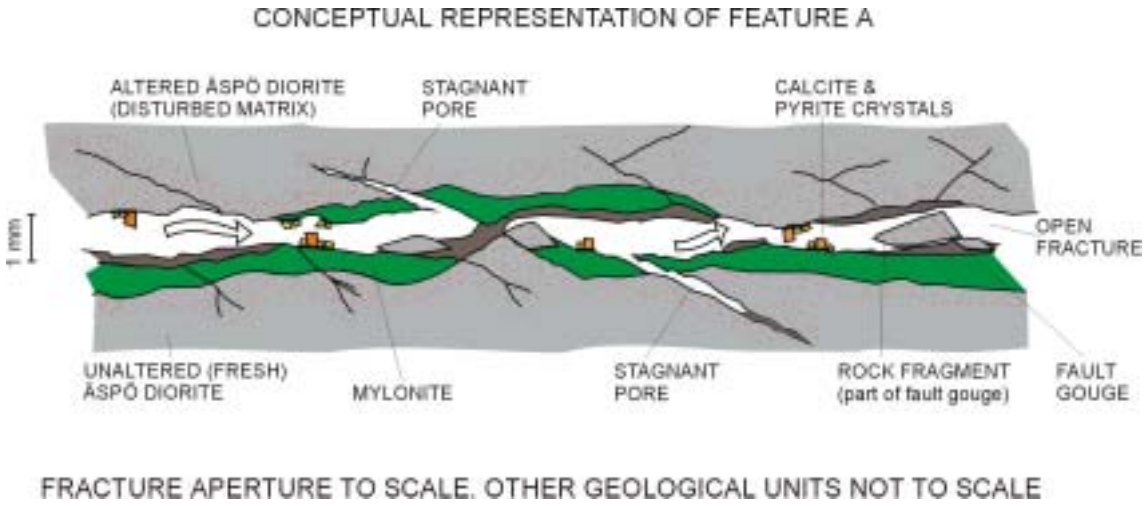

Figure 4-3. Conceptual Microstructure Model For Feature A (After Winberg et al., 2000)

4.4 Sorption Processes and Values

Mazurek (2001) presented a conceptual model for the internal structure of Feature A based on flow in master faults or splays, with available porosities for both surface sorption and matrix sorption. Porosities available for surface sorption include fracture coatings and altered or unaltered mylonites. Porosities available for matrix diffusion include fault gouge/breccia, lithified cataclasite, and granite (altered and unaltered). This is consistent with the

transport calibration which includes both surface and matrix sorption processes. The magnitude of calibrated Kd and Ka values are generally not far from the values from laboratory experiments, although a few tracers exhibit greater than expected retention. This is consistent with the variety of materials making up the immobile zone porosity and the predominance of granitic and breccia materials rather than clay minerals.

4.5 Pathway Width

The calibrated transport path width on the order of 1.5 meters with some portions as large as 5 meters. This is very large for such a short path length, on the order of 5 meters. The transport path width is used in the transport model primarily to define the pathway perimeter for calculation of surface sorption and matrix diffusion. While it is possible that the path width is this large, the path is not completely consistent with a model of Feature A with variable apertures and infillings, which would tend to produce a more constrained path.

Alternatively, transport path width could be normalized by the number of available surfaces. So, if there were on the average only two surfaces available for diffusion and sorption along the path, the width would be 1.5 meters. However, if the presence of minerals and mylonites resulted in an average of 8 surfaces available along the path, the effective path width is reduced to 0.375 m, which is more consistent with the channelized radial flow geometry expected.

5. CONCLUSIONS

This report studied the mechanisms behind the surprisingly good match between DFN model predictions and measurements for the STT-2 sorbing tracer experiment. The parameters used in the DFN model appear to be consistent with geological evidence and the fracture models. The model calibration studies support the use of matrix diffusion and sorption as well as surface sorption mechanisms for tracer retention. Observed enhanced matrix and surface sorption appear to be consistent with the occurrence of mylonite and other fracture infillings which provide both an increase in reactive surface area and a limited immobile zone volume with increased matrix porosity. The transport aperture of only 0.3 mm supports the observed rapid advective transport.

6. REFERENCES

Dershowitz, W., M. Uchida, T. Cladouhos, and A. Fox : Discrete Fracture Network Sorbing Tracer Predictive Modeling: Aspo Task 4EF. Swedish Nuclear Fuel and Waste Management Co, ICR-01-XX, 2000.

Dershowtz, W. D. Shuttle, T. Foxford, and E. Sudicky : PAWorks, Pathways Analysis and Solute Transport, User Documentation, Version 1.5, Golder Associates, Redmond, WA, 1998.

Mazurek, M. Geological Model for Feature A : Paper Presented at TRUE-1 Seminar, Aspo Sweden, 2001. (in press)

Winberg A, P. Andersson, J. Hermanson, J. Byegård, V. Cvetkovic, and L. Birgersson : Äspö Hard Rock Laboratory, Final report of the first stage of the tracer retention understanding experiments, Swedish Nuclear Fuel and Waste Management Co, TR-00-07, 2000.

APPENDIX C

LEARNING FROM RECOVERY:
THOUGHTS ON FEATURE A TRANSPORT EXPERIMENTS

Learning from Recovery: Thoughts on Feature A Transport Experiments

Bill Dershowitz [2], Masahiro Uchida [1],
Thomas Doe[2], Aaron Fox[2], Trenton Cladouhous[3]

1. Japan Nuclear Fuel Cycle Development Corporation,
2. Golder Associates Inc
3. WebPE.com

ABSTRACT

This paper summarizes discrete fracture network (DFN) analysis of the Tracer Retention Understanding Experiments "TRUE-1" carried out at the Äspö Hard Rock Laboratory in Sweden from 1995 through 2000. These studies confirmed the ability of the DFN approach, together with conventional advection-dispersion-diffusion assumptions to calibrate and predict solute transport in a single fracture at the 5 to 10 meter scale. The analysis also indicated the possibility that alternative formulations of reactive transport constitutive laws may also be useful.

In addition to addressing issues of ADD transport, the "TRUE-1" experiment raised and addressed important issues regarding solute transport pathways and the effect of fracture network connectivity on flow and transport in fractured rock.

1. INTRODUCTION

Solute transport in fractured rock is controlled by unique combinations of transport properties, transport pathway geometry, and hydraulic head field. Minor changes in the head field can radically alter the transport pathways, producing completely different transport results.

The Tracer Retention Understanding Experiments (TRUE) are part of a research program at Äspö, the Swedish Hard Rock Laboratory, designed to study the transport of radionuclides in crystalline rock (Winberg, ed., 2000). The TRUE-1 experiment was carried out in a 50-m scale block of fractured rock at the northern end of the Laboratory, at the 450 m level (Figure 1). Tracer experiments focused on a geologically and hydrogeologically identified structure, "Feature A" (Figure 2) at the 5 to 20 meter scale. The purpose of this paper is to point out several of the interesting aspects of this experiment, particularly as they relate to improving the understanding of flow and transport in fractured rocks.

The JNC/Golder modeling group used stochastic discrete feature network (DFN) models for analysis and modeling of the TRUE-1 experiment (Dershowitz et al., 2000). This effort included identification of conductive features, their geometry, and properties, stochastic discrete fracture simulations, and flow and transport modeling. Most DFN analyses were carried out as stochastic models, reflecting the underlying uncertainty in fracture geometry and properties even for as well characterized a rock block as TRUE-1. However, by the end of the project, transport was reduced to a network of less than 10 pipes between injection and collection boreholes, with deterministically calibrated properties. The details of these analyses are described in Dershowitz et al. (1996) and Dershowitz et al. (2001).

This paper will address four major issues, which arose during the project:

1. Identification of flow and transport pathway geometry
2. Network connectivity and head

3. Transport process constitutive approaches
4. Calibration and prediction

Resolution of these issues is essential to understa nding solute transport processes in fractured rock, and developing an ability to predict tran sport at larger time and distance scales.

2. PATHWAY GEOMETRY

Figure 3 shows the geometry of tracer tests carried out in "Feature A". Although the goal of the experiment was to test a single discrete fracture, evidence from borehole images clearly demonstrates that at the 10 meter scale of the experiment, "Feature A" is not a single fracture, but rather a structure made up of multiple fractures, intersected by and interacting with a fracture network. The orientation of "Feature A" at each of its intersections with the five experimental boreholes is illustrated in Table 1. The strike of these intercepts varies from N25W to N46W, with dips between 76 and 80 degrees. Thus, even while "Feature A" is a relatively well defined feature at the scale of 10 to 50 meters, it is clearly not a single planar structure. In particular, at borehole KXTT4, "Feature A" consists two distinct fractures with hydraulic response – which indicates that at least two distinct transport pathways should not be unexpected (Figure 4).

Figure 5 illustrates the orientation distribution of potentially conductive features identified by the project geologist, Jan Hermanson from bor ehole images, borehole flow logging and hydraulic interference measurements. The in tensity of potentially conductive fractures in each of the boreholes defining "Feature A" is shown in Figure 6. Based on this analysis, the conductive fracture intensity P_{32} in the rock block of "Feature A" is on the order of 3.15 m^2/m^3. For a five meter transport path, this results in 3 to 7 intersecting conductive fractures with transmissivities similar to "Feature A", i.e, on the range of 10^{-6} to 10^{-8} m^2/s. This is illustrated in the DFN model of Figures 7, 8, and 9.

The network aspect of "Feature A" is confirmed by the results of flow dimension analysis of hydraulic tests conducted in "Feature A". From the five boreholes intersecting "Feature A", Dershowitz et al. (1996) evaluated the flow dimension based on fractional dimension type curve approaches (Doe, 1991). The flow dimension from four of five of these tests is 2.6 – indicating a leaky aquifer or fracture network behavior. Only one test, at KA3005A, away from the focus of the tracer experiments is near 2.0, the dimension for a single fracture or confined aquifer.

Given this level of structural complexity, it is to be expected that transport in "Feature A" will follow multiple pathways, and it is perhaps so meway surprising when breakthrough exhibits only a single peak, possibly indicating a single path way! Further, borehole intersections show that "Feature A" itself is a combination of multiple splays and coalesced fractures, as can be seen in the borehole image logs. Additional path way structure can be provided by the internal structure of the fracture including mylonites, breccia, and gouge, as well as variations in fracture aperture (Figure 10).

3. CONNECTIVITY AND HEAD

Hydraulic interference was used to evaluate the connectivity of the rock block containing "Feature A." This hydraulic testing indicates that "Feature A" is connected hydraulically to many of the discrete features in the surr ounding 100 m scale rock volume, but is also hydraulically isolated many conductive structures within the rock block, even at distances as low as ten meters from "Feature A". This is consistent with interfe rence behavior observed

elsewhere at Äspö and other fractured rock sites (Uchida et al., 2001). During the tracer experiments, heads and drawdowns were to be predicted together with tracer breakthrough. In many cases, this proved to be one of the more difficult aspects of the modeling, particularly for the DFN approach. In the early tracer experiments, there was a clear "groundwater" divide within "Feature A", caused by intersections between "Feature A" and different fractures connecting hydraulically to the Aspo tunnels. Over time, as the heads in the "Feature A" rock block equilibrated, this groundwater divide disappeared, and the natural gradient of 0.1% toward the drift was asserted throughout "Feature A". (Figure 11).

Hydraulic responses are thus the key to understanding the connectivity of "Feature A", and its place in the surrounding fracture network. For any realization of a discrete fracture network, stochastic fracture properties and the connectivity to boundary conditions are different. This results in differences in drawdown patterns between different DFN realizations. Figure 12 illustrates drawdown patterns for 10 DFN realizations of the PDT-4 tracer test. Each of these realizations is consistent with the fracture statistics and hydraulic tests in the TRUE-1 rock block. However, each realization also produces different heads and thus significantly different gradients and flow fields within "Feature A". This allows the quantification of the level of uncertainty in tracer prediction due to geometry and connectivity of intersecting fractures. For the purposes of "prediction" however, JNC/Golder took the DFN realization which provided the best match for the drawdown pattern of PDT-4, and used this for prediction of sorbing tracer transport along the same pathways and under the same boundary conditions.

Table 2 illustrates the use of the calibrated DFN model to produce a probabilistic prediction of drawdown in response to PDT-4.

A variety of stochastic continuum approaches have been used to model "Feature A", placing emphasis on the pattern of transmissivity and transport aperture within the single fracture, and generally ignoring connectivity to the intersecting fracture networks. This approach has the advantage of simplicity, but misses the important physical phenomena described above – it is easier to calibrate heads when you don't need to consider the uncertainty in fracture intersections and connectivity, but it is not necessarily better!

This is illustrated by the distance drawdown relationship from tracer tests carried out on "Feature A". Figure 13 shows the drawdown at borehole KXTT4 as a result of pumping from borehole KXTT3, only 4.7 m away. At the same pumping rate of 0.2 liters/minute, the drawdown during experiment STT-2 is four times greater than that observed in experiment PDT-2. At the same time, the recovery from PDT-2 is over 10 percent larger than for STT-2, even though the hydraulic response is smaller. The pumping rate of experiments RC-1 and PDT-3 is 0.4 liters/minute, doubled that of STT-2. However, the drawdown due to RC-1 is lower than that from STT-2, and the recovery of STT-2 is similar to that in RC-1. Neither of these behaviors can be predicted by a model which does not consider the complexity of the connectivity of the fracture network in the TRUE-1 block, and the interaction between fractures and the changing head field during the TRUE-1 experiment.

This enigma of connectivity is further illustrated in Figure 14. Experiments between KXTT4 and KXTT3, and between KXTT1 and KXTT3 show strong connectivity, with on the order of 90 to 100% recovery for conservative tracers. At the same time, experiments between KXTT1 and KTXX4 in Feature A show only 5% recovery! This behavior is inconsistent with the idea of pathways controlled by the stochastic pattern of apertures on fractures. However, it is reasonably, when considering that the actual connections are through the multiple fractures which make up "Feature A", and that small changes in the head field can completely change the transport pathways in the fracture network. Clearly under the head field based on pumping in KXTT4, the transport pathways do not follow the route via KXTT3!

4. TRANSPORT PROCESSES

One of the goals of the TRUE-1 experiments was to improve our understanding of transport processes. It is hoped that deeper evaluation of the results from the TRUE-1 experiments will help to clarify the fundamental uncertainties re garding flow and transport in porous media:

- What is dispersion and what is the best wa y to parameterize dispersion to understand both symmetric (Gaussian) and non-symmet ric dispersion? Can non-symmetric dispersion be explained in terms of multi-rate advection, or is it related solely to mobile-immobile exchange?
- What is the nature of exchange between mobile and immobile zones along transport pathways. Is this primarily a diffusional phenomenon, or are there other mechanisms such as locally turbulent mixing involved?

Going into the TRUE-1 project, JNC/Golder assumed that the important processes for transport are:

- Advection – transport of solutes at the same velocity as groundwater motion
- Dispersion – variations in solute transport velocity due to variations in groundwater velocity
- Immobile zone exchange – exchange of mass between the mobile (advective) portions of the fracture pore-space and imm obile zones such as infillings, stagnant pools, altered rock, fracture coating minerals, and the rock itself
- Sorption – chemical attachment between certain tracers and certain minerals

Of these processes, there is the most uncertainty concerning immobile zone exchange. Is this purely a diffusive process proportional to differences in concentration, or is it the result of local turbulent mixing (advective exchange). Is immobile zone exchange controlled strictly by the available surface area, as some theorize, or is it controlled by the geological structure and material distribution within the fracture ?

JNC/Golder utilized three different solute tr ansport approaches to examine the extent to which the important issues of immobile zone exch ange can be resolved within the context of the TRUE-1 experiments: Conventional a dvection/dispersion/diffusion (ADD), Immobile zone exchange (IMX), and Continuous time ra ndom walk (CTRW; Berkowtz et al, 2000).

The ADD approach is illustrated in Figure 15 (Dershowitz et al., 1998). The Laplace Transform Galerkin solution for solute tr ansport ADD assumes steady-state flow and a second-order approach to describe the diffusive mass transfer of a solute between the groundwater in a pipe and the multiple immobile porosity zones attached to it, the advective-dispersive transport of solute species n in a pipe network is given by (Sudicky, 1990):

$$A\left[R_n(\ell)\frac{\partial C_n}{\partial t} + q(\ell)\frac{\partial C_n}{\partial \ell} - \frac{\partial}{\partial \ell} D_{l_n}(\ell)\frac{\partial C_n}{\partial \ell} + R_n(\ell)\lambda_n C_n - R_{n-1}(\ell)\lambda_{n-1} C_{n-1} \right]$$
$$\pm \sum_{\ell'} \dot{M}\,\delta(\ell - \ell') + \sum_{\ell^*} Q(C_n - C_n^*)\delta(\ell - \ell^*) + \sum_{im=1}^{IM} V_{im}\theta_{im} D_{im} \frac{\partial C_n^{im}}{\partial w}\Big|_{w=0} = 0 \qquad \text{(Equation 1)}$$

where:

n	=	nuclide index [-]
im	=	immobile zone class number (note: if desired *im* can equal 0) [-]
$IM(\ell)$	=	total number of immobile zones attached to pipe ℓ [-]
$A(\ell)$	=	pipe cross-sectional area [L^2]
$R_n(\ell)$	=	retardation factor [-]
$q(\ell)$	=	specific discharge (≡ Pipe velocity v) [L/T]

$D_{\ell_n}(\ell)$ = dispersion coefficient = $\alpha v + D_n^o$ [L^2/T]

α = pipe longitudinal dispersivity [L],

D_n^o = free-solution diffusion coefficient [L^2/T]

λ_n = decay constant [1/T]

$\dot{M}(t)$ = internal solute mass source/sink [M/T]

Q = external fluid source/sink [L^3/T]

$\delta(\ell - \ell')$ = dirac delta [1/L]

$\delta(\ell - \ell^*)$ = dirac delta [1/L]

V_{im} = block surface area per unit volume of matrix and fissures [1/L]

D_{im} = matrix effective diffusion coefficient [L^2/T]

θ_{im} = immobile zone porosity for immobile zone "im"

C_n = pipe concentration [M/L^3]

C_n^* = concentration of injectate in external fluid source [M/L^3]

C_n^{im} = Immobile zone concentration [M/L^3]

ℓ = Distance along interconnected pipe network [L]

ℓ' = Location of solute mass source/sink [L]

ℓ^* = Location of external fluid source/sink [L]

w = Distance perpendicular to plane of fracture [L]

t = time [T]

The second order approach implemented for diffu sive exchange of solute mass between the pipes and any on the *im* immobile zones attached to them is described by:

$$\theta_{im}(im,\ell)R_n^{im}(im.\ell)\frac{\partial C_n^{im}}{\partial t} - \frac{\partial}{\partial w}\theta_{im}(im,\ell)D_{im}\frac{\partial C_n^{im}}{\partial w} + \theta_{im}(im,\ell)R_n^{im}(im,\ell)\lambda_n C_n^{im} - \theta_{im}(im,\ell)R_{n-1}^{im}(im,\ell)\lambda_{n-1}C_{n-1}^{im} = 0 \qquad \text{(Equation 2)}$$

where:

$\theta_{im}(im, \ell)$ = Immobile zone porosit y for immobile zone "*im*" attached to pipe "ℓ" [-]

$R_n^{im}(im, \ell)$ = Immobile zone retardati on factor for immobile zone "*im*" attached to pipe "ℓ" [-]

C_n^{im} = Concentration in matrix [M/L^3]

D_{im} = Matrix effective diffusion coefficient [L^2/T]

= $D_n^0\ \tau$

D_n^o = Free-solution diffusion coefficient [L^2/T]

τ = Tortuosity [-]

The above equations used for the ADD approach recognize that we do not fully understand immobile zone exchange by providing the optio n of multiple immobile zones, each with its own diffusion rate, thickness, tortuosity, and por osity. Providing for mu ltiple immobile zones is particularly useful in considering transpor t at multiple time and distance scales. While fracture infillings may be the primary immobile zone for transport at the 5 meter and one month scale, intact rock is more likely to be the most important immobile zone for distance scales of kilometers and time scales of hundreds or thousands of years. For the purposes of the TRUE-1 experiment, only a single immobile zone is used, and this immobile zone represents the short terms, small capacity imm obile zone of gouge, breccia, and altered rock

which is most likely to be important in the short time and distance scale. However, the same model can be used for longer time frames by adding additional immobile zone porosities to the porosities in the TRUE-1 model.

Advective exchange (AX) (Miller, 1996) assumes that the process of exchange between mobile and immobile zones occurs at a fixed rate of exchanges per meter of advection, rather than at a rate proportional to differences in concentration. This model is illustrated in Figure 16. The approach is based on two parameters: β, the number of advective exchanges per meter, and f_{imm}, the ratio of the immobile zone volume to the mobile zone volume.

Continuous Time Random Walk (CTRW) was developed by Berkowitz et al. (2000) to explain the frequent occurrence of non-symmetrical (non-Gaussian) dispersion on the basis of multi-rate advection. CTRW treats both diffusion and Gaussian dispersion as special cases of multi-rate advection, and can reproduce both diffusive and Gaussian transport on the basis of a single parameter β, the power for the assumed powerlaw (Pareto) distribution of velocity. The CTRW method is summarized in Figure 17 (after Berkowitz et al, 2000).

While it was hoped that the TRUE-1 experiments would distinguish between different fundamental theoretical approaches to dispersion and immobile exchange, all three of the approaches implemented were able to fit experiments to some level of accuracy. Example ADD, AX, and CTRW fits to TRUE-1 experiments are shown in Figures 18, 19, and 20. In addition, the LaSar approach for multi-rate advection (Cvertkovic et al., 1999) was also successful in matching the TRUE-1 experiments. The only conclusion from this is that, at present, multiple and conflicting theories about transport in fractures can reproduce the TRUE-1 experiments, and additional experiments will be required to distinguish between them.

5. CALIBRATION AND PREDICTION

JNC's goal in participating in the TRUE-1 project was to improve our understanding of transport in fractures and fracture networks, not to demonstrate the predictive abilities of DFN approaches. Nevertheless, we are somewhat gratified when our calibrated DFN models demonstrate a certain degree of predictive power. The calibration process itself was quite edifying, since it showed to what extent model parameters needed to be adjusted to provide a match to transport experiments.

Over the course of four years JNC/Golder used a series of increasingly refined DFN models to produce predictions for tracer breakthrough in "Feature A". These experiments went from the initial radially converging tests RC-1 and RC-2, dipole tests DP-1 through DP-4, and sorbing tracer experiments of the tracer retention experiment STT-1, STT-2, and STT-1b. The accuracy of calibrations and predictions improved continuously over this period, and in the end the prediction of STT-2 and STT-1b was quite accurate. Predictions for breakthrough of STT-2 tracers are summarized in Table 3 and illustrated in Figures 18, 21, 22, and 23. These predictions were based on calibrations to STT-1b transport behavior, and it should therefore not be too surprising that the predictions, although blind, are fairly accurate.

The key parameter which determined the success of transport calibrations and predictions was the immobile zone exchange parameters in Equation (4) above. In particular, the calibrated immobile zone retardation factor R_{im}

$$R_{im} = 1 + \rho_{im} K_d' / \theta_{im} \qquad \text{(Equation 3)}$$

where ρ_{im} is the immobile zone bulk density, θ_{im} is the immobile zone porosity, and K_d' is the effective distribution coefficient for the immobile zone. The calibrated value of R_{im} indicates

that either the effective distribution coefficien t is 10 times the laboratory measured values, or the immobile zone porosity is on the order of 15%. Geological information (Hermanson, 2000) indicates that the porosity of 15% is not unreasonable if immobile zone diffusion is primarily to gouge materials. This is also s upported by research described in Altamann et al. (2001).

The other important immobile zone transport parameter is the perimeter of the pipe pathways. This controls the rate and amount of possibl e diffusion. The calibrated value for this parameter is on the order of 5 to 7 meters, for a pipe flow width of 2.5 to 3.5 meters divided by the number of surfaces on which diffusion o ccurs. For a simple tabular channel, the number of surfaces is 2. However, with ma trix infillings, the effective number of surfaces may be much larger, resulting in effective trans port path widths more on the expected order of magnitude of 0.1 to 1 m.

Unfortunately, the TRUE-1 experiments did not resolve the issue of the actual mechanism behind the parameters which work for calibra ting and predicting ADD solute transport. However, they did demonstrate that, at least for "Feature A", the ADD transport assumptions are not inconsistent with observations.

6. CONCLUSIONS

The TRUE-1 experiment made major progress in improving the understanding of flow and transport in fractured rock. The experiment w as successful in demonstrating the usefulness of discrete fracture network methods for characterizing fracture rock and understanding the geometry of transport pathways, and the possi bility of calibrating DFN models for transport predictions. The experiment did not succeed in resolving the nature of transport within fracture planes, or in resolving between competi ng constitutive approaches to solute transport. It is hoped that future transport experiments on single fractures and fracture networks will further advance the scientific understanding of flow and transport in fractured rock.

7. REFERENCES

Altmann S., M. Uchida, and V. Tidwell, 2001. Visualization and Quantification of Heterogeneous Diffusion Rates in Granodiorite Samples by X-ray Absorption Imaging - Diffusion within Gouge Materials, Altered Ri m and Intact Rock Matrix. Proceedings, TRUE-1 Seminar. September 2000. SKB, Stockholm.

Berkowitz, B., H. Scher and S. E. Silliman, 200 0. Anomalous transport in laboratory-scale, heterogeneous porous media, Water Resources Research, Vol. 36, No. 1, pp.149-158.

Cvertkovic, V. J.-O. Selroos, and H. Cheng., 1999. Transport of Reactive Solute in Single Fractures. Journal of Fluid Mechanics, Vol. 318. pp 335-356.

Dershowitz, W. T. Cladouhos, and M. Uchida, 2001. Tracer Tests with Sorbing Tracers. SKB International Cooperation Report ICR-2001-XX. SKB, Stockholm.

Dershowitz, W., A. Thomas, and R. Busse, 1996. Discrete Fracture Analysis in Support of the Äspö Tracer Retention Understanding Expe riment. SKB International Cooperation Report ICR-96-05. SKB, Stockholm.

Dershowitz, W., Foxford, T., Sudicky, E., Shuttle, D, and Eiben, T., 1998. PAWorks: Pathway Analysis for Discrete Fracture Networks with LTG Solute Transport. User Documentation. Version 1.5. Golder Associates Inc, Seattle.

Dershowitz, W., G. Lee, J. Geier, T. Foxford, P. LaPointe, and A. Thomas, 2000. FracMan Interactive Discrete Fracture Data Analysis, Geometric Modeling, and Exploration Simulation. User Documentation. Version 2.6. Golder Associates Inc, Seattle.

Doe, T. W., 1991. Fractional Dimension Analysis of Constant-Pressure Well Tests. Presented at the 66th Annual Technical Conference & Exhibition of the Society of Petroleum Engineers, Dallas, TX, Oct. 6-9, 1991. SPE Technical Paper No. 22702. Society of Petroleum Engineers, Richardson TX.

Miller, 1996. Advective Exchange: A New Conceptual Approach for Solute Transport in Fractured Rock. Internal Report. Golder Associates Inc., Seattle.

Sudicky, E.A., 1990. The Laplace Transform Galerkin Technique for Efficient Time-continuous Solution of Solute Transport in Double-porosity Media, Geoderma, 46, 209-232.

Uchida, M., Sawada, A. Shimo, M., Yamamoto, H. Takahara, H. , and Doe, T., 2001. Anisotropy, Reversibility and Scale Dependence of Transport Properties in Single Fracture and Fractured Zone --Non-sorbing Tracer Experiment at the Kamaishi Mine. Proceedings, TRUE-1 International Seminar. SKB, Stockholm.

Winberg, A. , ed., 2000. Final Report of the First Stage of the Tracer Retention Understanding Experiments. SKB Technical Report TR-00-07. SKB, Stockholm.

APPENDIX D

DEMONSTRATION SIMULATIONS TASKS 6 PERFORMANCE ASSESSMENT MODELING USING SITE CHARACTERIZATION DATA

APPENDIX D

Demonstration Simulations Task 6 Performance Assessment Modelling Using Site Characterisation Data (PASC)

W. Dershowitz (JNC/Golder)
H. Benabderrahmane (Andrea)
J-O. Selroos (SKB)
M. Uchida (JNC)
A. Winberg (Conterra AB)

October, 2000

TABLE OF CONTENTS

1. BACKGROUND 1

2. OBJECTIVES 2

3. FRAMEWORK AND PROPOSED SITE 3

4. SCOPE 4

5. EXAMPLE TASK 6 SIMULATION CS-135 TRANSPORT IN FEATURE A 5

5.1 3D DFN Model 6

5.2 Conclusions 9

6. DETAILED SUGGESTIONS 10

7. PERFORMANCE MEASURES/OUTPUT 11

8. EXPECTED FINAL PRODUCTS 12

9. APPENDIX – AVAILABLE DATA 13

LIST OF FIGURES

Figure 5-1 Feature A Transport Pathways 5
Figure 5-2 Conductive Fractures Intersecting “Feature A” 5
Figure 5-3 Features NW, A, and A’ and background fractures 6
Figure 5-4 Mobile/Immobile Zone Transport JNC/Golder FracMan/PAWorks Concept 6
Figure 5-5 STT-2 Cesium Injection Time History 7
Figure 5-6 STT-2 Cesium Recovery Predicted within 3% 7
Figure 5-7 Task 6 “PA” Source and Recovery Cesium 8
Figure 5-8 Normalized Breakthrough Cesium-135 8
Figure 5-9 Cumulative Release Cesium-135 9
Figure 5-10 Mobile/Immobile Zone Transport JNC/Golder FracMan/PAWorks Concept 9

1. BACKGROUND

Solute transport is a key aspect of both performance assessment and repository site characterisation. Task 6 seeks to provide a bridge between site characterisation (SC) and performance assessment (PA) approaches to solute transport in fractured rock. Task 6 will focus on the 50 to 100m scale which is critical to PA according to many repository programs.

This document was prepared on behalf of the Äspö Task Force on Modeling of Groundwater Flow and Transport. Section 6 of this document presents example simulations prepared by Golder Associates for JNC. The remainder of this document was prepared by Golder Associates, incorporating discussions and comments by all of the authors on behalf of the sponsoring organizations.

Task 6 is developed in the context of arguments concerning the usefulness of *in situ* tracer experiments for PA, as discussed at the 1st GEOTRAP workshop held at Cologne in 1996. PA requires an understanding of slower processes which are sometimes difficult to observe during short duration tracer experiments; *in situ* tracer experiments are dominated by rather faster processes. At the same time, PA models are generally simpler and physically less realistic than SC models[1].

Task 6 tries to bridge the gap between PA and SC models by applying both approaches for the same tracer experiment, and also for PA boudary conditions. In other word, this exercise will try to look at ***how far in-situ tracer experiments can constrain PA models***. It is hoped this will help to identify the relevant conceptualisations (in processes/structures) for longer term PA predictions and identify site characterisation data requirements to support PA calculations.

- Task 6 combines the use of PA and SC models for both PA and SC boundary conditions.
- All modellers should first implement their models such that they can reproduce the results from relevant Äspö in situ tracer experiments.
- Modellers can make appropriate assumptions for PA modelling, while continuing to honour the in situ tracer experiment result.

Task 6 is phased from simple to complex, and includes sensitivity studies to maximise the amount of information obtained from the task to support both site characterisation and performance assessment efforts.

It is emphasised that up-scaling is not a primary objective of Task 6; this is a change of focus as compared to the presentation of Task 6 at the 13th Task Force meeting in Carlsbad. Up-scaling is now assumed to be an implicit part of the model approaches, whereas the goal of the exercise is to apply PA and SC models to Äspö data.

[1] PA model refers to a Performance Assessment model that typically is based on a number of simplifications concerning geometrical description and treatment of processes. A site characterisation, or process, model is more rigorous in description of primarily processes. However, the latter type of model typically describes a smaller or less complex system than a PA model does.

2. OBJECTIVES

The general objectives of Task 6 is to assess simplifications used in PA models, to assess the constraining power of tracer experiments for PA models, and to provide input for site characterisation programs from a PA perspective. The objectives may be elaborated as follows:

1. Identify key assumptions needed for long term prediction in PA and identify less important assumptions in PA.
2. Identify the most significant PA model components of the site.
3. Prioritise assumptions in PA modelling and demonstrate a rationale for simplifications in PA-models by parallel application of PA models of varying degree of simplification.
4. Understand the capability of in-situ tracer experiments to constrain PA models.
5. Understand the site-specific flow and transport behaviour at different scales using SC models.
6. Provide a benchmark for comparison of PA and SC models in terms of PA measures for radionuclide transport at PA temporal and spatial scales.
7. Establish how to transfer SC models using site characterisation data to PA models.
8. Provide support for site characterisation program design and execution aimed at delivering needed data for PA.

3. FRAMEWORK AND PROPOSED SITE

The objectives will be met by adopting a step-by-step process of model implementation, calibration to in situ experiments, PA type simulations, and sensitivity studies.
Task 6 will focus on the 50 to 100 meter scale which is frequently the critical scale for geosphere retention. However, in order to allow for a more direct comparison, initial simulations will be carried out on the TRUE-1 block at the 5-meter scale:

- Single fracture scale: the TRUE-1 block will be modelled. The purpose of the modelling study is to assess how different conceptualisations of a single fracture compare to each other.
- Fracture network scale: a synthetic block based on the Prototype Repository, TRUE Block Scale, TRUE-1 and FCC features. The purpose of the modelling study is to assess how different conceptualisations of a fracture network compare to each other.

Flow and transport at the two scales will be addressed in the following two steps by applying SC-type models and/or PA-type models:

- Traditional tracer experiment (SC time scale): the selected sets of TRUE-1 tracer experiment will be modelled. The purpose of the modelling study is to provide constraints to all the models before invoking assumptions for PA time scale predictions.
- PA time scale prediction: Nuclide transport or sorbing tracer transport with PA type boundary conditions will be performed. Modellers can make any assumptions as long as they honour the material properties used for TRUE-1 tracer transport modelling.

Flow and transport will be analysed for both current boundary conditions and for PA relevant time scales. Transport is considered from a virtual canister emplacement location in the Äspö HRL rock mass to a structural feature at a specified distance (starting from a few meters to 50-100 m). As an option, the addressed scale may be extended to the site scale (i.e., canister to biosphere). For this option, geochemical data may also be utilised similar to Task 5.

It is acknowledged that the distinction between SC and PA models may be somewhat ambiguous. However, it is stressed that all simplifications utilised when going from SC (tracer experiment) time scales to PA time scales and up-scaling procedures utilised when going from the single fracture scale to the network scale needs to be clearly stated by the modelling teams.

It is also foreseen that SC-type approaches and visualisation techniques be used to understand the nature of flow and transport of radionuclides at PA spatial scales. It is anticipated that different groups will provide visualisations of transport pathways and processes using a variety of tools including pathway analysis, velocity distributions, spatial distributions of F- and β factors, etc.

4. SCOPE

The specific tasks to be performed are:

Task 6A. Model and reproduce selected TRUE-1 tests with a PA model and/or a SC model. This task provides a common reference platform for all SC-type and PA-type modelling to be carried out as the project progresses. This ensures a common basis for future comparison.

Task 6B. Model selected PA cases in the TRUE-1 site with new PA relevant (long term/base case) boundary conditions and temporal scales. This task serves as a means to understand the differences between the use of SC-type and PA-type models, and the influence of various assumptions made for PA calculations for extrapolation in time.

Task 6C. Develop a 50-100m scale synthesised structural model using data from the Prototype Repository, TRUE Block Scale, TRUE-1 and FCC. The structural model should also be complemented with a hydraulic parameterisation. It is suggested that a deterministic rather than a stochastic model is constructed so that the differences between models will be results of variations in assumptions, simplifications, and implementation rather than in the structural framework. The structural model will include sufficient elements of the TRUE Block Scale experiment to make it possible to reproduce a TRUE Block Scale tracer experiment as part of Task 6D. It is also suggested that Task 6C is performed by a single group led by SKB.

Task 6D. Task 6D is similar to Task 6A, using the synthetic structural model and a 50 to 100 m scale TRUE-Block Scale tracer experiment. The flow and transport simulations will be carried out using both SC-type and PA-type models. The task will provide an improved understanding of how these approaches compare at in situ tracer test time and distance scales.

Task 6E. Task 6E extends the Task 6D transport calculations to a reference set of PA time scales and boundary conditions. In the first part of Task 6E, a basic set of PA and SC assumptions and simplifications should be used. These can be extended to alternative assumptions as part of the sensitivity study part of Task 6E.

Modellers are encouraged to apply different conceptual models of varying degree of simplifications. The possible range of simplifications could be from simple 1D uniform streamtubes to a 3D representation of the internal structure of the fracture, stagnant pools, in-plane heterogeneity of aperture distribution etc for Tasks 6A and 6B. However, it is noted that if a modelling group uses a PA model, they should also provide interim modelling assumptions and results to provide a platform for model comparison. For example, if a 1D PA model is going to be used, model assumptions (such as transmissivity, boundary conditions) and drawdown match of an interim model, e.g. a stochastic continuum flow model used for deriving streamlines, should be reported. For Task 6D and 6E, modelling groups are encouraged to apply various conceptual models which addresses network effects such as dilution, branching (dispersion at fracture intersections) or flow/transport along FIZs (fracture intersection zone).

5. EXAMPLE TASK 6 SIMULATION CS-135 TRANSPORT IN FEATURE A

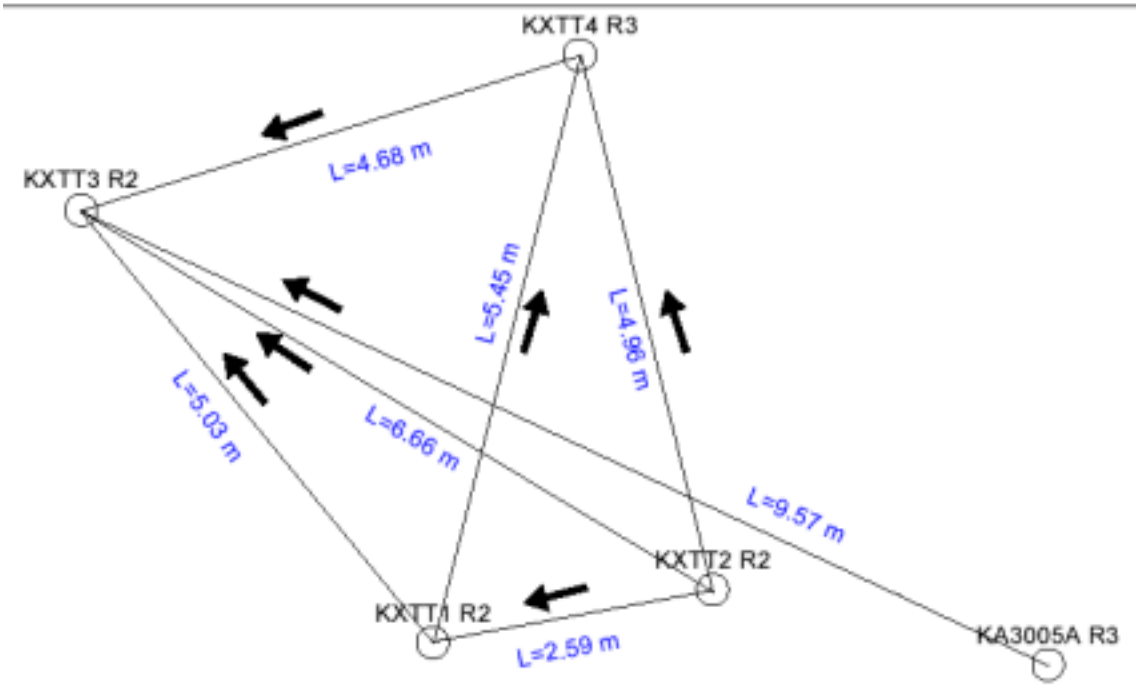

Figure 5-1 Feature A Transport Pathways

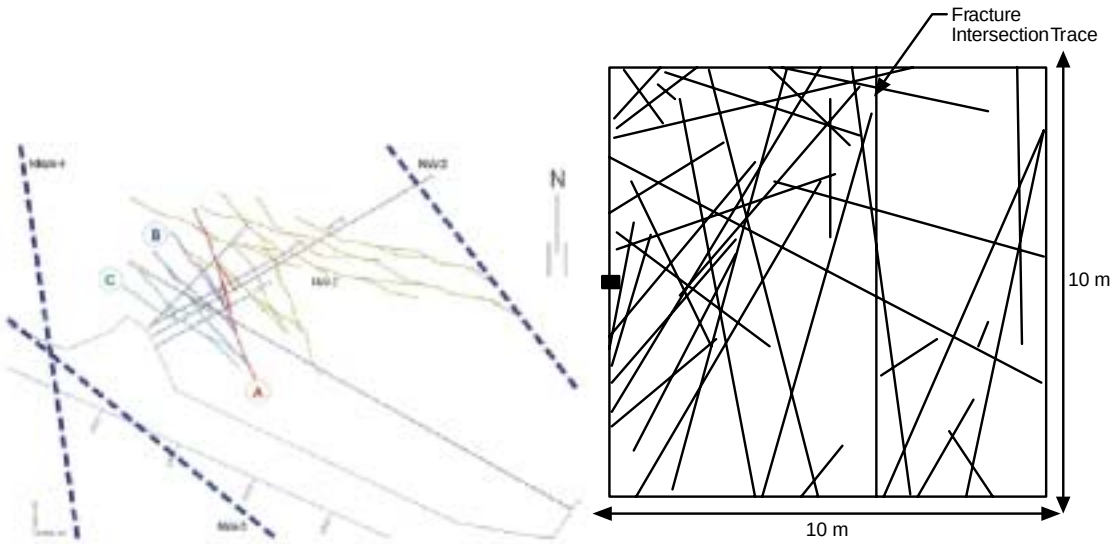

Figure 5-2 Conductive Fractures Intersecting “Feature A”

5.1 3D DFN Model

All 359 background fractures

5% background fractures

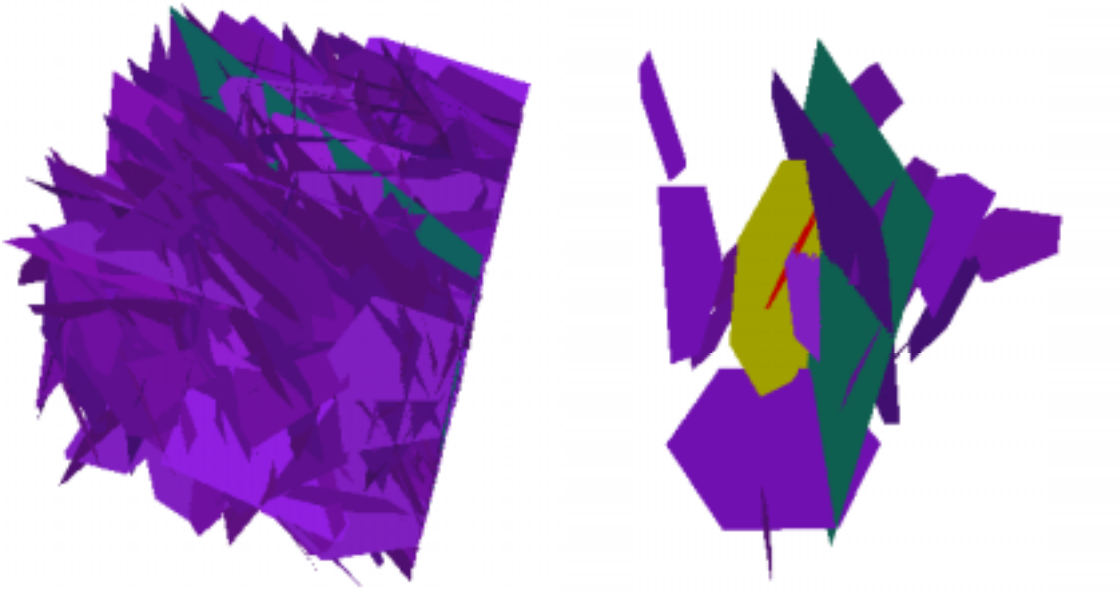

Figure 5-3 Features NW, A, and A' and background fractures

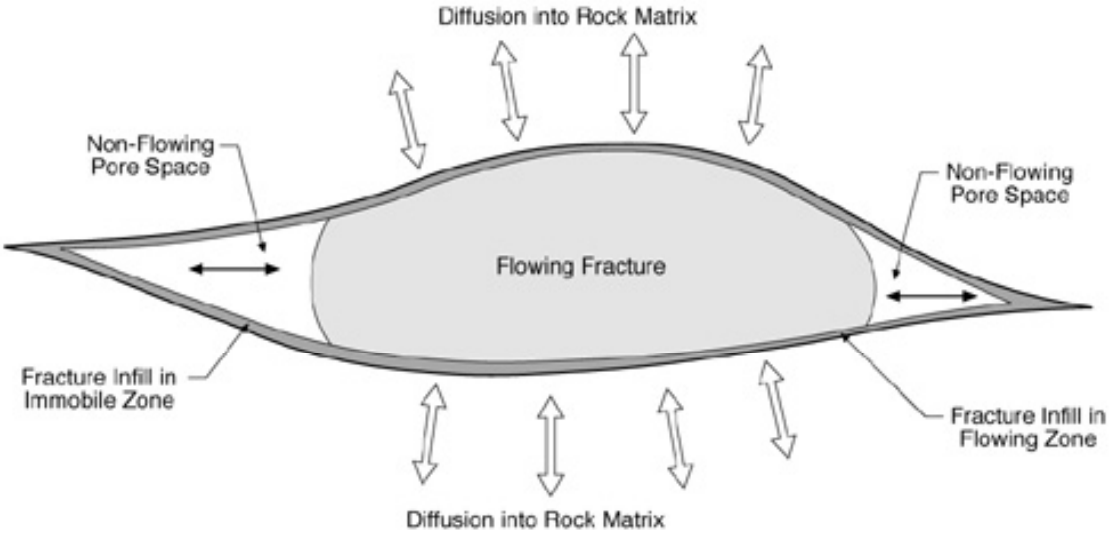

Figure 5-4 Mobile/Immobile Zone Transport JNC/Golder FracMan/PAWorks Concept

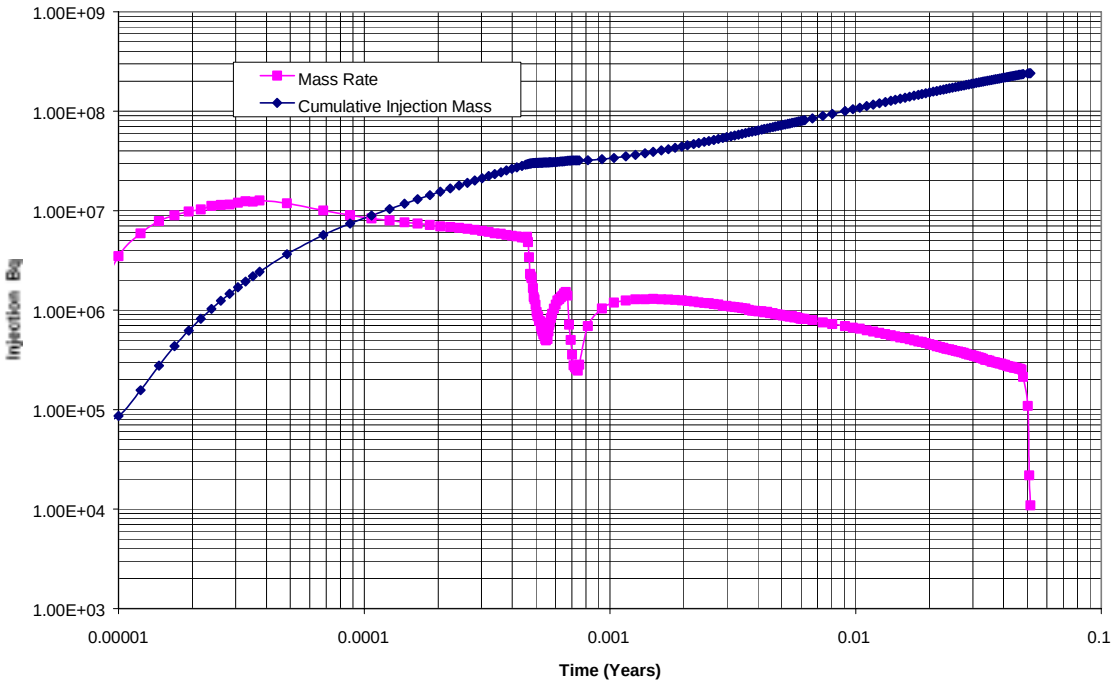

Figure 5-5 STT-2 Cesium Injection Time History

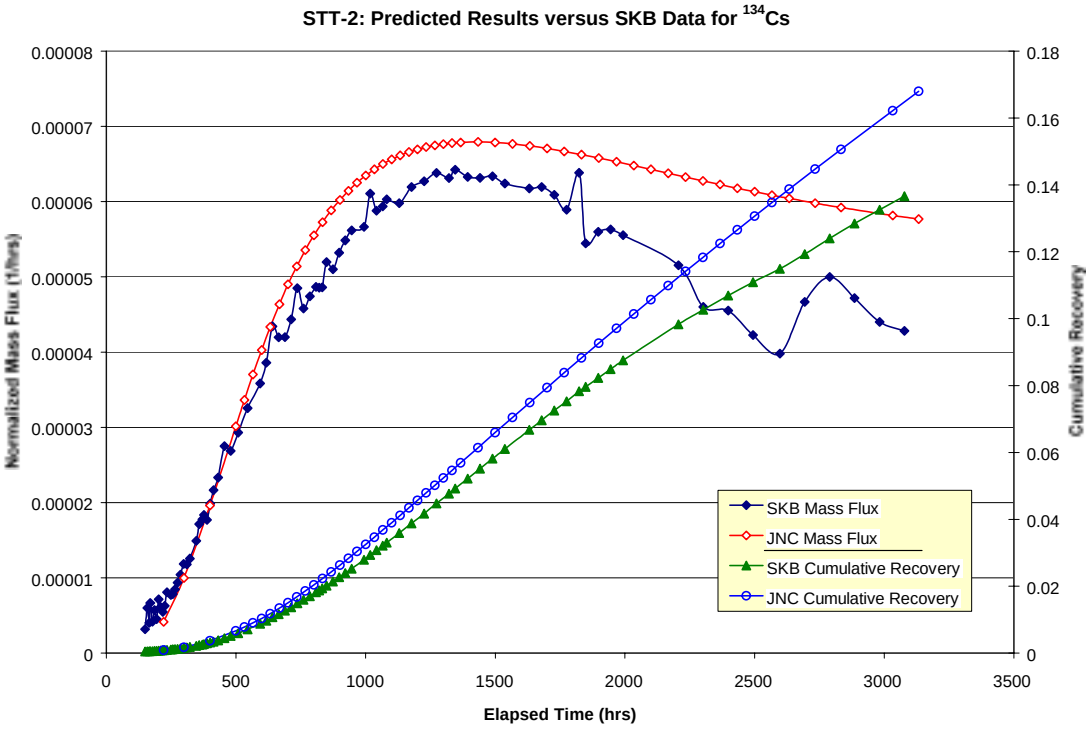

Figure 5-6 STT-2 Cesium Recovery Predicted within 3%

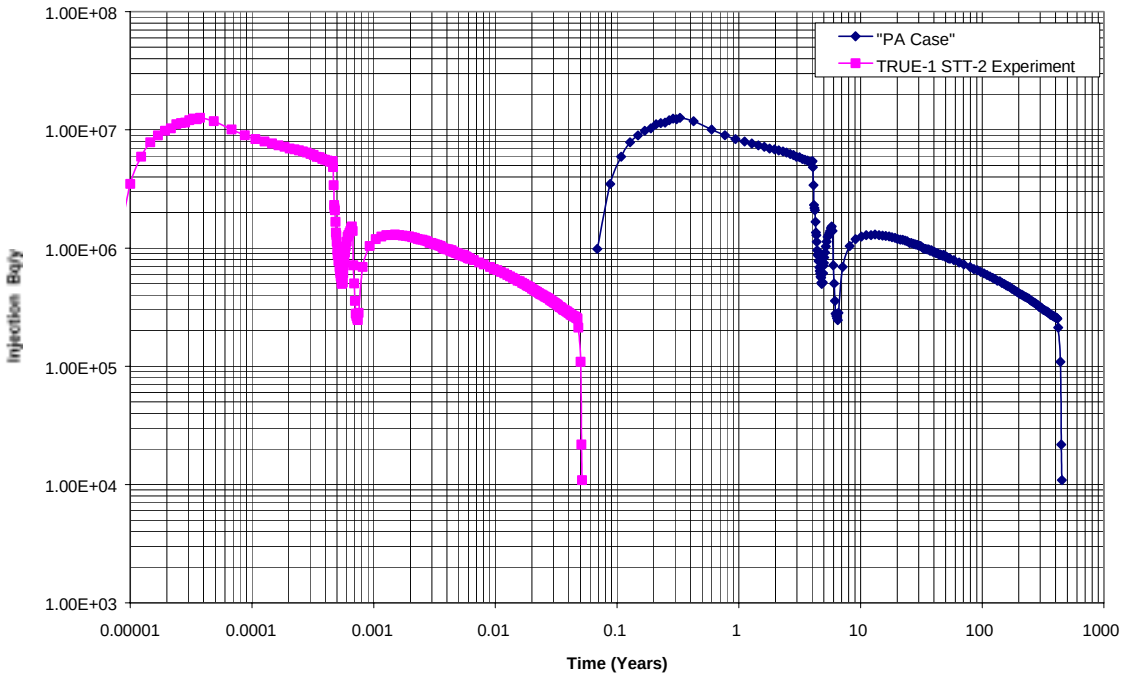

Figure 5-7 Task 6 "PA" Source and Recovery Cesium

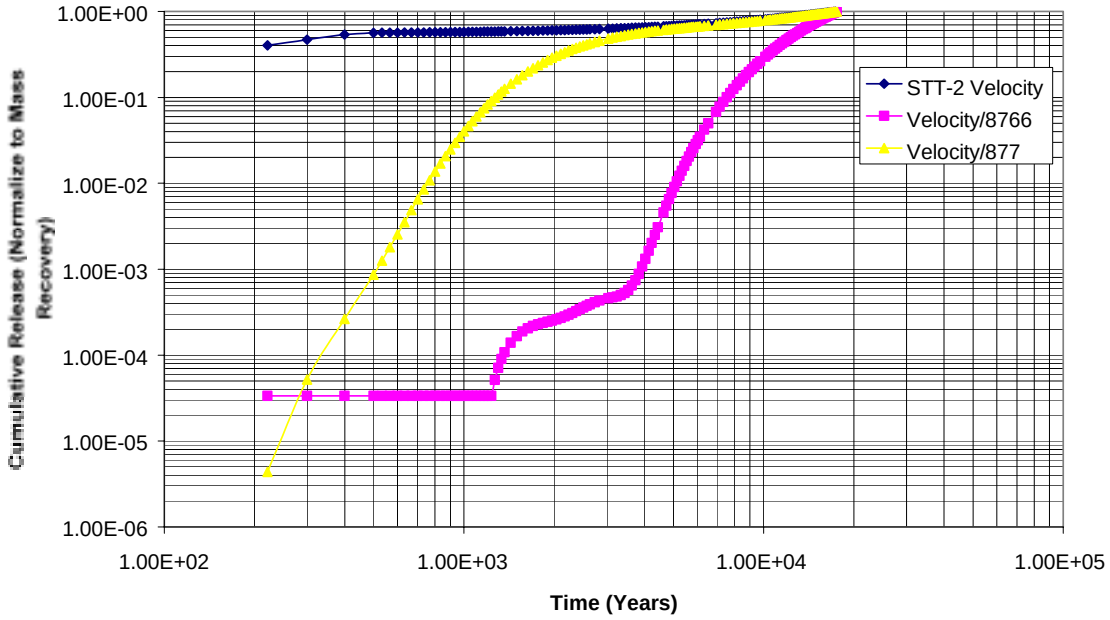

Figure 5-8 Normalized Breakthrough Cesium-135

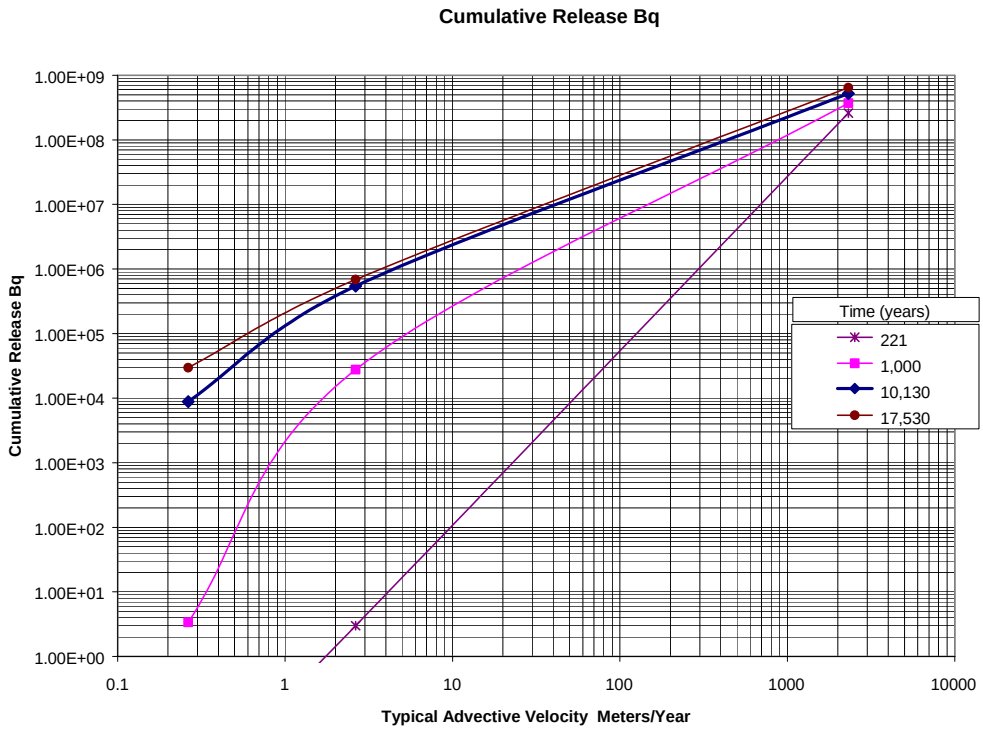

Figure 5-9 Cumulative Release Cesium-135

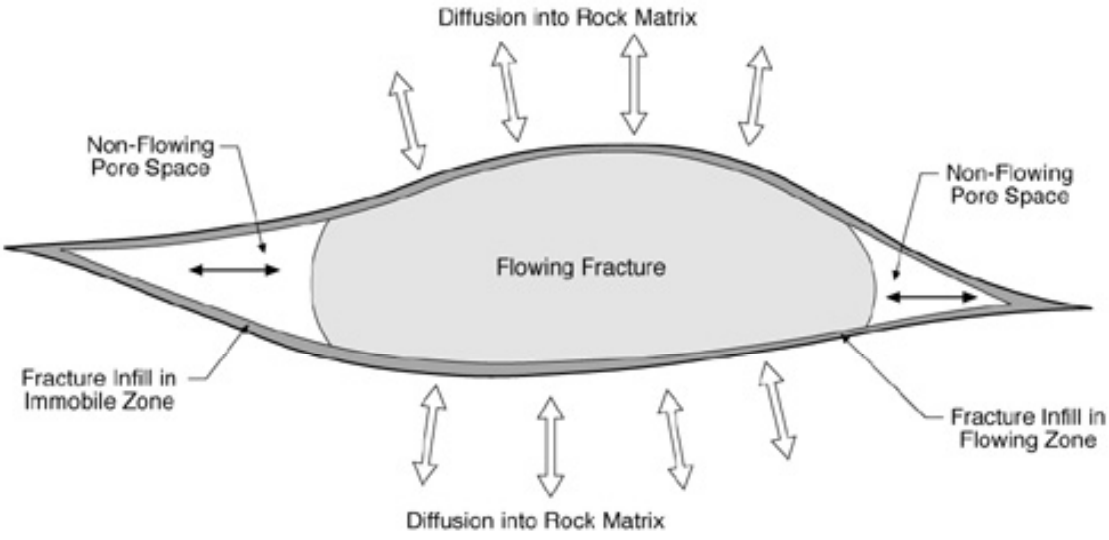

Figure 5-10 Mobile/Immobile Zone Transport JNC/Golder FracMan/PAWorks Concept

5.2 Conclusions

- Task 6 Potentially Provides a Link Between PA and Site Characterization Codes;
- Task 6 Potentially Supports Extension of Site Characterization Experiments to PA Time and Space Scales; and
- Task 6 Potentially Provides Guidance for Prioritization of Site Characterization.

6. DETAILED SUGGESTIONS

Below some specific suggestions for the successful execution of the task are given. The suggestions should not be seen as final decisions; additional suggestions from Task Force members are strongly encouraged at the Task Force meeting.

1. The project sequence from simulation of real tracer tests to PA scale calculations and from a relatively simple fracture to a fracture network should be followed to ensure that all models develop in a consistent, logical, and comparable fashion.
2. Modellers are encouraged to provide performance measures based on varying degree of simplification to quantitatively demonstrate the rationale for simplifications.
3. The task should be based on TRUE Block Scale site data, supplemented by information from fracture characterisation projects (FCC), TRUE-1 rock block, the Prototype Repository rock block, and possibly data from the Long Term Diffusion Experiment (LTDE).
4. PA time scale, i.e. ten thousand to one million years (Task 6B and 6E).
5. Common boundary conditions set by Task 6 project team such as fixed head at downstream fracture zones, fixed head at upstream edges of model.
6. The horizontal distance from canister to closest important fracture zones on order of 50 to 100 meters.
7. A select, limited group of radionuclides with a range of half-lives and sorption parameters such as Cs, I, Th, Se should be used.
8. Injection mode (pulse, slug etc) will be selected by the Task 6 project team. It is suggested that injection takes place during a long enough interval to obtain matrix diffusion effects (Task 6B and 6E).
9. Modelling groups can develop the SC and/or PA-type models to the level of geological, hydrogeological, geochemical, and transport in detail which they feel appropriate.
10. Details such as background fracture properties and locations and the framework structural model should be agreed between groups prior to modelling, and will be included in the structural framework. The project team needs to provide a structure to achieve this.
11. No treatment of engineered barriers and the disturbed zones.
12. Reference cases (Task 6A and 6D) need to be defined in sufficient detail such that groups could in theory produce at least one identical result (cross-comparison of models at least one common denominator).

7. PERFORMANCE MEASURES/OUTPUT

The three main output entities to be calculated are:

1. Cumulative release (Bq/yr) to fracture zone at downstream boundary for each radionuclide up to a certain time (e.g., time to peak or specified regulatory time).
2. Magnitude of peak release (Bq/yr) and time to peak release (yr) for each radionuclide.
3. Retention ratio [%] (e.g., ratio of peak release for radionuclide including sorption and diffusion processes to peak release with sorption and diffusion off, or ratio of mass retained in geosphere to total mass injected).

Additional deliverables may consist of specific analyses concerning e.g. used assumptions and analyses of flow field characteristics:

1. Sensitivity studies of alternative geological assumptions (such as mixing at intersections, FIZ effects, internal structure of fractures, effect of correlations between properties such as size, fracture type, internal structure, transmissivity, etc.).
2. Measures of the flow field such as the distribution of flow wetted surface normalised by flux (FWS/Q), and the distribution of groundwater travel time f(tau).

8. EXPECTED FINAL PRODUCTS

1. Guidance for site characterisation requirements in order to meet PA needs.
2. Increased confidence in the simplifications and assumptions used in PA-type flow and transport approaches by using both CS-type and PA-type models for identical in situ experiments.
3. Demonstration of rationale for abstraction process (assumptions and simplifications) when going from CS-type models to PA models.
4. Improved understanding of flow and transport at PA temporal and spatial scales based on studies using Äspö data.
5. Visualisation of flow and radionuclide transport pathways and processes at experimental and PA scales, using 3D pathway and transport process visualisations and statistical analysis of transport pathways.

9. APPENDIX – AVAILABLE DATA

Similar to previous Task 6 proposal presented at Task Force meeting #13 in Carlsbad.